UCGE Reports
Number 20245

Department of Geomatics Engineering

GPS and Galileo Performance Evaluations for Multiple Reference Station Network Positioning

(URL: http://www.geomatics.ucalgary.ca/research/publications/GradTheses.html)

by

Seema Phalke

September 2006

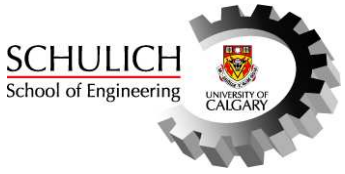

UNIVERSITY OF CALGARY

GPS and Galileo Performance Evaluations for Multiple Reference Station Network Positioning

by

Seema Phalke

A THESIS

SUBMITTED TO THE FACULTY OF GRADUATE STUDIES

IN PARTIAL FULFILMENT OF THE REQUIREMENTS FOR THE

DEGREE OF MASTER OF SCIENCE

DEPARTMENT OF GEOMATICS ENGINEERING

CALGARY, ALBERTA

September, 2006

Abstract

The European Galileo and the modernization of the current Global Positioning System (GPS) will substantially increase the available signals to Global Navigation Satellite Systems (GNSS) users. Past simulation studies have shown that Galileo performs better than the current GPS under high ionosphere conditions and for medium length reference-rover separations when using the Single Reference Station (SRS) approach. When the baseline increases beyond 30 km, ambiguity resolution performance deteriorates, and carrier phase fixed integer ambiguity kinematic positioning becomes difficult to achieve for either system. The Multiple Reference Station (MRS) approach reduces the effect of correlated errors more effectively than the traditional SRS approach and hence provides better positioning accuracies over increased baseline distances. The Multiple Reference Station Tightly Coupled (MRS-TC) approach is an efficient MRS technique developed at the University of Calgary. This study extends past research through an evaluation of Galileo compared to GPS for the MRS approach. The focus is on an independent assessments of the MRS-TC approach dual frequency Galileo and a GPS using 24/27 GPS/Galileo and 29/30 GPS/Galileo constellations, in terms of positioning accuracy and ambiguity resolution reliability. Several networks of varying sizes are analysed under different ionospheric conditions using a measurement simulation software system.

The analysis shows that for all the simulated baselines and error levels, the MRS-TC approach applied to Galileo always offers the best results compared to SRS GPS and Galileo and the MRS-TC GPS cases. The study concludes that, for low ionospheric error

conditions, the MRS-TC for Galileo delivers reliable cm-level positioning errors for extended baselines up to 120 km, whereas for medium and high ionospheric conditions, it provides reliable cm-level positioning errors for baselines up to 90 and 30 km, respectively. For high ionospheric conditions and extended baselines beyond 30 km, none of the systems provide reliable results under the simulation conditions and algorithms used. These results obtained here are based on 24/27 GPS/Galileo and 29/30 GPS/Galileo constellations however they will vary depending upon the constellation, i.e. the number of satellites deployed for each system in the future since the ambiguity resolution performance is in part a function of the number available satellites.

Acknowledgement

I would like to thank all my colleges, friends and family members who supported and contributed to this thesis work. I would like to express my gratitude especially

- To my supervisor, Dr. Elizabeth Cannon. I appreciate her constant guidance, encouragement through out my M. Sc. program. Without your support this thesis work was impossible.
- To Dr. Gerard Lachapelle, for providing access to all the resources and encouragement throughout the M. Sc. course
- To my husband Santosh who has been a constant source of love and encouragement ever since he entered my life. You are the one who understand me most.
- To my 5 month old daughter Saee to push me up to complete this work. You are so wonderful, beautiful, and adorable, I love you so much.
- To my parents and my sister, for your love and support throughout my life.
- To my parents in Laws, for taking care of Saee while I was writing the thesis and for your endless love and support.
- To all my friends and colleagues, Mark Petovello, Sanjeet Singh, Dharshaka Karunanayake, Minmin Lin, Paul Alves, Ning Luo, Deip Dao, Shahin Charkhandeh for the interesting discussions we had.
- To "Geoide", for providing the financial support for this thesis work.

Table of Contents

List of Tables

List of Figures

List of Symbols

$\varepsilon\phi$	Effect of carrier phase noise plus the multipath (m)
εp	Effect of pseudorange noise plus the multipath (m)
λ_1	GPS carrier L1 wavelength (m)
λ_2	GPS carrier L2 wavelength (m)
$d\rho$	Satellite orbital errors (m)
d_{trop}	Tropospheric delay (m)
Φ	Carrier phase observation (m)
$\nabla\Delta$	Double difference (DD) operator
ρ	Geometric Range (m)
d_{ion}	Ionospheric delay (m)
P	Pseudorange observable (m)
dt	Receiver clock offset (s)
dT	Satellite clock offset (s)
c	Speed of light (m)
λ	Wavelength of the carrier chosen (m)
f	Frequency of the carrier phase (Hz)
I	Ionosphere error (m)
N	Initial phase ambiguity
ppm	Parts per million
v	Innovative sequence in Kalman filter

w	Processing noise
x	Estimation state vector in Kalman filter
z	Observation vector in Kalman filter

List of Abbreviations

AR	Ambiguity Resolution
CAR	Cascading Ambiguity Resolution
CIR	Cascading Integer Resolution
CORS	Continuous Reference Stations
CS	Commercial Service
DD	Double Difference
DGPS	Differential GPS
DoD	US Department of Defence
EC	European Commission
ECC	European Commission Communication
ESA	European Space Agency
EU	European Union
EWL	Extra Wide Line
FARA	Fast ambiguity resolution approach
FASF	Fast ambiguity search filter
FLYKIN+TM	Single reference processing software by the University of Calgary
FOM	Figures Of Merit
GJU	Galileo Joint Undertaking
GNSS	Global Navigation Satellite System
GPS	Global Positioning System
IF	Ionosphere-Free

IGS	International GPS Station
IOV	In-Orbit Validation
L1	GPS frequency band centred in 1575.42 MHz
L2	GPS frequency band centred in 1227.6 MHz
L2C	Modernized GPS frequency band centred in 1227.6 MHz
LAMBDA	Least-squares Ambiguity Decorrelation Adjustment
LC	Linear Combination
LSQC	Least-Squares Collocation
ML	Medium Lane
MRS	Multiple Reference Station
MRS-TC	MRS Tightly Coupled
MTTCF	Mean Time To Correct Fix
MultiRef™	MRS approach developed by the University of Calgary
NGS	National Geodetic Survey
NICE	New and Improved Clock and Ephemeris
NL	Narrow-Lane
NOAA	National Oceanic and Atmospheric Administration
NWP	Numerical Weather Prediction
OS	Galileo Open Service
PC	Percentage of correct ambiguity fixes
PRN	Pseudo-Random Noise
PRS	Public Regulated Service
PVT	Position, Velocity and Time information

RMS	Root Mean Square
RTK	Real Time Kinematic
SA	Selective Availability
SAR	Search and Rescue Service
SIS ICD	Galileo Open Service Signal In Space Interface Control Document
SOL	Safety of Life service
SPS	Standard Positioning Service
SRS	Single Reference Station
TCAR	Triple Frequency Cascading Ambiguity Resolution
TEC	Total Electron Content
UERE	User Equivalent Range Error
US	United States
USCG	United States Coast Guard
UV	Ultra-Violet
WGS84	Earth-Centred-Earth-Fixed reference frame
WL	Wide-Lane

Chapter 1 Introduction

1.1 Background

The U.S. Department of Defence (DoD) developed the Global Positioning System (GPS) to provide precise estimates of position, velocity, and time to users worldwide. The DoD approved the basic architecture of the GPS in 1973. The first satellite was launched in 1978, and the GPS was declared operational in 1995. GPS has been widely used in civilian applications during the past few decades. However, the GPS integrity, availability, and accuracy still need further improvement for Real Time Kinematic (RTK) applications like surveying, geodesy, structural monitoring (of dams, buildings, etc.), and automated machine control, which always demand more and more accuracy (Enge 2003). A GPS modernization program was started in the late 1990's to upgrade GPS performance for both civilian and military applications. The decrease of Selective Availability (SA) to 0 was the first step taken on May 1, 2000 and this enabled the improvement of the Standard Positioning Service (SPS) from a horizontal accuracy of 75.0 to 22.5 m 95% of the time (Sandhoo et al. 2000). Further GPS modernization steps for civil users consist of the broadcast of a second civil signal on L2 (L2C), and a third civil signal on an additional civil frequency, namely L5. The first GPS satellite with L2C was launched on September 25, 2005 and the L5 signal will be introduced on a new generation of satellites called Block IIF, of which the first one is scheduled for launch in late 2007 or early 2008. The capabilities of RTK systems will be significantly boosted

with the availability of three carriers and will thus provide exciting new benefits for civil users.

While GPS is undergoing modernization, the European community has been developing an independent and civilian satellite navigation system: Galileo, which is a joint undertaking of the European Commission (EC) and the European Space Agency (ESA). Modernized GPS and Galileo will be the parts of the 2nd generation Global Navigation Satellite System (GNSS). The Galileo constellation is expected to consist of 30 satellites (27 active plus three active spare) evenly placed in three orbital planes with one-degree higher orbital inclination angle than GPS and it is expected to become operational by 2010. Galileo users will be able to access three free-of-charge signals modulated on three frequencies, namely E1, E5b and E5a, through an Open Service (OS), which is expected to enable equivalent or even better positioning accuracy compared to modernized GPS (European Commission 2006a).

A stand-alone GPS user can typically estimate location with accuracy better than 10 metres. To improve positioning accuracy, the correlation property of GPS errors is utilised by means of carrier phase Differential GPS (DGPS), which uses a Single Reference Station (SRS) receiver at a known location to calculate and transmit the corrections to a roving user. For GPS, this SRS approach performs well under normal atmospheric conditions for baselines less than 30 km (Gao and Wojciechowski 2004). However, the approach does not provide reliable and precise solutions under high ionosphere conditions and for extended baselines since the carrier phase integer

ambiguities are difficult to resolve. This is mainly due to the reduction in the correlation of ionospheric errors (Misra and Enge 2006; Dao et al. 2004).

To overcome the limitation of the SRS approach when using longer baselines, network-based positioning methods were developed which use a network of reference stations to measure the correlated GPS errors (e.g. ionosphere and troposphere) over a region and to predict their effects spatially and temporally within the network. In case of a stand-alone GPS, this Multiple Reference Station (MRS) approach, also known as Network RTK has proven to reduce the effects of the correlated errors much better than the traditional SRS approach. It also allows the reference stations to be located further apart, thereby covering a larger service area than the traditional approach while still providing the same (or higher) level of performance (Raquet 1998; Wübbena 1996; Vollath et al. 2000).

The MRS Tightly Coupled (MRS-TC) approach is a recently developed MRS algorithm, which combines all the L1 and L2 observations from the reference stations and the rover into one unique filter to estimate the rover positions. This MRS-TC algorithm has shown to provide more accurate position results than the traditional SRS and Least-Squares Collocation (LSQC) MRS approaches under both quiet and active ionospheric conditions (Alves 2004; Dao 2005).

1.2 Motivation

Two main findings from past studies motivate the need for this research. In the first series of research efforts, Alves (2001), Julien et al. (2003), Julien et al. (2004) and Zhang et al.

(2003) simulated GPS constellation consisting of 24 modernized GPS satellites and a Galileo constellation consisting of 27 active satellites as designed originally. Using these simulations they showed that in the case of the SRS approach, Galileo outperforms modernized GPS for single, dual and triple frequency cases, and for baselines up to 70 km, mainly because of its greater number of satellites resulting in more measurements and better geometry. Until now, past studies have evaluated stand-alone Galileo and compared these results to stand-alone GPS, only for the SRS approach. Secondly the various MRS algorithms are very well evaluated for the dual frequency case in past studies only for stand-alone GPS. For example, the evaluation by Ahn (2005) showed that for stand-alone GPS, the network approach succeeds in making consistent improvements in the range of 9% to 22% over SRS in terms of reducing the effect of measurement errors on all observables. However the performance of MRS algorithms deteriorate in terms of positioning accuracy and ambiguity resolution with an increase in baselines beyond 100 km and in the case of high ionospheric conditions (Dao 2005).

Since past studies have shown that stand-alone Galileo performs better than GPS for the dual frequency SRS approach, the intent herein is to determine what advantages Galileo can provide for the MRS dual frequency approach. Specifically, it needs to be determined if it will provide reliable results for extended baseline lengths and for high atmospheric conditions.

Until now, studies have simulated the GPS constellation consisting of 24 modernized GPS satellites and a Galileo constellation consisting of 27 active satellites as designed

originally. However since there are 29 operational GPS satellites present in space (US Coast Guard 2006), and if all 30 Galileo satellites are set active then the new constellation will consist of 29/30 GPS/Galileo satellites. Hence, it needs to be determined if this new 29/30 GPS/Galileo constellation with a higher number of satellites will further improve results for extended baseline lengths and for high atmospheric conditions.

1.3 Thesis Objectives and Scope of the Research

The main purpose of this research is to evaluate stand-alone Galileo compared to GPS for the SRS and MRS approaches using dual frequency measurements, and to determine if stand-alone Galileo MRS can extend the maximum achievable baseline beyond 100 km to provide reliable kinematic positioning under different ionospheric conditions. This overall objective is subdivided into several sub-objectives, namely:

1. To understand the modernized GPS and Galileo signals, their error sources, and possible phase combinations,
2. To study various SRS and MRS algorithms used in kinematic positioning and the benefits offered by modernized GPS and Galileo for SRS ambiguity resolution,
3. To evaluate and compare the performance of the SRS and MRS-TC techniques for stand-alone GPS and Galileo case using the SimGNSSII™ software simulator developed at the University of Calgary for baselines ranging from 30 km to 120 km for different simulated ionospheric conditions using 24/27 GPS/Galileo constellations and to investigate if stand-alone Galileo with MRS-TC case can improve performance in terms of accuracy and reliability,

4. The same evaluation experiment described for 24/27 GPS/Galileo constellations discussed earlier is repeated using the 29/30 GPS/Galileo constellations to investigate if the results obtained with the first evaluation can be improved further because of an increased availability of satellites.

In order to achieve these objectives, GPS and Galileo constellations were simulated, for four different MRS networks with baseline lengths from 30 km to 120 km. GPS and Galileo observations were generated for low, medium and high ionosphere levels for the simulated MRS networks. The processing of the simulated data was done in four different modes: SRS stand-alone GPS, SRS stand-alone Galileo, MRS-TC stand-alone GPS and MRS-TC stand-alone Galileo. The results obtained from simulation processing in four different modes were analysed and compared in terms of positioning accuracy and ambiguity resolution performance. This analysis leads to determine what improvements the MRS-TC stand-alone Galileo approach can provide over the other three approaches.

Since stand-alone GPS MRS approaches have already been well evaluated through previous studies using dual frequency data, this study extends this work to the stand-alone Galileo MRS dual frequency case. The next interesting step which is outside the objectives of this thesis would be to determine the advantages of stand-alone Galileo MRS for the triple frequency case.

This study is simulation-based work and all the data processing is done in post mission mode, however the results will be informative for the real-time case.

1.4 Thesis Outline

Chapter 2 gives an overview of the modernized GPS and Galileo in terms of performance, signals in space, and interoperability. It reviews GNSS differential error sources such as: satellite orbital errors, tropospheric errors and ionospheric errors. Various phase combinations and stochastic ionospheric modelling techniques currently used in GPS carrier phase positioning are also discussed.

Chapter 3 presents a review of the SRS approach for kinematic positioning. It describes the Kalman Filtering (KF) estimation technique utilised in SRS positioning. It explains both dual frequency and triple frequency techniques for ambiguity resolution which can be used for modernized GPS and Galileo. It also discusses the benefits of modernized GPS and Galileo in terms of ambiguity resolution for the SRS approach.

Chapter 4 describes the MRS algorithm for kinematic positioning and reviews existing approaches including the tightly coupled approach. It then discusses present MRS kinematic positioning performance with GPS using dual and triple frequency techniques.

Chapter 5 presents the simulation approach employed in this study. It describes the GPS/Galileo SimGNSSII™ software simulator, the simulated GPS and Galileo constellations, four different simulated networks and the simulated error levels. It then details the test scenarios and data processing used in this study.

Chapter 6 first describes the Figures Of Merit (FOM) utilised in the analysis. It then presents and analyzes the results based on different test scenarios as explained in Chapter 5 and the FOMs. Various comparison plots are generated and results are summarized at the end of the chapter.

Finally, Chapter 7 draws conclusions from this research and makes recommendations for future work.

Chapter 2 GPS and Galileo Fundamentals

2.1 GPS I and Modernization

GPS has performed extremely well and has generally exceeded expectations in the past three decades, however some significant improvements are needed to satisfy both military and civil users (McDonald 2002). The goals of the GPS Modernization program are to protect the services for military users, to prevent adversaries from exploiting the system, and preserve civil use with enhancements (Swider 2001). The first GPS modernization step was the cancellation of Selective Availability (SA) in 2000 (Sandhoo et al. 2000). It was then followed by the launch of a satellite with the addition of a new military signal (M-code) and a second civil code on L2 (L2C) in September 2005. The first satellite with the third civil frequency (L5) is expected to be launched by 2008. Further modernization i.e. GPS III, will consist of new civil signal L1C proposed as common baseline L1 open service signal for GPS and Galileo. This signal is backward compatible to the present GPS L1 signal. GPS III will also support increased signal power levels, which will help to prevent jamming. The launch of GPS-III satellites with L1C is expected by 2013 (Alexander 2006). The assessment and design of a new generation of satellites to meet military and civil requirements will continue through 2030. In addition, the Operational Control Segment (OCS) will continue to expand to improve the monitoring of signals and to predict satellite orbital positions and clock data in the satellite broadcast messages more accurately.

Figure 2.1 represents the GPS signals before September 2005, the present GPS signals and the proposed modernized signals. Table 2.1 lists the Modernized GPS signal frequencies, wavelengths and chipping rate. Table 2.2 includes a summary of the launch schedule of the modernized GPS satellites (Hothem 2006).

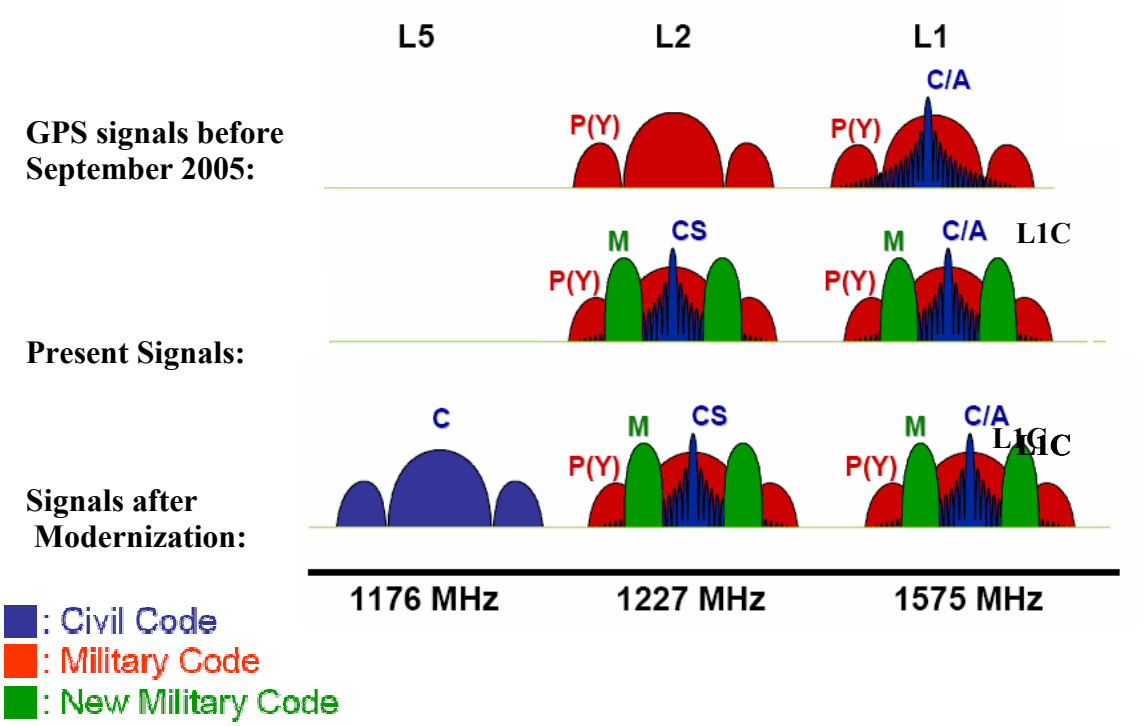

Figure 2.1 Comparison of the Present GPS Signals and the Post-Modernization GPS Signals (From ICDGPS-200C 2004)

Table 2.1 Modernized GPS Signals

Modernized GPS signals	Frequency (MHz)	Wavelength (m)	Chipping rate (Mc/s)
L1	1575.42	0.190	10.23
L2C	1227.60	0.244	1.023
L5	1176.45	0.254	10.23

Modernized GPS expects to enhance the performance in accuracy, integrity, continuity, and availability of current GPS due to following improvements:

- Frequency Diversity: As shown in Table 2.1 modernized GPS users will have access to three civil signals rather than one. Thus, GPS modernization provides redundancies and robustness in the civil signal services to meet today's increasing dependency on GPS and safety-of-life applications (Jan 2003).
- Improved Ionospheric Delay Measurement: Presently ionosphere delays can be estimated with the semi-codeless cross correlation on L2. However, it can introduce a bias (Litton et al. 1996). A multi-frequency GPS user can directly estimate the frequency dependent ionosphere error using the available multi-frequency measurements. This leads to robust ionosphere estimation, and reduces the User Equivalent Range Error (UERE) to about 2 m, which will enable the Standard Positioning Service (SPS) stand-alone horizontal accuracy to be improved to 3 to 8 m, 95% of the time (McDonald 2002).
- Improved Satellite Clock and Ephemeris: The New and Improved Clock and Ephemeris (NICE) will further reduce the GPS satellite clock and ephemeris errors to approximately 1.2 m, so that the SPS horizontal accuracy will be further improved to 2 to 5 m 95% of the time (Perz 2004; Rodriguez et al. 2004).

With the increased signal power in GPS-III and technology advancement in the reduction of code noise and code multipath, further improvement in the GPS SPS performance is expected (Zhang 2005).

Table 2.2 GPS Modernization Program (Alexander 2006)

Activity	Implementation Date
SA set to zero	May 2000
GPS IIR-M Enhancements - New L2 civil (L2C) signal - M-code on L1 & L2	1st satellite operational on December 16, 2005 2nd Launch 14 Sept. 2006
GPS IIF Enhancements - L2 civil (L2C) signal - M-code on L1 & L2 - New L5 civil signal	1st launch currently scheduled for May 2008
GPS III Enhancements - L2 civil (L2C) signal - M-code with greater power - L5 - New L1C civil signal	1st launch ~ 2013
OCS Enhancements	On going

2.2 Galileo

The Galileo constellation will comprise of satellites in a Medium Earth Orbit (MEO) and its associated ground segment, and it will be the European contribution to the Global Navigation Satellite System (GNSS). Galileo is being designed as an independent system but at the same time, this design is optimized for use with other systems, notably GPS (European Commission 2006b). It will be a civil system, operating under public control and jointly managed and financed by the European Commission (EC) and the European Space Agency (ESA).

2.2.1 Status of the Galileo Project

Since the 1990s, the EC and ESA began preparatory activities in order for Europe to have its own global satellite navigation system for better and guaranteed coverage over

northern Europe. This navigation system named Galileo and it is to be realised in three phases: project definition, development and implementation. The Galileo Definition Phase was carried out in the year 2000. A tentative Galileo frequency and signal plan (Hein et al. 2001) was then published and has been the baseline for the development of Europe's satellite navigation system. The development phases of Galileo were decided in 2002. The Galileo frequencies and signals were redefined in the same year to incorporate compatibility and interoperability with GPS, and another frequency and signal plan was published (Hein et al. 2002). In mid 2004, a few more important changes were carried out in the waveforms on the L1 and E6 signals as a consequence of the agreement made between the US and EU in the same year (Rodriguez et al. 2004). In addition, the orbit selection for the Galileo constellation was finalized and published in Zandbergen et al. (2004). The first experimental In-Orbit Validation (IOV) GIOVE-A Galileo satellite was launched in December 2005 (GPS World 2006a). The development of the IOV satellites and ground segment is on-going and the IOV satellites and the IOV ground segment will be deployed before the end of 2008.

The performance objectives of Galileo in terms of position accuracy and availability are geared to be competitive with respect to existing GNSS's and further planned evolutions (European Commission 2006a). Based on a 10-degree mask angle and global availability 99.8% of the time, the Galileo OS horizontal and vertical accuracies are expected to be 4 m and 8 m (95%) respectively (European Commission 2006b).

The development of Galileo consists of three phases:

- Development and Validation: During this first phase (2002 to 2005), the mission requirements were consolidated, the satellites and ground-based components were under development, and the overall IOV of Galileo was IVO includes the delivery of the first four satellites in the Galileo constellation of 30, along with a number of ground control and monitoring stations. The first Galileo prototype satellite was launched in December 2005.
- Deployment phase: Presently Galileo is in the deployment phase (2006-2007) which covers the entire network of ground infrastructure and the launch of the remaining Galileo satellites.
- Commercial operation: The third phase will start in 2008, whereby the whole system will become commercially operational. The information contained in the Galileo Open Service Signal In Space Interface Control Document (SIS ICD) is now made available to the public by the Galileo Joint Undertaking (GJU), an undertaking jointly created by the European Commission and the European Space Agency (ESA and GJU 2006).

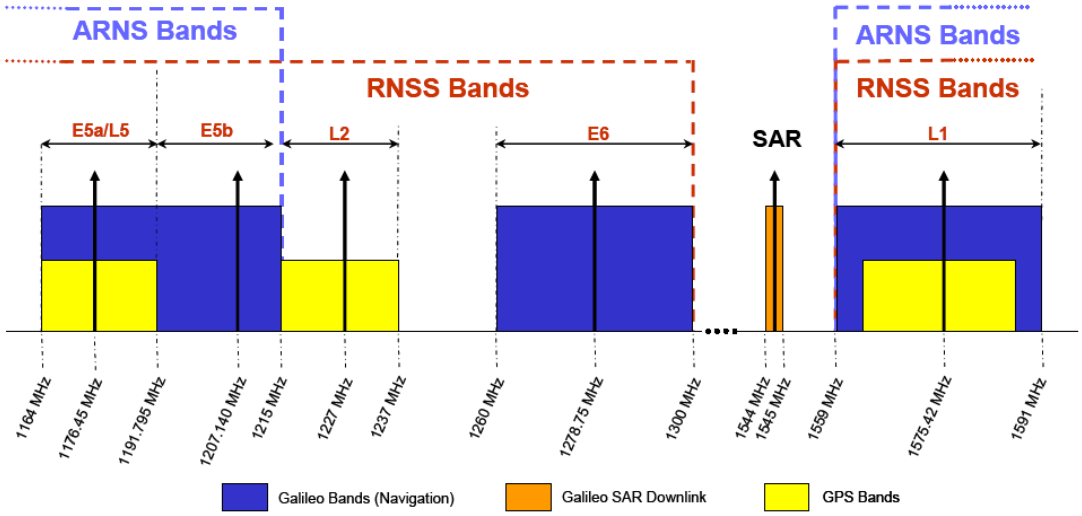

Figure 2.2 Galileo Frequency Plan (ESA and GJU 2006)

2.2.2 Galileo Signals in Space

Galileo will provide 10 signals in the frequency ranges 1164-1215 MHz (E5A and E5B), 1260-1300 MHz (E6) and 1559-1591 MHz (E1), in the Radio-Navigation Satellite Service (RNSS) and Aeronautical Radio Navigation Services (ARNS), allocated frequency bands (ESA and GJU 2006). Figure 2.2 describes the selection of these signals. Out of these ten signals, four signals will be transmitted in the frequency range 1164-1215 MHz (E5a-E5b), three signals will be transmitted in the frequency range 1260-1300 MHz (E6), and the last three signals will be transmitted in the frequency range 1559-1591 MHz (L1). Among those signals, six will be accessible to all Galileo civil users on E5a, E5b and L1 as an Open Service (OS). Two signals on E6 with encrypted ranging codes will only be accessible to some commercial users, and the remaining two (one in the E6 band and one in the E2-L1-E1 band) with encrypted ranging codes and data will be

accessible to authorized users of the government approved Public Regulated Service (PRS). The details of the each Galileo signal characteristic are as shown in the Table 2.3.

Table 2.3 Galileo Signal Characteristics (European Commission 2006b)

Signals Id.	Signals	Central Frequency	Frequency Modulation	Chipping Rate	Code Encryption	Data Rate	Data Encryption
1	Data Signal In E5A	1176 MHz	BPSK(10)	10 Mcps	No	50 Sps/25 Bps	No
2	Pilot Signal In E5A	1176 MHz	BPSK(10)	10 Mcps	No	No Data	No Data
3	Data Signal In E5B	1207 MHz	BPSK(10)	10 Mcps	No	250 Sps/125 Bps	No
4	Pilot Signal In E5B	1207 MHz	BPSK(10)	10 Mcps	No	No Data	No Data
5	Spilt-Spectrum Signal In E6	1278 MHz	BOC(10,5)	5 Mcps	Yes – Governmental Approved	250 Sps/125 Bps	Yes
6	Commercial Data Signal In E6	1278 MHz	BPSK(5)	5 Mcps	Yes - Commercial	1000 Sps/500 Bps	Yes
7	Commercial Pilot Signal In E6	1278 MHz	BPSK(5)	5 Mcps	Yes - Commercial	No Data	No Data
8	Spilt-Spectrum Signal In L1	1575 MHz	BOC(N,M)	M Mcps	Yes – Governmental Approved	250 Sps/125 Bps	Yes
9	Data Signal In L1	1575 MHz	BOC(2,2)	2 Mcps	No	250 Sps/125 Bps	No
10	Pilot Signal In L1	1575 MHz	BOC(2,2)	2 Mcps	No	No Data	No Data

2.3 System Compatibility and Interoperability

Galileo is being designed as an independent GNSS, providing Position, Velocity and Time information (PVT) in combination with an assessment of the quality of the provided information to users as well as support to the COSPAS-SARSAT Search and

Rescue system through broadcasts of alert messages (Leonard et al. 2002). This information is provided through different signals allocated for different services like the OS, the Commercial Service (CS), the Safety-of-Life service (SOL), the Publicly Regulated Service (PRS) and the Search and Rescue Service (SAR). With demanding user requirements, the combined use of Galileo with other existing Satellite Navigation Systems, notably GPS**,** is a key driver to gain access to the future GNSS market (Leonard et al. 2002). Hence, Galileo is being designed as an independent system but at the same time, this design is optimized for use with other systems. To facilitate interoperability of Galileo with GPS at the receiver level, different studies have identified the following main interoperability issues (European Commission 2006a):

a) Signals in Space
b) Constellation
c) Time reference frame
d) Geodetic datum

These four issues regarding the compatibility and interoperability of Galileo and GPS from a system architectural design level were discussed in Dellago et al. (2003a, 2003b). Fyfe et al. (2002), Miller et al. (2004), Ganguly et al. (2004) and Spiller et al. (2001) discuss the range of applications such as telecommunications systems, civil aviation, and vehicle navigation, etc. and possible user benefits that can be gained from a hybrid of complementary and compatible GPS/Galileo services. An agreement signed in June 2004 between the US and EC ensures non-interference and compatibility between the GPS and Galileo. Key elements of the agreement include (GPS World 2004):

- A Common signal structure for future open services, and a suitable signal structure for the encrypted Galileo Public Regulated Service (PRS), and
- Confirmation of interoperable time and geodetic standards to facilitate the joint use of GPS and Galileo.

2.4 GNSS Observables and Error Sources

Two observables, namely the pseudorange and carrier phase, are mainly utilised while estimating the position with any GNSS. The pseudorange observable is determined by measuring the difference between the transmission time and reception time of the satellite signal. The observation equation relating the pseudorange observable P in unit of length (usually metres) in terms of time difference is expressed as (Spilker and Parkinson 1994):

$$P = \rho = c(t - T) \tag{2.1}$$

Using the user and satellite coordinates, the geometric range measurement can be expressed as:

$$\rho = \sqrt{(x^s - x)^2 + (y^s - y)^2 + (z^s - z)^2} \tag{2.2}$$

where (x^s, y^s, z^s) are the three components of the satellite coordinate, and (x, y, z) is the unknown user position defined as the receiver antenna phase centre coordinate, which needs to be estimated. Both satellite and receiver coordinates are referred to the Earth-Centred-Earth-Fixed reference frame (WGS84). t is the time of signal reception in seconds, and T is the time of transmission in seconds, whereas c is the speed of light in

metres per second. Equation (2.1) is a theoretical expression and in practice, the GNSS signal is corrupted by many error sources. These include the satellite clock error, satellite coordinate error, and atmospheric effects (including tropospheric and ionospheric components); therefore, the complete equation relating the pseudorange in metres and the unknown error parameters is given by:

$$P = \rho + d\rho + c(dt - dT) + d_{ion} + d_{trop} + \varepsilon p \tag{2.3}$$

where, $d\rho$ is the satellite orbital errors in metres, d_{trop} is the tropospheric delay in metres, d_{ion} is the ionospheric delay in metres, dt is satellite clock offset in seconds, dT is receiver clock offset in seconds and εp is the effect of pseudorange noise plus multipath in metres (Wells et al. 1986).

Similarly the carrier phase observation, Φ in metres can be given as:

$$\Phi = \rho + d\rho + c(dt - dT) + \lambda N - d_{ion} + d_{trop} + \varepsilon_{\phi} \tag{2.4}$$

where λ is the wavelength of the carrier chosen in metres (per cycle), N is the integer phase ambiguity, and ε_{ϕ} is the effect of carrier phase noise plus multipath in metres (Lachapelle 2004). The ionospheric error for the carrier phase observable is the same as the pseudorange observable, however since the ionosphere causes an advance to the carrier and a delay in the pseudorange, they differ in sign (Klobuchar 1996).

2.4.1 GNSS Measurement Differencing

For positioning using carrier phase observations, Double Difference (DD) phase observations are usually used. Double differencing reduces the effect of orbital and

atmospheric errors, and eliminates satellite and receiver clock errors, and therefore helps to resolve integer ambiguities more efficiently and effectively (Lachapelle 2004).

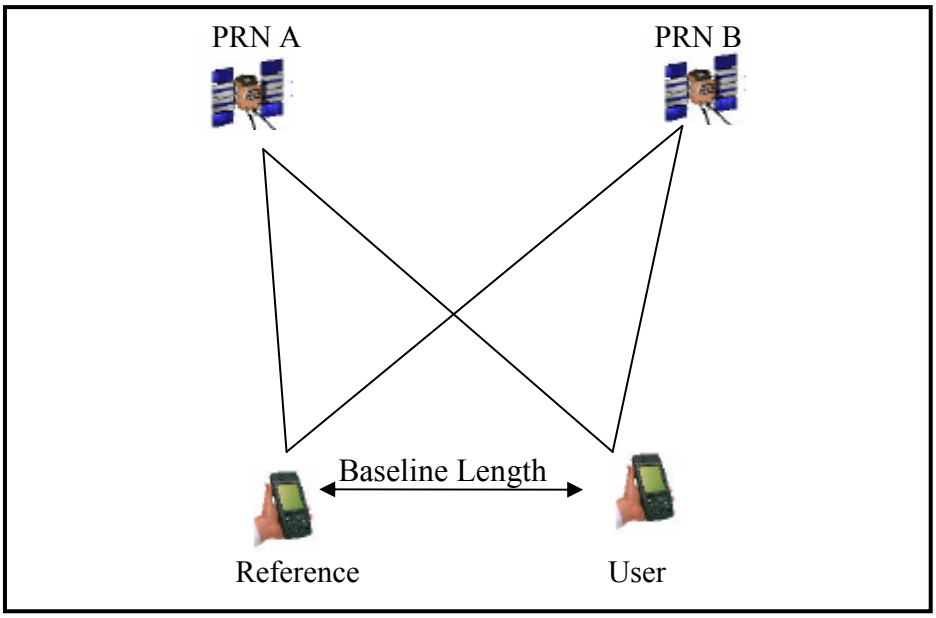

Figure 2.3 Double Differencing

The double difference pseudorange and carrier phase observations can be expressed as: (Lachapelle 2004)

$$\nabla\Delta P = \nabla\Delta\rho + \nabla\Delta d\rho + \nabla\Delta d_{ion} + \nabla\Delta d_{trop} + \nabla\Delta\varepsilon p \tag{2.5}$$

$$\nabla\Delta\Phi = \nabla\Delta\rho + \nabla\Delta d\rho + \nabla\Delta\lambda N - \nabla\Delta d_{ion} + \nabla\Delta d_{trop} + \nabla\Delta\varepsilon\phi \tag{2.6}$$

where $\nabla\Delta$ is the double difference operator.

2.4.2 GNSS Error Sources

After eliminating the satellite and receiver clock errors by DD processing, the remaining five different errors are as mentioned in Equations (2.5) and (2.6). These errors can be classified as spatially correlated or uncorrelated. Spatially correlated errors tend to cancel between a reference receiver and a rover receiver for shorter baselines, but increase in proportion with the baseline length. Errors such as satellite orbital error, tropospheric error and ionospheric error are examples of spatially correlated errors. Spatially un-correlated errors depend upon the user receiver or its environment. These errors do not relate to the baseline length and do not cancel through DD processing. Multipath and measurement noise are the examples of spatially uncorrelated errors. All DD error sources are discussed in detail in the following subsections.

2.4.3 Satellite Orbital Error

The orbital error is due to inaccuracies in the predicted satellite position computed from the broadcast ephemeris. The effect of a satellite position error on a position is the projection of this error onto the line-of-sight of the observation vector (Parkinson 1996). According to IGS (2005), the satellite orbit computed from the broadcast ephemeris has an RMS accuracy of 1.6 m.

A satellite orbital error is spatially correlated and is reduced with DD processing. Wells et al. (1986), state that the relationship between a satellite orbital error and the resulting baseline error after differencing is:

$$\frac{\Delta d}{d} = \frac{\Delta \rho}{\rho} \tag{2.7}$$

where Δd is the total error in length for the baseline d (m), $\Delta \rho$ is the total error in the coordinates of a satellite position (m), and ρ is the mean distance from the receiver stations to the satellite (m). From Equation (2.7), the baseline error due to a 2 m satellite position error will be less than 1 cm for baseline lengths of up to 100 km, for an average satellite receiver distance of 20,200 km. Hence, for most baselines the effect becomes negligible and typically remains below the centimetre level in magnitude (e.g. for a 100 km baseline, a typical differential orbital error would be less than 1 cm).

2.4.4 Tropospheric Error

Satellite signals are refracted by the lower neutral part of the earth's surface extending from zero to 16 km which is known as troposphere, and which is composed of dry gases and water vapour. The troposphere is a non-dispersive medium and therefore the refraction here does not depend on the GNSS signal frequencies (Misra and Enge 2006). The magnitude of the tropospheric error depends on the satellite elevation angle, and it is about 2.5 m in the zenith direction and over 25 m for an elevation of 5 degrees (Misra and Enge 2006). The troposphere error can be compensated using the different models like the Hopfield or Saastamoinen model (Parkinson 1996; Misra and Enge 2006). After applying a model, the differential troposphere error varies typically from 0.2 to 0.4 parts per million (ppm), (Lachapelle 2004).

2.4.5 Ionospheric Error

The ionosphere is the region of ionized gases, which is about 50 to 1000 km above the earth. It is formed by the ionization of the neutral atmosphere by solar Ultra-Violet (UV) radiation and X-ray radiation coming from the corona of the Sun at low and middle altitudes and by energetic particles at high altitude (Skone 1998). The variability of the earth's ionosphere is much larger than that of the troposphere, and it is more difficult to model (Klobuchar 1996). The carrier phase velocity exceeds that of light in a vacuum due to ionosphere significant enough to affect precise positioning. The first-order carrier phase advancement I (in metres) caused by the ionosphere is given as (Misra and Enge 2006):

$$I = \frac{-40.3}{f^2} TEC \tag{2.8}$$

where 40.3 is an empirically derived constant with units of m^3/s^2/electrons, TEC represents the Total Electron Content along the signal path in units of electrons/m^2, and f is the frequency of the carrier phase. The ionospheric error can reach 15 m in the zenith direction and more than 150 m at elevations near the horizon under extreme conditions (Wells et al. 1986). From Equation (2.8) it can be seen that the ionospheric delay is a function of the signal frequency. Thus, a multiple frequency navigation system can use this dispersive property to estimate the ionospheric effect on measurements (Alves 2004).

The magnitude of the ionospheric error varies according to the process of ionization, which depends mainly on the nature of solar activities. It is, therefore, different for day time and night time and from one season to another. Diurnally, the ionospheric error

usually reaches the first peak at 14:00 local time, the second peak at 22:00 local time and drops to the minimum before sunrise (Skone 2003). The ionosphere is the largest error source for differential processing and varies from one parts per million (ppm) of the inter-antenna distance during low ionospheric periods at mid latitudes to greater than 10 ppm at low geomagnetic latitudes during midday (Alves 2004). In GNSS, double differencing the residual error grows with the baseline distance. Various ionospheric estimation techniques are discussed for different GNSS measurement processing algorithms through out this thesis.

2.4.6 Multipath and Noise

Multipath effects occur when reflected satellite signals from surfaces or under the antenna, interfere with the direct satellite signal. It distorts the signal modulation and thus degrades the measurement accuracy (Garin et al. 1996). The level of multipath is a function of the tracking technology, the antenna type, and the antenna environment, namely the distance from the reflecting object and reflectiveness of the environment (Alves 2004). Multipath error is spatially uncorrelated and is highly dependent on the local receiver environment. The code pseudorange multipath can be as long as half of a code chip, which is equivalent to 150 m. The carrier phase multipath is much smaller than that of the pseudorange, with a maximum magnitude of one quarter of a carrier wavelength, i.e. about 5 cm for GPS L1 and 6 cm for L2 (Lachapelle 2004). However, in practical applications, the reflected signal is attenuated to some extent and the typical phase multipath values are generally about 1 cm or less (Lachapelle 2004). To reduce the impact of multipath, careful selection of the antenna site is essential to avoid any

potential reflectors (Liu 2003). The research described herein concentrates on the ionospheric effects since it is generally the dominant source of error for long baselines, so the effects of multipath are not considered herein.

Receiver noise is mainly due to thermal noise and dynamic stress of the receiver (Lachapelle 2004). Noise is the sum of all other un-modeled and second order effects (Alves 2004). It has a very small effect, i.e. about millimetres in magnitude, while using precise carrier phase positioning. Differential processing as mentioned in Equations (2.5) and (2.6) approximately doubles the receiver noise, as compared to single point positioning.

2.5 Phase Combinations

Equation (2.6) represents the DD carrier phase observation in units of metres, after eliminating the receiver and satellite clock offsets in the differencing operation. Presently, GPS dual frequency L1 and L2 observations are normally utilised for precise positioning using carrier phase observations. Under the current Anti-Spoofing (AS) environment, direct matching of the Y-code and reconstruction of L2 carrier phase is not possible by unauthorized users. L2 signal can be reconstructed by either squaring the signal or cross-correlating between dual-band signals. The most effective semi-codeless tracking technique of the L2 carrier phase has at least 14 dB loss in signal to noise ratio with respect to the direct P code correlation (Ashjaee and Lorenz 1993). With the Modernized L2C signal it will provide less noisy measurement due to possibility of direct reconstruction.

The advantage of having two frequencies is that various errors react to the different frequency signals in a different way. For example, the troposphere affects both frequencies to the same degree while the ionosphere affects them differently. These error properties between the various measurements are manipulated using frequency combinations to reduce the overall measurement errors. Frequency combinations are formed by linearly combining measurements from the two frequencies. This approach can be used to improve ambiguity resolution performance by reducing measurement errors in units of cycles, relative to the wavelength of the carrier. Thus, the effect of these errors on ambiguity resolution is reduced (Alves 2004). Various linear phase combinations for dual frequency observations can be formed as (Liu 2003):

$$\nabla\Delta\phi_{i,j} = i\nabla\Delta\phi_1 + j\nabla\Delta\phi_2 \tag{2.9}$$

where i and j are combination coefficients and ϕ_1 and ϕ_2 are the GPS L1 and L2 carrier phase observations (in cycles) respectively. The wavelength $\lambda_{i,j}$ in metres for this phase combination can be written as:

$$\lambda_{i,j} = \left(\frac{i}{\lambda_1} + \frac{j}{\lambda_2} \right)^{-1} \tag{2.10}$$

Also the ambiguity (in cycles) of this combination is given as:

$$\nabla\Delta N_{i,j} = i\nabla\Delta N_1 + j\nabla\Delta N_2 \tag{2.11}$$

where λ_1 and λ_2 are the wavelengths in metres and N_1 and N_2 are the ambiguities in cycles of GPS L1 and L2 carrier phase observations, respectively. In practice, many different carrier phase combinations such as the Narrow-Lane (NL), Wide-Lane (WL)

and Ionosphere-Free (IF) can be formed using dual frequency measurements as explained in Table 2.4 (Liu 2003, Dao 2005). I_1 is the ionospheric error on L1 in units of metres, and σ_1 is the standard deviation of the observation noise on L1 carrier in cycles. Out of these combinations, the Narrow-Lane has a very short wavelength of 10.7 cm and therefore makes the resolution of NL ambiguities difficult. This NL combination is hence not used in practical positioning applications unless very short baselines and quiet atmospheric conditions are involved (Liu 2003).

Table 2.4 Linear Phase Combination Properties (From Liu 2003)

Combinations	i	j	$\lambda_{i,j}$ (cm)	$N_{i,j}$	Ionosphere Error		Noise(1-sigma)	
					M	cycle	m	cycle
L1	1	0	19.03	N_1	I_1	$\frac{I_1}{\lambda_1}$	$19\sigma_1$	σ_1
L2	0	1	24.42	N_2	$\left(\frac{77}{60}\right)^2 I_1$	$\frac{77}{60}\frac{I_1}{\lambda_1}$	$24\sigma_1$	σ_1
WL	1	-1	86.19	$N_1 - N_2$	$-\frac{77}{60} I_1$	$\frac{17}{60}\frac{I_1}{\lambda_1}$	$121\sigma_1$	$1.41\sigma_1$
NL	1	1	10.70	$N_1 + N_2$	$\frac{77}{60} I_1$	$\frac{137}{60}\frac{I_1}{\lambda_1}$	$15\sigma_1$	$1.41\sigma_1$
IF	1	$-\frac{\lambda_1}{\lambda_2}$	48.44	$N_1 - \frac{\lambda_1}{\lambda_2} N_2$	0	0	$60\sigma_1$	$1.26\sigma_1$

Thus, in practice, the applications for GPS carrier phase positioning employs single frequency observations using L1, dual frequency WL and dual frequency IF and dual

frequency observations with stochastic ionosphere modelling and are discussed in the following sections.

2.5.1 Single Frequency

Many users who have access to only single frequency L1 observation use L1 carrier phase and code measurements to estimate the state vector. The L1 DD carrier phase and code observations are expressed as:

$$\nabla\Delta\phi_{L1} = \nabla\Delta\rho + \nabla\Delta N_1\lambda_1 + \nabla\Delta\varepsilon_{\phi_1} \tag{2.12}$$

$$\nabla\Delta P = \nabla\Delta\rho + \nabla\Delta\varepsilon_P \tag{2.13}$$

where $\nabla\Delta\rho$ is the true differential geometric range, $\nabla\Delta N_1$ is the L1 DD ambiguity, and $\nabla\Delta\varepsilon$ is the sum of the residual DD errors: ionospheric residuals, the tropospheric residuals, multipath and noise. The definition of epsilon here is not consistent with equation 2.6. From Table 2.4 it can be seen that the L1 single frequency observation produces the advantages of less ionospheric and noise effects, as compared to L2 observations. The ionospheric error cannot be effectively estimated here or else can be partially modelled using the broadcast ionospheric model or an ionospheric map from an external source. Therefore, single frequency observations do not work effectively for long baseline lengths when the ionospheric error cannot be effectively compensated (Liu 2003).

2.5.2 Dual Frequency WL

The DD Wide-Lane (WL) observations are given by:

$$\nabla\Delta\phi_{WL} = \nabla\Delta\rho + \nabla\Delta N_{WL}\lambda_{WL} + \nabla\Delta\varepsilon_{\phi_{WL}} \tag{2.14}$$

$$\nabla\Delta P = \nabla\Delta\rho + \nabla\Delta\varepsilon_{P} \tag{2.15}$$

where $\nabla\Delta N_{WL}$ is the WL DD ambiguity given by $\nabla\Delta N_1 - \nabla\Delta N_2$, $\nabla\Delta\varepsilon$ is the sum of the residual DD errors: comprised of ionospheric residuals, tropospheric residuals, multipath and noise. The wavelength of the WL phase observation is 86 cm, which is the widest of all linear phase combinations when using dual frequency GPS data. If an ionospheric error is equivalent to one L1 cycle for the L1 observable, then the corresponding error for the WL observable would only be 17/60 of a cycle. Therefore, this linear combination is more resistant to the ionospheric error (in cycles) than L1 and thus, it is more reliable to resolving WL ambiguities under high ionospheric conditions.

However, as seen in Table 2.4, the ionospheric error is effectively amplified when measured in metres, which is $\frac{77}{60}$ times the ionosphere error of L1. In addition, the noise is amplified in the WL combination compared to the single frequency L1 and L2 observables (in metres). Hence, it is common that the position estimate derived using the WL linear combination has a higher position error than the position errors determined with the L1 observable (Liu 2003).

2.5.3 Dual Frequency IF

The Ionosphere Free (IF) combination removes the first order effects of the ionosphere. There are two strategies while dealing with the Ionosphere Free (IF) combination: IF Float and IF Fixed.

2.5.3.1 IF Float:

The IF float observables are given by:

$$\nabla\Delta\phi_{IF} = \nabla\Delta\rho + \nabla\Delta N_{IF}\lambda_{IF} + \nabla\Delta\varepsilon_{\phi_{IF}} \tag{2.16}$$

$$\nabla\Delta P = \nabla\Delta\rho + \nabla\Delta\varepsilon_{P} \tag{2.17}$$

where $\nabla\Delta N_{IF}$ is the IF DD ambiguities given by $\nabla\Delta N_1 - \frac{\lambda_1}{\lambda_2}\nabla\Delta N_2$, $\nabla\Delta\varepsilon$ is the sum of the residual DD errors from the ionosphere, troposphere, multipath and noise. The disadvantage of this linear combination is that the IF ambiguities are no longer integer. Also the IF combination is noisier than L1 and L2 being combination of L1 and L2 (Liu 2003). In many cases, this is compensated by the removal of the first order (over 99%) ionospheric error.

2.5.3.2 IF Fixed

IF fixed is the cascading scheme which first uses the WL combination to fix the WL ambiguities. After fixing the WL ambiguities a modified IF observation given by

$\nabla\Delta\phi_{L1} - \frac{\lambda_1}{\lambda_2}\nabla\Delta\phi_{L1} - \frac{\lambda_1}{\lambda_2}\nabla\Delta N_{WL}$ is formed. By rearranging the terms this newly constructed observable can be expressed as:

$$\nabla\Delta\phi_{L1} - \frac{\lambda_1}{\lambda_2}\nabla\Delta\phi_{L1} - \frac{\lambda_1}{\lambda_2}\nabla\Delta N_{WL} = \frac{\rho}{\lambda_{IF}} + \frac{\lambda_1 - \lambda_2}{\lambda_2}N_1 \qquad (2.18)$$

This equation is utilised to estimate the N_1 ambiguities. The wavelength in this case is $\lambda_{IF}\frac{\lambda_1 - \lambda_2}{\lambda_2}$ (10.7 cm) which is much shorter than the λ_1 (19 cm). The first disadvantage of this combination is that it is three times noisier than L1 (Liu 2003). The second disadvantage of this combination is that the effective wavelength is very small, i.e. only 10.7 cm which means a longer convergence time to resolve the ambiguities (Liu 2003). After these N_1 ambiguities are estimated and resolved as integers, the ionosphere-free fixed (IF Fixed) position estimates can be computed (Liu 2003)

2.5.4 Dual Frequency Stochastic Ionosphere Modelling

Teunissen (1997), Odijk (1999, 2000) and Liu and Lachapelle (2002) discuss three methods for modelling ionosphere biases: the ionosphere float, ionosphere fixed, and ionosphere weighted models. The ionosphere float model estimates the double difference slant ionospheric bias from the code and carrier phase measurements. In this model there is no previous knowledge about the ionosphere or direct ionosphere observations. One problem with the dual frequency ionosphere float model is the instability of stochastic ionosphere modelling during initial convergence of the filter. This is due to the addition of the ionosphere parameters to the ambiguity states that decreases the degrees of freedom of the filter. The ionosphere fixed model does not estimate the ionosphere but

the code and carrier phase observations are reduced with an external ionosphere value. The ionosphere weighted model uses the properties of the L1 code and L1 and L2 carrier phase observations as listed in Table 2.4 to stochastically model and estimate the ionospheric error. The state vector in this case includes the rover's position, velocity, ambiguities and the ionospheric error (Julien 2004). The observation equations used in this strategy are given as:

$$\begin{aligned}
\nabla\Delta\Phi_{L1} &= \nabla\Delta\rho + \nabla\Delta N_1\lambda_1 - \nabla\Delta I_1 + \nabla\Delta\varepsilon_{\phi_1} \\
\nabla\Delta\Phi_{L1} &= \nabla\Delta\rho + \nabla\Delta N_2\lambda_2 - \frac{f_1^2}{f_2^2}\frac{\nabla\Delta I_1}{\lambda_2} + \nabla\Delta\varepsilon_{\phi_2} \\
\nabla\Delta P_{L1} &= \nabla\Delta\rho + \nabla\Delta I_1 + \nabla\Delta\varepsilon_P \\
\nabla\Delta P_{L2} &= \nabla\Delta\rho + \frac{f_1^2}{f_2^2}\nabla\Delta I_1 + \nabla\Delta\varepsilon_P
\end{aligned} \tag{2.19}$$

where $\nabla\Delta\Phi$ is the double difference carrier phase measurement in metres, f is the frequency of the signal, I_1 is the ionosphere delay of the L1 frequency in metres, and ε is the sum of measurement errors to be estimated as residuals. Thus, the ionosphere-weighted model mitigates the problem of instability in the float model due to the addition of the external ionosphere values as observations that increases the redundancy of the system (Liu 2003).

Liu (2003) showed that stochastic ionospheric modelling using the ionosphere weighted model provides the best positioning and ambiguity resolution performance over medium baseline lengths. Also another study performed in Dao (2005) showed that the stochastic modelling of ionospheric error assures a comparable or even better performance, as

compared to an IF combination seen before. Therefore, the weighted ionosphere model is used for stochastic ionosphere modelling in this research.

Chapter 3 Single Reference Station Kinematic Positioning

Stand-alone GPS positioning provides only a few metres of accuracy. In order to achieve a higher accuracy, a DD setup as described in Section 2.4.1 is utilised where a reference station with precisely known coordinates is used to compute rover positions differentially with respect to a reference stations.

Consider the simplified form of the GPS DD carrier phase observable derived from Equation (2.6):

$$\nabla\Delta\Phi = \nabla\Delta\rho + \nabla\Delta N\ \lambda + \nabla\Delta\varepsilon \tag{3.1}$$

In order to solve for the true range and to extract the rover coordinates, the ambiguities need to be resolved first. Successful ambiguity resolution is the key to high precision positioning using the carrier phase observables, and to reach centimetre level accuracy the ambiguities must be resolved correctly (Liu 2003).The following steps need to be performed in order to proceed from a float solution to a precise and accurate fixed solution (Lachapelle 2004):

1. Float filter solution
2. Integer ambiguity resolution and validation
3. Fixed (integer ambiguity) solution

Figure 3.1 shows the flowchart of three step DD GNSS carrier phase observable processing, and the details of this implementation are discussed in the following sections:

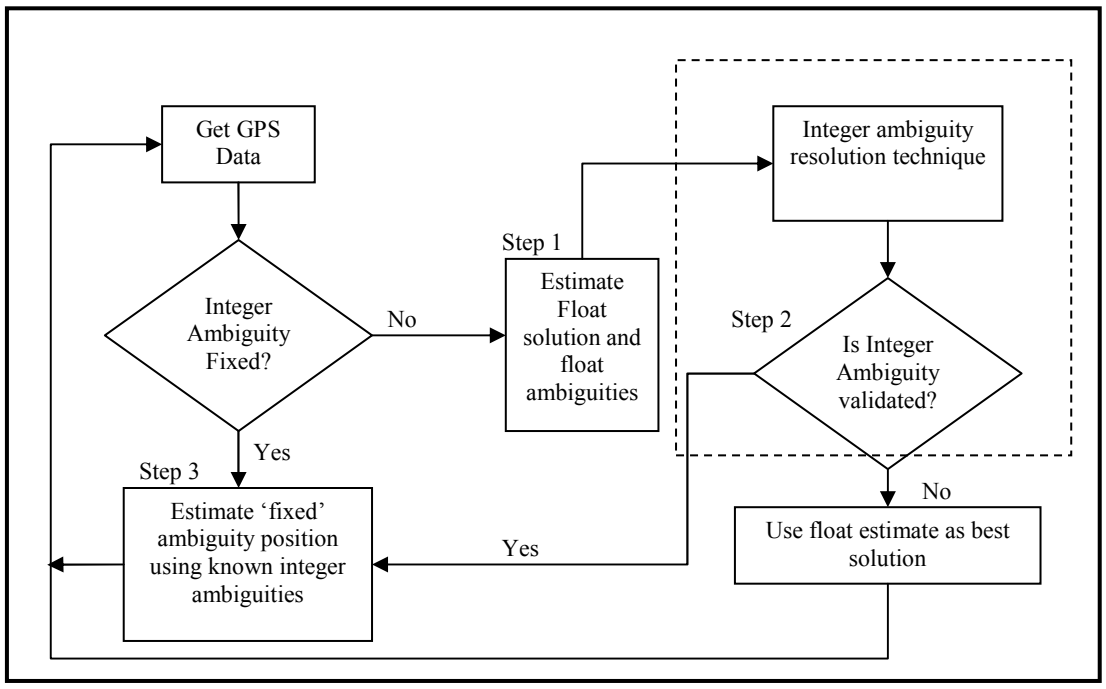

Figure 3.1 DD Carrier Phase Positioning Flowchart (Lachapelle 2004)

3.1 Kalman Filtering

The first float filter step in Figure 3.1 is usually implemented using a Kalman filter as shown in Figure 3.2 below. The Kalman filter is executed in four steps: prediction, computation of the innovation sequence, computation of the Kalman gain, and the update. In Figure 3.2 the x_k is the state vector estimated at epoch k, C_k is the variance-covariance matrix of the state vector x_k at epoch k, z_k is the observation vector at epoch k, ϕ is the transition matrix, Q_k is the system process noise matrix at epoch k, R_k is the variance-covariance matrix of the observation vector z_k, I is an identity matrix, and H is the design matrix which is the matrix computed by taking the derivatives of the observables with respect to the estimated states. The - sign is used with any matrix or

state vector before the *Update* step, while the + sign is used with any matrix or state vector after the *Update* step. More details on Kalman filtering are offered in Brown and Hwang (1992).

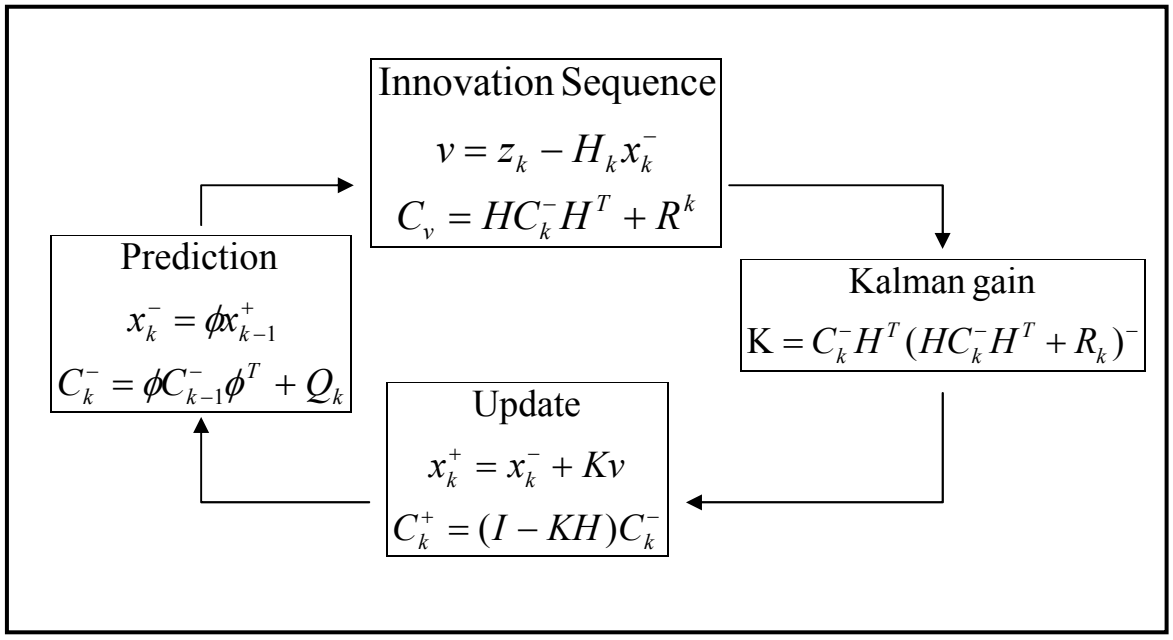

Figure 3.2 Linearized Kalman Filter Loop (Brown and Hwang 1992)

The state vector usually contains the three position states, three velocity states and the DD ambiguity state for each DD observable. Assuming there are 'n' DD's available, the complete state vector is given by:

$$x = \left(\phi, \lambda, h, \dot{\phi}, \dot{\lambda}, \dot{h}, \nabla\Delta N_1, \nabla\Delta N_2, \ldots \nabla\Delta N_n \right) \tag{3.2}$$

where (ϕ, λ, h) represents the rover's latitude and longitude in radians and the rover's height in metres, respectively. $\left(\dot{\phi}, \dot{\lambda}, \dot{h} \right)$ represents the rover's latitude rate in radians per

second, its longitude rate in radians per second and the rover's rate of change in height in metres per seconds. The term $\nabla\Delta N_i$ stands for the double-difference ambiguities for satellite-receiver pair *i*. The Kalman filter uses two sets of models: the dynamic and the measurement models to estimate the state vector. The dynamic model is based on knowledge of the system dynamics. It describes how the state vector evolves from the current epoch to the next via a transition matrix and how the covariance of the state vector is used in this transition (Liu 2002). In most of the navigation solutions, the random walk or Gauss-Markov model is used to model the dynamics of the system (Brown and Hwang 1992). Assuming a random walk model for the velocity state $\left(\dot{\phi},\dot{\lambda},\dot{h}\right)$ with corresponding driving noise vector $\left(w_\phi, w_\lambda, w_h\right)$ the transition matrix for the position and velocity state vector is derived as:

$$\phi_1 = \begin{bmatrix} 1 & 0 & 0 & \delta t & 0 & 0 \\ 0 & 1 & 0 & 0 & \delta t & 0 \\ 0 & 0 & 1 & 0 & 0 & \delta t \\ 0 & 0 & 0 & 1 & 0 & 0 \\ 0 & 0 & 0 & 0 & 1 & 0 \\ 0 & 0 & 0 & 0 & 0 & 1 \end{bmatrix} \tag{3.3}$$

If a spectral density for the driving noise vector is $\left(sp_\phi, sp_\lambda, sp_h\right)$ in units of m^2/s^3, the subsystem noise matrix for the position and velocity state vector is derived as (Liu 2002):

$$Q_1 = \begin{bmatrix} \frac{sp_\phi}{3}\delta t^3 & 0 & 0 & \frac{sp_\phi}{2}\delta t^2 & 0 & 0 \\ 0 & \frac{sp_\lambda}{3}\delta t^3 & 0 & 0 & \frac{sp_\lambda}{2}\delta t^2 & 0 \\ 0 & 0 & \frac{sp_h}{3}\delta t^3 & 0 & 0 & \frac{sp_h}{2}\delta t^2 \\ \frac{sp_\phi}{2}\delta t^2 & 0 & 0 & sp_\phi \delta t & 0 & 0 \\ 0 & \frac{sp_\lambda}{2}\delta t^2 & 0 & 0 & sp_\lambda \delta t & 0 \\ 0 & 0 & \frac{sp_h}{2}\delta t^2 & 0 & 0 & sp_h \delta t \end{bmatrix} \tag{3.4}$$

The ambiguity states do not change unless there is a loss of phase lock; hence, these are modelled as random constants. The transition matrix for the ambiguity state vector is an identity matrix given by:

$$\phi_2 = \begin{bmatrix} 1 & 0 & 0 & 0 & 0 & 0 \\ 0 & 1 & 0 & 0 & 0 & 0 \\ 0 & 0 & 1 & 0 & 0 & 0 \\ 0 & 0 & 0 & 1 & 0 & 0 \\ \vdots & \vdots & \vdots & \vdots & \ddots & \vdots \\ 0 & 0 & 0 & 0 & 0 & 1 \end{bmatrix} \tag{3.5}$$

Hence the complete state transition matrix is given by:

$$\phi = \begin{bmatrix} \phi_1 & 0 \\ 0 & \phi_2 \end{bmatrix} \tag{3.6}$$

and the complete system noise matrix is given by:

$$Q = \begin{bmatrix} Q_1 & 0 \\ 0 & Q_2 \end{bmatrix} \tag{3.7}$$

where Q_2 is the zero matrix. The measurement model relates the state vector to the GPS observations through the design matrix *H*. This design matrix is derived by taking the derivatives of the measurements with respect to the state vector (Cannon 1991).

3.2 Ambiguity Resolution

The ambiguities coming from the float filter need to be resolved to their correct integer values in order to achieve the desired high accuracy. Least-squares ambiguity decorrelation adjustment method (LAMBDA) by Teunissen (1993) is chosen for ambiguity resolution in Step 2 of the Kalman filtering approach described in Figure 3.1. This technique resolves ambiguities so that the following error function *e* is minimized (Teunissen 1993).

$$e = (\hat{N} - N) C_N^{-1} (\hat{N} - N)^T \tag{3.8}$$

where N stands for fixed integer ambiguities, $\hat{N}$ represents the estimated DD float ambiguities, and C_N^{-1} is the covariance matrix of the float ambiguities. The ratio test described in Han and Rizos (1996) is used to validate the best-estimated ambiguities using Equation (3.8) above.

$$ratio = \frac{(\hat{N} - N_1) C_N^{-1} (\hat{N} - N_1)^T}{(\hat{N} - N_2) C_N^{-1} (\hat{N} - N_2)^T} >= \delta \tag{3.9}$$

where N_2 is the ambiguity set that has the smallest sum of squared ambiguity residuals, and N_1 is the second-best ambiguity set by virtue of having the second smallest sum of squared ambiguity residuals.

3.3 Benefits of GPS Modernization and Galileo in Ambiguity Resolution

Dual frequency techniques applied to the stand-alone GPS case have been discussed so far. This section presents improved estimation techniques when applied to modernized GPS and Galileo. In Chapter 2, various phase linear combinations and ionospheric modelling methods were discussed for carrier phase positioning using dual frequency observations. These various approaches can reduce the effect of the ionospheric error and help to resolve the integer ambiguities and hence are very important in the field of ambiguity resolution. Both Galileo and modernized GPS will provide three frequencies to civil users in future and more linear combinations are possible using these triple frequencies.

3.3.1 Triple Frequency Cascading Ambiguity Resolution

Similar to Equation (2.9), the following equation provides a general form for the triple frequency Linear Combination (LC):

$$\nabla\Delta\phi_{i,j,k} = i\nabla\Delta\phi_1 + j\nabla\Delta\phi_2 + k\nabla\Delta\phi_3 \tag{3.10}$$

where ϕ_1, ϕ_2, and ϕ_3 represent the phase observations on L1, L2 and L5 for the stand-alone GPS or on E1, E5b and E5a for stand-alone Galileo in cycles. Integers *i, j* and *k* are the coefficients and $\phi_{i,j,k}$ is the linearly combined phase. The wavelength $\lambda_{i,j,k}$ of this linearly combined phase $\phi_{i,j,k}$ is given by:

$$\lambda_{i,j,k} = \left(\frac{i}{\lambda_1} + \frac{j}{\lambda_2} + \frac{k}{\lambda_3} \right)^{-1} \tag{3.11}$$

Also the ambiguity of this three frequency combination in cycles is given as:

$$\nabla\Delta N_{i,j,k} = i\nabla\Delta N_1 + j\nabla\Delta N_2 + k\nabla\Delta N_3 \tag{3.12}$$

where λ_1, λ_2 and λ_3 are the wavelengths in metres and N_1, N_2 and N_3 are the ambiguities in cycles of the phase observations on L1, L2 and L5 for the GPS, or on E1, E5b and E5a for Galileo. Zhang (2005) discusses these triple frequency combinations in detail.

For GPS and Galileo, a common characteristic exists between the two systems' signal frequencies: two of the frequencies are very close to each other while the third is much further away (Zhang et al. 2003). This characteristic allows for different linear frequency combinations such as the Extra-Wide-Lane (EWL), Wide-Lane (WL) and Medium-Lane (ML) as described in (Zhang 2005).

The longer the wavelength, the easier it is to fix the ambiguities, hence WL ambiguities are easier to resolve compared to each single frequency. The Cascading Ambiguity Resolution (CAR) method uses WL phase linear combinations with cascading wavelengths to fix the ambiguities in several steps in order of the length of the lanes from the longest to the shortest, so that all the ambiguities are fixed (Zhang 2005). As described in Table 3.1, the available frequency combinations, EWL, WL, ML, have stepwise decreasing wavelengths for both GPS and Galileo.

Table 3.1 Practical Triple-frequency Integer Linear Combinations (Zhang 2005)

System	LC	Coefficients			$\lambda_{i,j,k}$	Noise (1- sigma)		Ionosphere Error	
		i	j	k	(m)	(m)	(cycles)	(m)	(cycles)
GPS	EWL	0	1	-1	5.861	$0.464\,\sigma_1$	$0.079\,\sigma_1$	$-1.719\,I_1$	$0.056\,\frac{I_1}{\lambda_1}$
	WL	1	-1	0	0.862	$0.079\,\sigma_1$	$0.079\,\sigma_1$	$-1.283\,I_1$	$-0.283\,\frac{I_1}{\lambda_1}$
	ML	1	0	-1	0.751	$0.059\,\sigma_1$	$0.079\,\sigma_1$	$-1.339\,I_1$	$-0.339\,\frac{I_1}{\lambda_1}$
	L1	1	0	0	0.190	$0.010\,\sigma_1$	$0.056\,\sigma_1$	I_1	$\frac{I_1}{\lambda_1}$
Galileo	EWL	0	1	-1	9.768	$0.773\,\sigma_1$	$0.079\,\sigma_1$	$-1.748\,I_1$	$-0.034\,\frac{I_1}{\lambda_1}$
	WL	1	-1	0	0.814	$0.064\,\sigma_1$	$0.079\,\sigma_1$	$-1.305\,I_1$	$-0.305\,\frac{I_1}{\lambda_1}$
	ML	1	0	-1	0.751	$0.059\,\sigma_1$	$0.079\,\sigma_1$	$-1.339\,I_1$	$-0.339\,\frac{I_1}{\lambda_1}$
	E1	1	0	0	0.190	$0.010\,\sigma_1$	$0.056\,\sigma_1$	I_1	$\frac{I_1}{\lambda_1}$

This stepwise decrease in wavelengths implies the use of CAR to increase the ambiguity resolution performance. CAR, introduced by Zhang et al. (2003), is performed in three steps for this three-frequency system:

1. Resolve the ambiguities with the longest wavelength i.e.: EWL
2. Use the fixed ambiguities to resolve the ambiguities with the WL frequency
3. Use the WL fixed ambiguities to resolve the ambiguities on E1 or L1.

It was shown using the CAR method that the percentage of correctly fixed ambiguities of combined GPS/Galileo remains over 90% even on a 70 km baseline at the 6 ppm ionospheric level (Zhang 2005).

3.3.2 Triple Frequency Ambiguity Resolution using Stochastic Ionospheric Modelling

To improve the positioning performance using triple frequency techniques, Julien et al. (2004) suggested using the triple frequency ambiguity resolution technique employing the weighted ionosphere model. In case of long baselines, the spatially correlated errors, especially ionospheric biases, restrain any attempt of resolving the carrier phase ambiguities. Similar to the weighted ionospheric model for dual frequency systems described in Section 2.5.4, this technique models the ionosphere bias as:

$$
\begin{aligned}
\nabla\Delta\phi_1 &= \nabla\Delta\rho + \nabla\Delta N_1\lambda_1 - \nabla\Delta I_1 + \nabla\Delta\varepsilon_{\phi_1} \\
\nabla\Delta\phi_2 &= \nabla\Delta\rho + \nabla\Delta N_2\lambda_2 - \frac{f_1^2}{f_2^2}\frac{\nabla\Delta I_1}{\lambda_2} + \nabla\Delta\varepsilon_{\phi_2} \\
\nabla\Delta\phi_3 &= \nabla\Delta\rho + \nabla\Delta N_3\lambda_3 - \frac{f_1^2}{f_3^2}\frac{\nabla\Delta I_1}{\lambda_3} + \nabla\Delta\varepsilon_{\phi_3} \\
\nabla\Delta P_1 &= \nabla\Delta\rho + \nabla\Delta I_1 + \nabla\Delta\varepsilon_P \\
\nabla\Delta P_2 &= \nabla\Delta\rho + \frac{f_1^2}{f_2^2}\nabla\Delta I_1 + \nabla\Delta\varepsilon_P
\end{aligned}
\qquad (3.13)
$$

Simulation tests performed in this study show that the ionosphere-weighted model with integrated triple frequency GPS and Galileo performs well in terms of ambiguity resolution performance and positioning accuracy for long baseline lengths up to 70 km.

The float 3D position improves by 5, 7.5 and 10 cm on average for the 30, 50 and 70 km baselines, respectively (Julien et al. 2004). High levels of improvement in the float ambiguity domain were reflected by good ambiguity resolution performance.

3.3.3 Tightly coupled Combination

This approach leverages the existence of common frequencies between GPS and Galileo to couple the two systems tightly using the hybrid measurements. As discussed in Chapter 2, E1 and L1, as well as E5a and L5 will have common carrier frequencies. Therefore, it will be possible to difference GPS and Galileo carrier-phase measurements without affecting the integer property of the ambiguities (Julien et al. 2003). This leads to hybrid measurements called Extra Measurements (EM) that complement a classical coupling of the GPS and Galileo measurements. This gain in information provided by these hybrid EMs link the two constellations tightly and translates into an improvement in carrier-phase ambiguity resolution. Julien et al. (2003) simulated baselines from one to 20 km and evaluated this tightly coupled approach for a triple frequency GPS/Galileo system. His study showed that the tightly coupled combination demonstrated a 10% improvement over the classical combination of GPS and Galileo in terms of mean time to correctly fix ambiguities and percentage of correctly fixed ambiguities for a 20 km baseline and an ionospheric error level of 6 ppm (90% of the time) using three frequencies. Julien et al. (2004) extended this tightly coupled approach along with stochastic ionosphere modelling as described earlier and showed that ionosphere modelling with and without tight coupling, produced comparable results in the float

ambiguity domain. However, with the tight coupling approach, it decreases the mean time to fix by nearly half while maintaining a high level of reliability.

3.4 FLYKIN+^{TM} for Galileo

FLYKIN+^{TM} is a powerful DGPS processing software package developed by the PLAN Group of the University of Calgary. It implements Kalman filtering and the LAMBDA method as explained earlier (Liu 2003). It can implement the phase linear combinations and stochastic ionosphere modelling for GPS observations as explained in Section 2.5. In order to process the Galileo observations in differential mode, this software has been modified for this research and a version FLYKIN+^{TM} for stand-alone Galileo was developed. Similar to stand-alone GPS FLYKIN+^{TM}, this software implements the dual frequency linear phase combinations excluding the ML and EWL combinations for Galileo as described in Table 3.1. Galileo FLYKIN+^{TM} software also implements the stochastic ionosphere modelling using the E1 and E5b Galileo frequencies. This newly implemented Galileo FLYKIN+^{TM} software has been utilised to evaluate the SRS stand-alone Galileo cases in the subsequent chapters.

Chapter 4 Multiple Reference Station Algorithm

4.1 Introduction to Multiple Reference Station Algorithm

Single reference station (SRS) differential GPS performs well under normal atmospheric conditions when the inter-antenna distances are less than 30 km and provides centimetre level accuracy under normal conditions. To overcome the limitation of the SRS approach when using longer baselines, network-based real-time positioning methods were developed which use a network of reference stations to measure the correlated GPS errors (e.g. ionosphere) over a region and to predict their effects spatially and temporally within the network.

4.2 Multiple Reference Station Algorithms for GPS RTK

The MRS approach for carrier phase-based DGPS offers several advantages over the traditional SRS approach. The MRS approach generates the corrections based on the observations from the network of reference stations with known precise coordinates placed around the rover. This yields a larger reduction in the spatially correlated differential errors compared to the equivalent SRS case (Dao 2005). As a result, the overall position solution accuracy is improved. Another important advantage of MRS is the increase in reliability and availability of the service (Fotopoulos 2000). For example, if one or two reference stations fail in the network, the remaining stations with MRS may yet provide a better solution than SRS where the failure of the reference station results in single point accuracy. The use of a network approach also allows for the quality control

of corrections generated from each reference station by checking it with the remaining corrections. Thus, if a particular station is generating erroneous corrections the network allows for the possible detection and elimination of this blunder from the final solution (Fotopoulos 2000). Under quiet and normal atmospheric conditions, the MRS approach allows a differential GPS RTK service with a specific number of reference stations to cover a relatively large geographical region compared to the standard SRS approach while maintaining standard accuracy requirements. Hence, a lower number of reference stations are required to provide a differential GPS service for a particular region when compared to the number of reference stations required while using the SRS approach. For instance, as shown in Figure 4.1, in order to cover an area of 200 km x 200 km, twenty-five reference stations are typically required while using the SRS approach, assuming the maximum inter-antenna distance necessary to maintain the service accuracy is 20 km. In contrast, while using the MRS approach, only five reference stations may be needed in an optimistic scheme, as shown in Figure 4.2.

The traditional correction-based MRS approach is mainly divided into four main steps (Odijk 2002):

1. Estimation and resolution of the network ambiguities
2. Determination of errors between network baselines
3. Interpolation of the network errors to the location of the rover
4. Transmission and application of the corrections by the rover

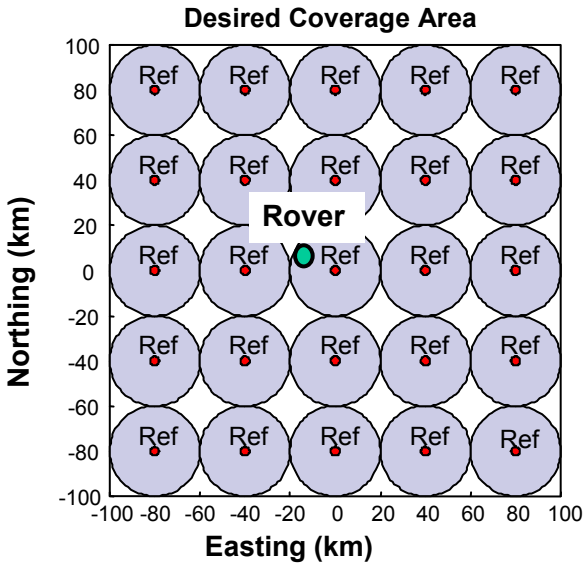

Figure 4.1 Number Of Reference Stations Required using SRS Concept (From Raquet 1998)

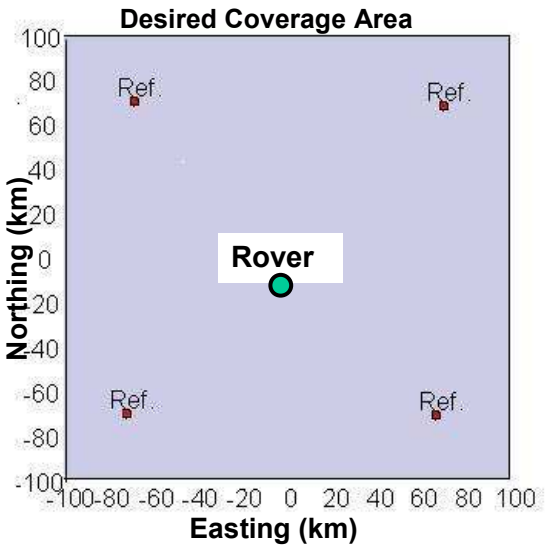

Figure 4.2 Number Of Reference Stations Required using MRS Concept (From Raquet 1998)

Various correction-based algorithms such as the linear combination algorithm (Han and Rizos 1996), the linear interpolation algorithm (Gao et al. 1997; Wanninger 1995), the partial derivative algorithm (Wübbena 1996) and the Least-Squares Collocation (LSQC) algorithm (Raquet 1998) have been developed using different approaches to interpolate the network errors to the rover. Dai et al. (2004) compared these correction based algorithms and demonstrated that their performances are almost equal.

The following practical issues need to be considered while using the MRS approaches especially for RTK applications (Dao 2005):

- Cost: A network of GPS reference stations is very expensive to establish and maintain.
- Geometry: Having an appropriate geometrical distribution of the reference stations is essential to attaining the highest efficiency of the MRS approach (Alves et al.2003).
- Minimal Multipath: The antennas must be positioned under open-sky tracking conditions, and in low multipath surroundings.
- Good Quality Receivers and Antennas: Receivers with narrow correlators and high quality antennas should be used to obtain high quality data.
- Accurate Coordinates: The accuracy of the network coordinates is an important consideration because it directly affects the network correction quality and, therefore, the performance of MRS approaches.
- Data Storage: Collection and storage of network data is very costly due to the requirement of a large hard drive capacity and needs good data management.
- Data Transmission: For real-time applications, a significant amount of data transmission from all reference stations to the network-processing centre where the corrections are generated and then transmission of these corrections to the rover is required. It is critical to have an effective communication link to address the issue of time latency (Alves et al.2003).

4.2.1 Tightly Coupled Approach

Until now, all the network RTK applications use a one-way communication model, i.e. from the reference stations to the rover or the network-processing centre. If a two-way communications model between a rover and the reference stations is used with the idea that a static or kinematic rover can also be treated as a reference station, the MRS algorithm can provide a better indication of the local environmental error conditions (Alves 2004). The rover can thus assist in the baseline configurations for the network. Since the rovers move in between two or more reference stations within the network, connecting baselines to the rovers as well as the reference stations will shorten the overall network inter-receiver separations within the network (Alves 2004). The ambiguity resolution performance is a function of the inter-receiver distance separation as the correlated errors increase in magnitude as the separation increases. Therefore the shorter baselines formed with the rover provides a higher likelihood of resolving the carrier phase ambiguities (Alves 2004).

In the traditional correction-based MRS approaches known as loosely coupled approaches, network ambiguities and the ionosphere are estimated using Bayes filtering. The estimated ambiguities are then searched, validated, and resolved. The resulting resolved ambiguities are then used to predict the errors to the locations of the rovers (Fortes 2002). The MRS Tightly Coupled (MRS-TC) approach is a recently developed MRS algorithm, which combines observations from all the reference stations and the rover into a one unique filter to estimate the rover positions (Alves 2004). The addition of the rover's information into the network filter maintains all the information used in the

least-squares collocation approach and adds the rover information. The covariance function determines the level of correlation between measurements. If the rover is involved in every baseline in the network, the reference station observations that are highly correlated with the rover are assigned a low variance and as a result, will be given more weight in the adjustment than an observation whose errors are different from those of the rover. Thus, all the four stages of a typical correction-based MRS approach, i.e. estimation and resolution of the network ambiguities, determination of errors, interpolation of the network errors, and application of the corrections by the rover are carried out in a single step using one network filter.

4.2.1.1 Implementation of MRS-TC

The state vector for this MRS-TC approach consists of the rover's position, ambiguities and ionospheric parameters, as well as the network's ambiguities and ionosphere parameters. The design matrix is give by Equation (4.1) below. The first 'n' rows of this matrix represent the double difference observations between the rover and one of the reference stations. The next 'm' rows correspond to double difference observations between the fixed reference stations with known coordinates. 'n' is the number of double difference observations between the rover and the reference station(s) and 'm' is the number of double difference observations between reference stations.

$$A = \begin{bmatrix} \frac{\partial \Delta\nabla\phi_1}{\partial x} & \frac{\partial \Delta\nabla\phi_1}{\partial y} & \frac{\partial \Delta\nabla\phi_1}{\partial z} & \lambda & 0 & & 0 & 0 & \\ \frac{\partial \Delta\nabla\phi_2}{\partial x} & \frac{\partial \Delta\nabla\phi_2}{\partial y} & \frac{\partial \Delta\nabla\phi_2}{\partial z} & 0 & \lambda & & 0 & 0 & \\ & & & & & \ddots & & & \\ 0 & 0 & 0 & 0 & 0 & & \lambda & 0 & \\ 0 & 0 & 0 & 0 & 0 & & 0 & \lambda & \\ & & & & & & & & \ddots \end{bmatrix} \quad (4.1)$$

The first three columns represent the rover's position estimates and the following 'n+m' columns correspond to the ambiguities of all of the double difference observations. For the last 'm' rows, no partial derivatives with respect to the coordinates exist between reference stations because their accurate fixed coordinates are known. This design matrix can be extended to accept any number of reference stations and rovers (Alves 2004). The selection of the double difference observables is based on the shortest inter-receiver separations, with the conditions of linear independence and connectivity being preserved (Alves 2004). Thus, a rover may be connected to one or several reference stations, depending on the reference station and rover receiver configuration.

4.2.1.2 Ionospheric Modelling

The MRS-TC model was extended by Alves (2004) to estimate the dual frequency slant ionosphere delay using the ionosphere free model as given in Odijk (1999). An

ionospheric parameter for each dual frequency satellite pair is estimated along with the rover's position, velocity and ambiguity states, and the network ambiguity states. The design matrix from Equation (4.1) can be written as:

$$A = \begin{bmatrix} A_{(1,1)} & A_{(1,2)} \\ A_{(2,1)} & A_{(2,2)} \end{bmatrix} \tag{4.2}$$

where the first row represents the set of measurements of the baselines including the rover as one of the stations, and the second row represents the set of measurements of baselines for only the network stations. Since there are no common parameters to be estimated between the network baselines and the rover to network baselines,

$$A_{(1,2)} = A_{(2,1)} = 0 \tag{4.3}$$

The sub-matrix $A_{(1,1)}$, representing the rover measurements is given by,

$$A_{(1,1)} = \begin{bmatrix} A_{pos} & \lambda_{L1} I & 0 & I \\ A_{pos} & 0 & \lambda_{L2} I & \frac{f_{L1}^2}{f_{L2}^2} I \\ A_{pos} & 0 & 0 & -I \\ A_{pos} & 0 & 0 & -\frac{f_{L1}^2}{f_{L2}^2} I \end{bmatrix} \tag{4.4}$$

This matrix represents the 'n' double difference observations between rover and one of the reference stations, where each row of the matrix correspond to different measurement types: L1 phase, L2 phase, L1 code and L2 code respectively. A_{pos} is a column sub-matrix which includes the partial derivatives of the double difference measurements with respect to the three position components of the rover as explained in Equation (4.1). λ is the measurement wavelength in metres, I is the identity matrix and f is the measurement frequency in Hertz. Since there are no position states for the network observations, the

sub-matrix $A_{(2,2)}$ representing 'm' double difference observations between the network stations is given by:

$$A_{(2,2)} = \begin{bmatrix} \lambda_{L1} I & 0 & I \\ 0 & \lambda_{L2} I & \frac{f_{L1}^2}{f_{L2}^2} I \\ 0 & 0 & -I \\ 0 & 0 & -\frac{f_{L1}^2}{f_{L2}^2} I \end{bmatrix} \tag{4.5}$$

Note that the L1 and L2 observations are used independently here without employing any frequency combination (Alves, 2004).

4.2.2 Other Approaches

Before the introduction of the tightly coupled approach, many correction-based approaches have been developed and evaluated for the MRS technique over the past few years and they can be categorised as:

1. Partial Derivative Algorithm (Wübbena et al. 1996; Varner et al. 1997)
2. Linear Interpolation Algorithm (Wanninger 1995; Gao et al. 1997; Han and Rizos 1996; Odijk et al. 2000)
3. Least Squares Collocation (Raquet 1998)

The Partial Derivative Algorithm (PDA) models the spatially correlated errors based on a first order partial derivative function, which can be interpolated to obtain the corresponding corrections for any user receiver within the network coverage area (Wübbena et al. 1996). The partial derivative algorithm essentially estimates network

field parameters for each satellite pair at a one controlling station known as master station, which are then transmitted to the rover receiver (Dao 2005). The choice of the appropriate PDA algorithm based on the spatial extent, the geometry of the network, and the number of reference stations, which define the level of complexity and accuracy of the PDA are discussed in Varner (2000) in detail.

In the case of the Linear Interpolation Algorithm (LIA), which is similar to the PDA, data is collected from all of the network reference stations and relayed to the master station, where ionospheric delay parameters are computed and broadcast to the rover for interpolation (Fotopoulos 2000). A distance-based LIA is used for modelling the ionospheric delays at a rover based on a network of reference stations, has been proposed by Gao et al. (1997). Han and Rizos (1996) came up with a similar LIA for modelling the spatially correlated errors and mitigating errors like multipath.

The Least Squares Collocation (LSQC) approach developed by Raquet (1998) computes corrections to the carrier phase measurements based on the estimated behaviour of the distance-dependent errors. This method uses the state vector and variance-covariance matrix from the ambiguity estimation and resolution stage to predict the errors of the reference stations to the measurements of a rover receiver within or around the network. The estimated corrections are effective in reducing the measurement errors at the rover and improving position accuracy (Alves 2004). These estimated corrections are applied to the raw measurements from the reference and rover receivers and then the double difference measurements are computed.

4.3 Current MRS RTK Performance Results with GPS

Various past studies have evaluated the effectiveness of MRS approaches compared to the traditional SRS approach. The following section presents an overview of these past studies carried out using single and dual frequency measurements.

The first study was carried by Raquet (1998) who introduced the LSQC approach. This approach was also evaluated in this study using a network of eleven GPS reference stations located in Norway. This network covered an area of 400 km x 600 km with inter-reference-station baseline lengths ranging from 100 to 300 km. Different network configurations were tested and compared to the equivalent SRS cases. The results showed a significant improvement produced by the MRS approach in observation, position and ambiguity resolution domains using L1 and WL observables under a very low (1-2 ppm) ionosphere level.

- For baselines less than 100 km, the MRS offered an improvement of 17% for the L1 position solution and of 11% for the WL position solution, compared to SRS case.
- For baselines beyond 100 km, the MRS approach offered an improvement of 44% for the L1 position solution and of 43% for the WL position solution, compared to SRS case.

Fortes (2002) improved the LSQC through refinement of the covariance functions, and separate modelling of the correlated errors. This modified MRS approach was tested for the St. Lawrence network with baselines ranging from 30 to 46 km and a Brazilian

network with baselines from 100 to 1000 km. When the ionosphere was active with intensity between 4 and 6 ppm because of the solar eclipse, a 50% to 60% improvement was observed using the MRS approach in L1 and WL modes. A very minor improvement of a few millimetres was observed when using the IF mode. However, it showed that the performance of MRS approaches is not very sensitive to the covariance function.

Pugliano (2002) evaluated the MRS LSQC approach using a reference station network in Campania, Italy with the baselines ranging from 50 to 100 km with an ionospheric level of 4 ppm, and compared it with the equivalent SRS baseline lengths ranging from 30 to 40 km. The analysis in the measurement, position and ambiguity resolution domains showed a significant improvement of 30% to 60% using the MRS approach over SRS for the L1 and WL modes.

Studies by Pany et al.(2001), Tsujii et al.(2001), Behrend et al.(2001), Jensen (2002), and Alves et al. (2004), introduced a Numerical Weather Prediction (NWP) model such as the NOAA real-time tropospheric correction model by the National Oceanic and Atmospheric Administration (NOAA). Alves et al. (2004) evaluated the effectiveness of the multiple reference station approach, for users of the United States Coast Guard (USCG) network, in relation to the single baseline RTK performance. Along with the network approach, i.e. using Multiple Reference Stations (MRS), real-time zenith tropospheric corrections supplied by the NOAA were utilised in this research. It was shown that these corrections assist with reducing the level of un-modeled, baseline length dependent errors, ultimately improving network and rover performance. Ahn (2005)

evaluated the network approach, MultiRef™, developed by the University of Calgary, together with NOAA-derived and independently modeled tropospheric corrections, as applied to three geographic regions: Florida, North Carolina, and the North Eastern regions, within the National Geodetic Survey (NGS) Continuous Reference Stations (CORS) network in the USA. It was concluded that the overall level of performance for the three chosen geographical regions demonstrated that the network approach succeeded in making consistent improvements in reducing the effect of measurement errors on all observables, for both the Modified Hopfield and NOAA tropospheric delay models. The mean value of the level of improvement was consistently in the range of 9% to 22%.

Alves (2004) first introduced the MRS-TC algorithm. It also evaluated and compared the MRS-TC method to the LSQC algorithm using two GPS networks located in Turkey with baselines of 25 to 74 km and in Southern Alberta with baselines of 30 to 60 km for normal atmospheric conditions (Alves 2004; Alves and Lachapelle 2004). It was found that the MRS-TC coupled approach performs quite similarly in some cases (Alves and Lachapelle 2004) and offered an improvement of 10% to 20% in other cases (Alves 2004).

Dao (2005) evaluated both the LSQC and TC MRS approaches for the Southern Alberta Network (SAN) with inter-station distances of 30 to 70 km and confirmed that the MRS approaches offer an improvement relative to the SRS approach. The degree of efficiency of the MRS LSQC approach depends mainly on the ability to estimate the ionospheric error and to resolve the ambiguities. The largest improvement of 70% was obtained under

medium ionospheric conditions with the use of L1 observations. Under high ionosphere conditions, the MRS LSQC approach yields improvements between 0% and 20% using L1 observations. The evaluation of the MRS-TC approach established that it offers the most accurate position solutions under either quiet or active ionospheric conditions compared to SRS and MRS LSQC approaches. Therefore, the MRS-TC approach was chosen for this simulation-based research to evaluate the MRS stand-alone Galileo compared to SRS and stand-alone GPS.

4.4 MRS-TC™ for Galileo

The MRS-TC™ is the GPS MRS processing software developed by University of Calgary that implements the Tightly Coupled (TC) approach. As explained in Section 4.2.1, it employs the TC approach with ionosphere modelling. In order to evaluate the MRS-TC approach for Galileo, the new MRS-TC™ Galileo software was developed which can process the simulated Galileo MRS Data. The MRS-TC™ Galileo evolves from the MRS-TC™ GPS processing software to process and handle Galileo E1-E5b dual frequency data. Similar to design matrix given by Equation (4.1), this Galileo processing software implements the ionosphere modelling as:

$$A_{(1,1)} = \begin{bmatrix} A_{pos} & \lambda_{E1} I & 0 & I \\ A_{pos} & 0 & \lambda_{E5_b} I & \frac{f_{E1}^2}{f_{E5_b}^2} I \\ A_{pos} & 0 & 0 & -I \\ A_{pos} & 0 & 0 & -\frac{f_{E1}^2}{f_{E5_b}^2} I \end{bmatrix} \tag{4.6}$$

$$A_{(2,2)} = \begin{bmatrix} \lambda_{E1} I & 0 & I \\ 0 & \lambda_{E5_b} I & \frac{f_{E1}^2}{f_{E5_b}^2} I \\ 0 & 0 & -I \\ 0 & 0 & -\frac{f_{E1}^2}{f_{E5_b}^2} I \end{bmatrix} \tag{4.7}$$

where λ_{E1} and λ_{E5_b} are E1 and E5b wavelengths and f_{E1} and f_{E5_b} are E1 and E5b frequencies respectively. This newly implemented MRS-TC™ Galileo software is thus utilised to evaluate MRS-TC approach for all stand-alone Galileo cases throughout the thesis.

Chapter 5 Simulation Design

5.1 GPS/Galileo Simulator

A software-based GPS/Galileo simulator, namely SimGNSSII™, developed at the University of Calgary (Luo 2001) was used for this research. This software simulates GPS and Galileo constellations and GNSS error sources, as well as the trajectory and dynamics of a rover platform. SimGNSSII™ takes the designed constellations of GPS or Galileo as an input to generate true geometric ranges. Pseudorange, carrier phase and Doppler observations are generated for all considered frequencies and all visible satellites at any specified location. All errors inherent to double difference observations: ionospheric and tropospheric delays, multipath-induced error, tracking noise and orbital error, are generated using complex models and are then added to these true ranges to produce the simulated observations. The following sections overview the different models used to simulate the ionospheric, tropospheric, orbital and multipath errors.

5.1.1 Ionospheric Error Simulation Model

The ionosphere model used in the software simulator is a combination of the Spherical Harmonics (SPHA) model and the grid model. It is globally optimised to simulate the global profile of the TEC distribution. This model uses the Global Ionosphere Map (GIM) files which contain the coefficients of spherical harmonics and other ionospheric parameters (Colombo et al. 2000). These GIMs can be obtained from the Centre for Orbit Determination in Europe (CODE), one of the Analysis Centres of the International GPS Service (IGS). The GIM coefficients give an approximation of the distribution of the

vertical TEC on a global scale by analyzing the geometry-free linear combination of GPS carrier phase data (Dong 2004). In order to improve the spatial variation, appropriate degree and order of SPHA components are chosen which yields the high frequency and reasonable magnitude variation of the ionospheric error. The degrees, orders, and SPHA coefficients in Table 5.1 are to add on the basic SPHA model to generate ionosphere error in SIMGNSSII^{TM} (Dong 2004).

Table 5.1 High degrees, orders and coefficients of SPHA model (Dong 2004)

Degree	Order	Coefficient
200	100	1
200	-100	1
100	50	1
100	- 50	1
50	25	1

In the next step a TEC grid-network is generated to the profile of the global TEC distribution. After building the grid network of the ionosphere, the TEC value at any point within the network is computed using interpolation.

Figure 5.1 shows an example of the double differenced ionospheric errors generated by this simulated ionosphere model. When the ionosphere is quiet, the RMS of the differential errors is about 1 ppm. For strong ionospheric activity, large differential errors with RMS of 10 ppm are simulated (Luo 2001).

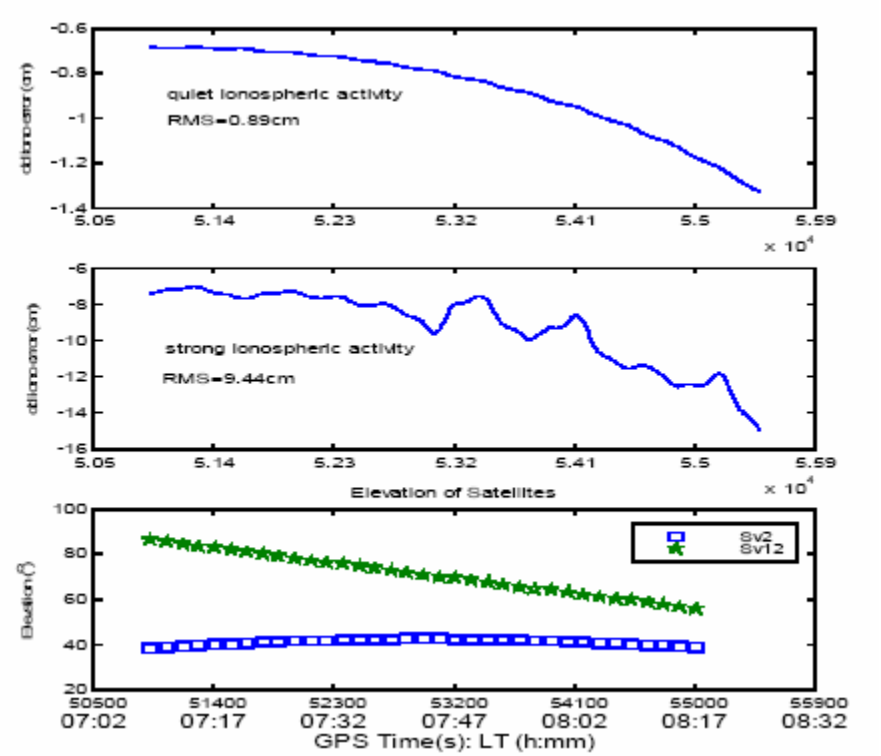

Figure 5.1 Example of Double Differenced (SV 2 and SV 12) Ionospheric Errors for a 10 Km Baseline (From Luo 2001)

5.1.2 Orbital Error Simulation Model

The orbital model used in the simulator is developed by analysing the statistical properties of the orbital error and then parameterizing these statistical properties as described in (Luo 2001). Here the orbital error is computed by subtracting the satellite's position, computed using the broadcast ephemeris, from an accurate reference orbit. The precise orbit is derived from JPL, which is one of the data analysis centres of the IGS, and is selected as the reference orbit (Luo 2001). After extracting the orbital error, several statistical tests were conducted to obtain the properties of the error. The probability distribution of the orbital error is modelled as a Gaussian distribution, and three different

correlation functions are derived for the orbital error in the along-track, cross-track and radial channels, respectively. Once the statistical properties of a random process are fully estimated, a simulated process with the same properties is generated by passing a white noise sequence through a shaping filter. Figure 5.2 presents the example of simulated orbital error using the model described above (Luo 2001).

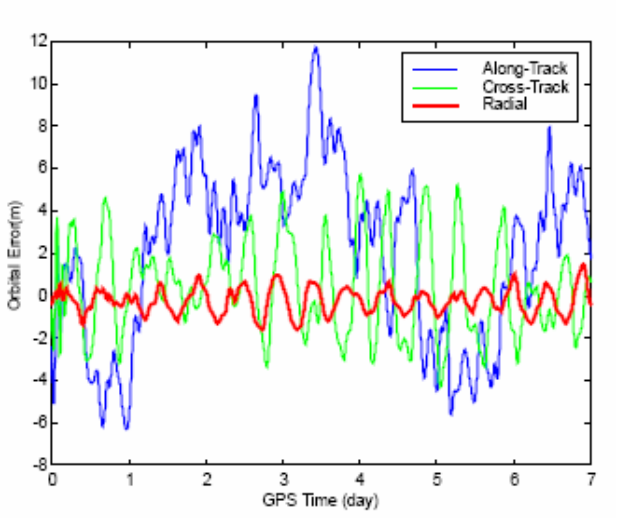

Figure 5.2 Sample of Simulated Orbital Errors (From Luo 2001)

5.1.3 Tropospheric Error Simulation Model

The tropospheric error model consists of two parts. One is the model of the vertical tropospheric delay, such as the Saastamoinen model (Saastamoinen 1972, 1973) and Hopfield model (Hopfield 1969). The other part is the mapping function, such as the B&E (Black and Eisner 1984), Chao (Chao 1974), Marini (Marini 1972) and Niell (Niell 1993) mapping functions. The simulator uses a new model based on the modified Hopfield model, which extends the Hopfield model to add the elevation angle mapping function (Black and Eisner, 1984). The temporal variation is realized by adjusting the

meteorological data with time (Luo 2001). The spatial variation is modelled using the grid algorithm over the simulated area. The size of the grid can be adjusted according to the spatial decorrelation rate required. The meteorological data is computed for each grid point. This meteorological data is interpolated at the desired user location using four-point bilinear interpolation. Although the meteorological data at each grid point is independent, the interpolation will generate the spatial correlation within the network. Thus, the resulting tropospheric delay is also spatially correlated (Luo 2001).

Figure 5.3 shows the diurnal variation of the meteorological data and related tropospheric parameters at the centre of a four-point grid network (100 km×100 km). It confirms that the relative humidity has the greatest effect on the tropospheric delay because the total vertical tropospheric delay changes in the same way as the relative humidity. Simulation results show the typical values of the vertical tropospheric delay (2.4 m) and its gradient (0.5 ppm) (Luo 2001).

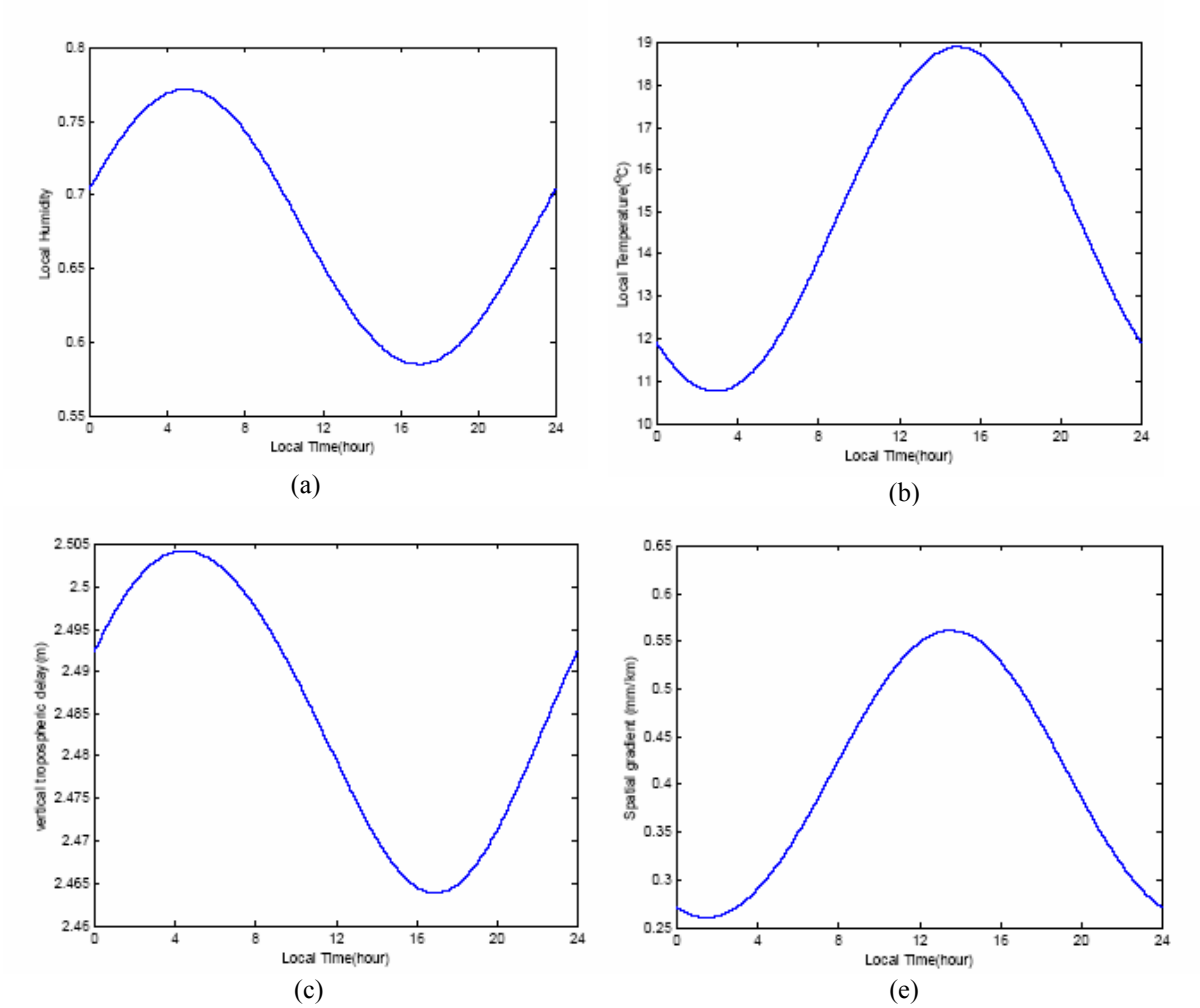

Figure 5.3 Temporal Variations of the Meteorological Data and Tropospheric Delay in a 100 km × 100 km Network (From Luo 2001)

5.1.4 Multipath Model

A sophisticated model for multipath has been developed by the Department of Geomatics Engineering at the University of Calgary (Ray 2000, Ryan 2000). This model is based on the mechanism for multipath generation. It contains three major parts: simulation of the reflecting environment, simulation of the antenna gain pattern, and simulation of the tracking loop (both code and carrier). This model is simplified further to simulate the

simplest reflecting environment, i.e. an infinite ground plane which has different reflecting coefficients (strength) at different reflecting points (Luo 2001). This model is called the simplified UofC model.

Figure 5.4 gives an example of multipath (both code and carrier) generated by the simplified model for a static platform (Luo 2001).

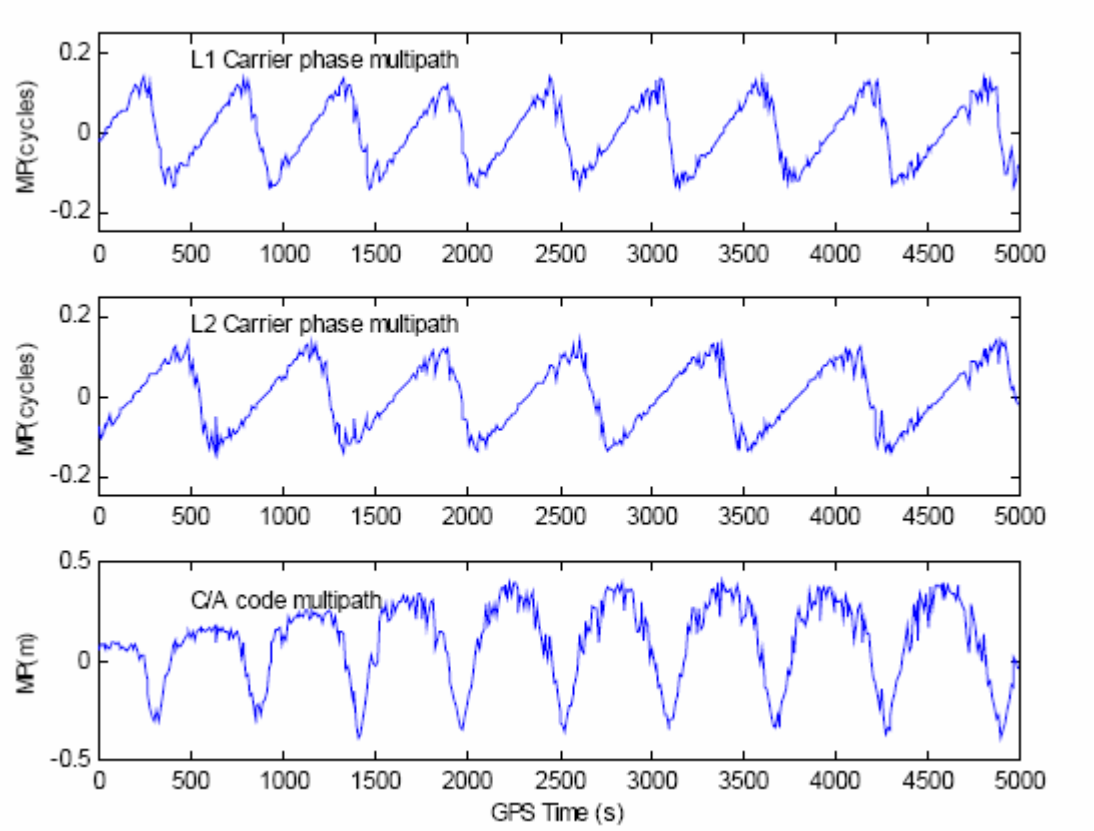

Figure 5.4 Simulated Multipath by the Simplified UofC Model (From Luo 2001)

The magnitude of each error to be simulated can be chosen according to the study requirement (Julien et al. 2004). This simulator has been used in many other GPS and

Galileo evaluations (e.g. Alves 2001, Lachapelle et al. 2002, Julien et al. 2003, Zhang et al. 2003).

5.2 Simulated Constellations

As per the original design of GPS and Galileo, the GPS constellation consists of 24 satellites unevenly distributed in six orbital planes inclined at 55º with a radius of 26,600 km, whereas the Galileo constellation consists of 30 satellites evenly distributed in three orbital planes, of which 27 active and 3 are spare satellites (European Commission 2006b). These three orbital planes are inclined at 56° with a radius of 29,994 km. Hence the 24/27 GPS/Galileo constellation is as shown in Table 5.2 (Salgado et al. 2001).

Table 5.2 GPS/Galileo 24/27 Constellations

GNSS	GPS	Galileo
Satellites	24	27
Planes	6	3
Inclination	55°	56°
Radius	26,600 km	29,994 km

However presently there are 29 operational GPS satellites in space (US Coast Guard 2006). If all 30 Galileo satellites designed to be in space are operational in the future, a new 29/30 GPS/Galileo constellation design can be created as shown in the Table 5.3.

Table 5.3 GPS/Galileo 29/30 Constellations

GNSS	GPS	Galileo
Satellites	29	30
Planes	6	3
Inclination	55°	56°
Radius	26,600 km	29,994 km

Thus this study simulates two different GPS/Galileo constellations: 24/27 and 29/30. The first one follows the original theoretical design and the second one is based on present GPS constellation status and the future Galileo constellation. Hence by utilising both theoretical and practical constellations in the simulations a full evaluation of the expected systems can be done.

5.3 Simulated Frequencies and Error Levels

As mentioned earlier in Chapter 1, the present study is based on dual frequency GPS and Galileo observations. The simulator software simulates two carrier frequencies: 1575.42 MHz (E1) and 1207.14 MHz (E5b) for Galileo and 1575.42 MHz (L1) and 1227.6 MHz (L2) for the GPS as listed in the Table 5.4.

Table 5.4 Simulated Signals for GPS and Galileo

System	Signal	Frequency (MHz)	λ (m)	Chipping Rate (Mc/s)
Galileo	E1	1575.42	0.190	2.046
	E5b	1207.14	0.248	10.23
GPS	L1	1575.42	0.190	1.023
	L2	1227.60	0.244	10.023

For all simulated observations, the ionospheric, tropospheric, and orbital errors, as well as receiver noise are included using different values of scale factors for the simulator software. For these simulated signals the magnitude of 1- σ single observation receiver noise errors generated are given in Table 5.5.

Table 5.5 Magnitude of Simulated Receiver Noise

	Signal	Receiver Noise
Galileo Code	E1	0.10 m
	E5b	0.10 m
GPS Code	L1	0.20 m
	L2	0.10 m
GPS/Galileo Phase	All	0.50 mm

The magnitude of the generated Double Difference (DD) troposphere and orbital errors are selected as listed in Table 5.6. The tropospheric error level shown in the table is the residual error, i.e. after applying a troposphere correction and double differencing.

Table 5.6 Magnitudes of Simulated Error Sources

Error source	Magnitude of DD error
Troposphere	0.2 ppm
Orbit	0.1 ppm

Typical pseudorange multipath varies from 0.5 m in a benign environment to more than 5 m in highly reflective environment; corresponding errors in the carrier phase are 1-5 cm (Misra and Enge 2006). The corresponding errors in the carrier phase measurements are less than a quarter cycle if the reflected signal has a lower signal strength than the direct signal (Ray 2000). These multipath errors are site dependant and are proportional to the number of reflectors present around the antenna (Misra and Enge 2006). However

multipath errors cannot be estimated in the differential positioning filter, and in the case of carrier phase based positioning algorithms it can typically result in unresolved, or incorrectly fixed, ambiguities. This thesis aims to evaluate and compare stand-alone GPS accuracy and ambiguity resolution performance to stand-alone Galileo for SRS and MRS-TC techniques, for different baselines and atmospheric conditions. Since the software simulator provides the ability to simulate a 'no multipath' multipath environment with only atmospheric conditions considered, one can focus on the performance effect due to atmospheric effects. Also since the same simulated positions of the reference stations and rovers are used for both GPS and Galileo to generate pseudoranges and carrier phase observations, the uncorrelated site-dependent multipath errors are not considered in this thesis for the evaluation and comparison of the two systems. Thus multipath errors are not simulated here and modelling the multipath and observing the effects of it is beyond the scope of this study.

Three different ionospheric conditions are simulated here using the magnitude of simulated error as shown in Table 5.7, where an ionospheric level of 3 ppm means that during a 24 hour test, the level of ionosphere error was within 3 ppm 90% of the time.

Table 5.7 Ionospheric Error Levels

Description	**DD Error level**
Low	1 ppm
Medium	3 ppm
High	6 ppm

For each carrier-phase measurement, an ambiguity of zero cycles is simulated. Therefore, the true value of each ambiguity is zero, which helps to check of the correctness of each ambiguity resolution trial.

5.4 Simulated Networks

In order to establish the reference networks located in Calgary with four sets of baselines ranging from 30 to 120 km are simulated. For each baseline, reference network stations are situated at four corners of a rectangle, with the rover at the centre of the rectangle to form a star topology as shown in Figure 5.5.

The diagonal distance from the rover to the reference station is the same as for the simulated baseline distance. For all four simulated networks of different baselines, the rover is located at the same fixed position.

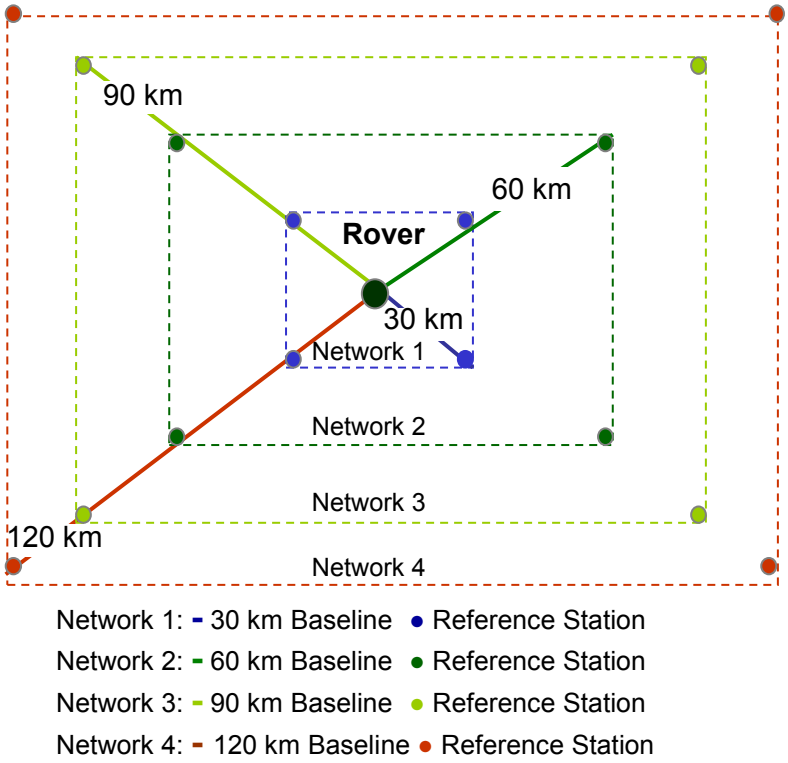

Figure 5.5 Simulated Baselines: 30 km, 60km, 90 km and 120 km Located in Calgary

5.5 PDOP and Number of Visible Satellites

For all the simulated networks, the rover is located at the same fixed position as shown in Figure 5.5. Figure 5.6 and Figure 5.7 represent the time series of the Position Dilution of Precision (PDOP) as well as the number of visible satellites at the rover position for 24/27 and 29/30 GPS/Galileo constellations, respectively.

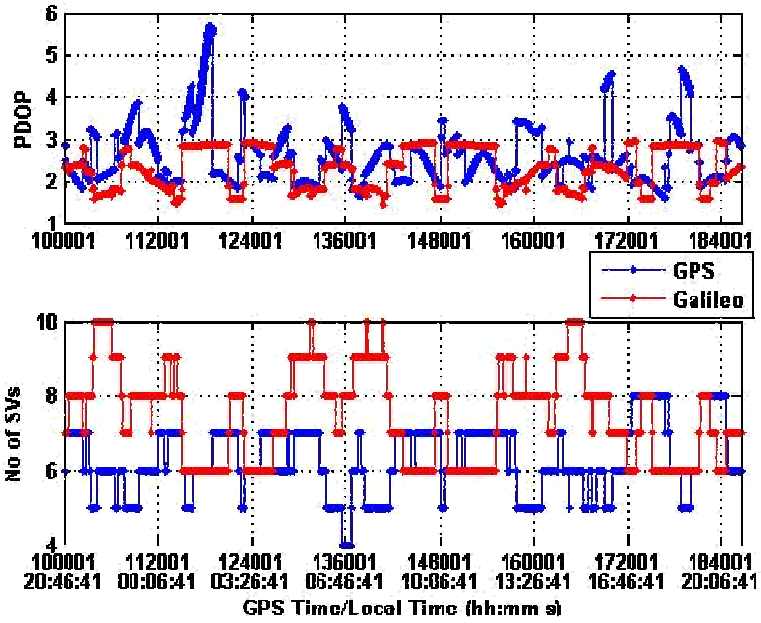

Figure 5.6 PDOP and Number of Satellites for 24/27GPS/Galileo constellation

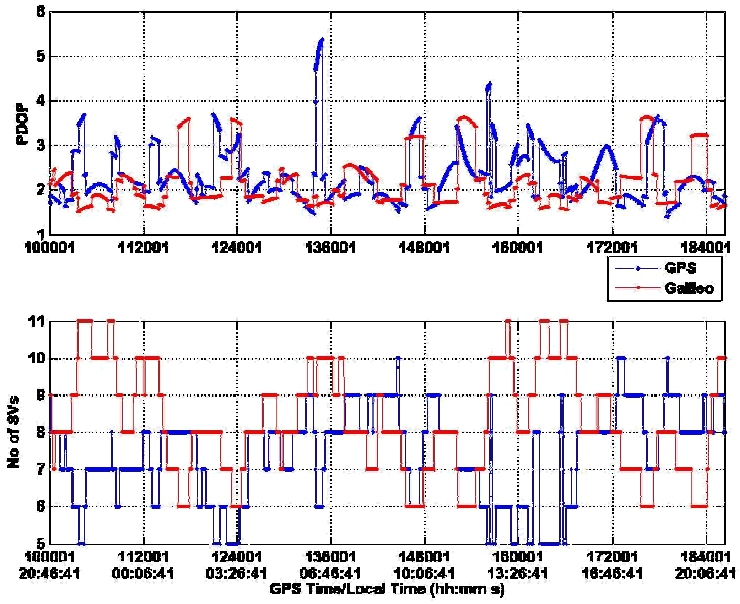

Figure 5.7 PDOP and Number of Satellites for 29/30 GPS/Galileo constellation

Table 5.8 represents the comparison statistics for the PDOP and number of visible satellites for all the simulated constellations. Both simulated cases, i.e. GPS/Galileo 24/27 and 29/30 stand-alone Galileo, show better PDOP and number of satellites than the stand-alone GPS case. Hence, it can be confirmed that the stand-alone Galileo constellation for the chosen location always provides better availability and geometry than the stand-alone GPS constellation.

Table 5.8 Comparison Chart for PDOP and Number of Satellites for Different Constellations

		GPS-24	GPS-29	Galileo-27	Galileo-30
PDOP	Min	1.6	1.5	1.5	1.5
	Max	5.8	5.4	3.3	3.0
Number of Visible satellites	Min	4.0	5.0	6.0	6.0
	Max	8.0	10.0	10.0	11.0

5.6 Test Scenarios and Data Processing

For each network ranging from 30 to 120 km, observations corresponding to three different error levels, i.e. low, medium and high ionospheric error, were generated in stand-alone GPS and stand-alone Galileo modes using the SimGNSSII^{TM} software. Thus four baselines and three ionosphere levels were simulated giving 12 different cases to analyse. For each of these simulated cases, the data was processed in four different modes:

1. SRS stand-alone GPS
2. SRS stand-alone Galileo

3. MRS-TC stand-alone GPS
4. MRS-TC stand-alone Galileo

Thus 12 different cases, each processed in four different modes gives 48 different scenarios. For the original constellation design of GPS and Galileo, i.e. the 24/27 GPS/Galileo constellation, all these 48 scenarios were generated, processed and analyzed. However, for the 29/30 GPS/Galileo constellation only the scenarios beyond a baseline of 30 km and for the medium and high ionospheric error cases were generated and analyzed. This was done to study the improvement in the case of active ionospheric conditions due to improved availably and geometry.

Even though the repeatability of the Galileo is about 72 hours, each simulation was done over a span of 24 hours since one day of simulation can provide statistically consistent results compared to longer simulation runs (Julien et al. 2003). For the entire data processing mission, dual frequency mode, i.e. L1/L2 for GPS and E1/E5b for Galileo, and a satellite elevation mask of 13 degrees were used.

In order to process the simulated data in SRS stand-alone GPS or and Galileo, the FLYKIN+^{TM} software is used. FLYKIN+^{TM} is a GPS differential positioning software which can process double differenced carrier phase data both in static and kinematic modes (Liu 2003). It uses a Kalman filter to estimate the three position and velocity components and ‘N’ float ambiguities, where ‘N’ is the total number of double difference observations formed between the rover and reference station as explained in the Chapter 3 earlier. The Least Squares Ambiguity Decorrelation Adjustment (LAMBDA)

(Teunissen 1994) is used to shrink the ambiguity search space. For this study newly implemented FLYKIN+^{TM} for Galileo software was utilised to process the SRS Galileo observations. FLYKIN+^{TM} for Galileo and FLYKIN+^{TM} for GPS are thus used herein to process the rover and one of the reference stations in differential mode and using stochastic ionosphere modelling to produce the SRS results for each simulated Galileo and GPS scenario respectively. In order to evaluate the MRS-TC approach for GPS and Galileo, MRS-TC^{TM} for GPS and newly implemented MRS-TC^{TM} for Galileo softwares are used to process the rover and all the given reference station's observations using the MRS-TC approach as explained in Chapter 4 previously. Since the ionosphere error is the major source of simulated errors, this simulated error level is compared with the estimated ionosphere error using the MRS-TC and SRS approaches.

Chapter 6 Results and Analysis

GPS and Galileo observations were simulated for different baselines and error conditions and these were then processed according to the simulation parameters and the test scenarios as described in Chapter 5. The results thus obtained are analysed here using three Figures of Merit (FOM) and ionosphere estimation error.

6.1 Figures of Merits

Similar to the study performed by Julien et al. (2003), three FOMs namely: Three Dimensional (3-D) Root Mean Square (RMS) of the position errors, Percentage of Correctly Fixed Ambiguities (PCFA) and Percentage of Fixed Ambiguities (PFA) have been utilised in order to assess the positioning and ambiguity resolution performance of different simulation scenarios throughout this research. These FOMs are defined below:

- **3-D RMS Accuracy**

The rover position accuracy is calculated as 3-D RMS values given by the differences between the estimated and simulated rover coordinates, for the entire simulation duration. This 3-D RMS accuracy is calculated for all the simulated epochs, i.e. in all cases of ambiguity fixed status: correctly fixed, partially fixed or the float case.

- **Percentage of Correctly Fixed Ambiguities**

The PCFA is the FOM that measures the percentage of carrier phase ambiguities that are estimated to the correct integer value (Julien et al. 2003). The PCFA is calculated as the

total number of ambiguities that are fixed to the correct integer values divided by the total number of ambiguities fixed to integer value for the simulation duration.

- **Percentage of Fixed Ambiguities**

The PFA is the total number of fixed ambiguities divided by the total number of ambiguities for the entire test scenario (Julien et al. 2003). In a comparison of the two systems in terms of ambiguity resolution performance, the PCFA is meaningful only when there are equivalent PFA for both systems. Even though the PCA and PCFA are closely related, they are important parameters to monitor separately in order to assess the system reliability.

In order to assess these FOMs, time series of the 3-D RMS error and times series of the ambiguities are plotted for four data processing modes for each simulated case as explained in Section 5.6. For the SRS approach, the time series of the ambiguities consists of the number of double difference L1 and L2 ambiguities for GPS, and E1 and E5b ambiguities for Galileo. Considering the 'n' double difference single frequency observations formed between the rover and the reference station for an epoch, there will be '2n' total ambiguities to be calculated for dual frequency data for that epoch. Similarly, for the MRS-TC approach, this time series consists of the number of double difference L1 and L2 ambiguities for GPS, and E1 and E5b ambiguities for Galileo, for all the network stations. Since four reference stations are utilised for each simulated network, four network baselines are formed corresponding to each reference station and the rover. Hence, assuming that all the reference stations observe the same number of

satellites, and ‘n’ single frequency double difference observations are formed per network baseline for an epoch, there will be ‘4n’ number of ambiguities formed per frequency for a total of ‘8n’ ambiguities to be calculated for dual frequency data for that epoch. For a detailed analysis, a time series of the 3-D RMS error and the number of float and fixed ambiguities are plotted for each simulated scenario. These time series are utilised to generate the 3-D RMS error, PFA and PCFA. The four sets of results obtained for each data processing mode are compared in terms of PFA, PCFA and the rover position accuracy.

6.2 Test Results with 24/27 Constellation

For the 24/27 GPS/Galileo constellations as per the original designs, all four baselines and three different atmospheric conditions were simulated, as explained in Chapter 5. Table 6.1 and Table 6.2 list the overall 3-D RMS position errors, Table 6.3 and Table 6.4 represent the PFA values and Table 6.5 and Table 6.6 represent the PCFAs for the SRS and MRS-TC for all the simulated scenarios of the test with the 24/27 GPS/Galileo constellations.

Table 6.1 3-D RMS Error in cm for SRS

Baseline (km)	Low Ionosphere		Medium Ionosphere		High Ionosphere	
	GPS	GAL	GPS	GAL	GPS	GAL
30	2.0	1.5	5.1	3.3	26.8	20.7
60	4.6	3.1	14.0	10.0	38.8	26.1
90	7.4	4.4	24.5	19.2	51.9	38.6
120	7.6	7.1	28.6	20.8	61.5	46.0

Table 6.2 3-D RMS Error in cm for MRS-TC

Baseline (km)	Low Ionosphere		Medium Ionosphere		High Ionosphere	
	GPS	GAL	GPS	GAL	GPS	GAL
30	0.4	0.3	0.5	0.4	0.7	0.6
60	0.5	0.4	0.6	0.6	1.8	1.0
90	0.6	0.5	1.1	0.6	8.8	6.7
120	0.7	0.6	2.5	0.9	26.4	18.0

Table 6.3 Percentage of Fixed Ambiguities for SRS

Baseline (km)	Low Ionosphere		Medium Ionosphere		High Ionosphere	
	GPS	GAL	GPS	GAL	GPS	GAL
30	99.94	99.95	96.87	99.31	24.15	13.31
60	95.81	99.78	61.61	71.48	16.28	3.13
90	89.59	98.69	27.12	19.83	16.00	2.58
120	86.84	92.70	18.18	12.18	9.19	2.04

Table 6.4 Percentage of Fixed Ambiguities for MRS-TC

Baseline (km)	Low Ionosphere		Medium Ionosphere		High Ionosphere	
	GPS	GAL	GPS	GAL	GPS	GAL
30	99.87	99.92	99.60	99.85	79.84	95.62
60	99.06	99.76	95.09	99.03	39.21	45.78
90	95.64	98.74	76.07	95.73	16.27	22.07
120	90.00	90.96	59.69	77.69	6.83	8.36

Table 6.5 Percentage of Correctly Fixed Ambiguities for SRS

Baseline (km)	Low Ionosphere		Medium Ionosphere		High Ionosphere	
	GPS	GAL	GPS	GAL	GPS	GAL
30	100.00	100.00	100.00	100.00	41.08	45.46
60	100.00	100.00	96.25	97.53	6.55	10.32
90	100.00	100.00	51.04	81.92	6.33	10.15
120	100.00	100.00	50.41	80.94	2.29	3.36

Table 6.6 Percentage of Correctly Fixed Ambiguities for MRS-TC

Base line (km)	Low Ionosphere		Medium Ionosphere		High Ionosphere	
	GPS	GAL	GPS	GAL	GPS	GAL
30	100.00	100.00	100.00	100.00	75.05	92.36
60	99.47	100.00	94.15	99.07	24.78	55.46
90	92.00	98.24	79.04	90.57	15.02	41.94
120	86.49	89.79	68.01	73.37	11.34	26.66

A detailed discussion of the test results for each simulated scenario is given below.

6.2.1 Results for the 30 km Baseline

Figure 6.1, Figure 6.2, and Figure 6.3 presents time series plots for the number of ambiguities and 3-D RMS error for the 30 km baseline. As shown in Figure 6.1a, a very small 3-D RMS error is obtained for all four processing modes for the low ionospheric error case. The PFA figure is more than 99% for all cases. Both stand-alone GPS and Galileo MRS-TC results show very good performance demonstrating a low 3-D RMS error of about 0.4 cm with an approximately 99.9% PFA and 100% PCFA. For a medium ionospheric error level (Figure 6.2), there is a small increase in the 3-D RMS errors for both the stand-alone GPS and Galileo SRS cases. Even though these errors are still at the decimetre level (5.1 cm and 3.3 cm, respectively), the reliability of the solution falls to 96.8% and 99.3% for the PFA, whereas the PCFA figure is fixed at 100%. However, the MRS-TC results are still comparable to the low ionosphere results with around a 0.4-0.5 cm 3D RMS error and PFA and PCFA values of more than 99% and 100%, respectively for both systems. For the high ionospheric error case (Figure 6.3), the SRS results

deteriorate further to a 3-D RMS error of more than 20 cm for both cases. The PFA figures declined to 13.3% and 24.2% for each system, and the PCFA to 45.5% and 41.1%. The number of fixed ambiguities frequently drops to zero, causing discontinuities in the 3-D position estimates. The MRS-TC in this case provides much improved results with smooth position error plots for both the stand-alone Galileo case with a 0.6 cm 3-D RMS error, a 95.6% PFA and a 92.4% PCFA. For GPS the RMS error is 0.7 cm, the PFA is 79.8% and the PCFA is 75.0%. The Galileo MRS-TC case provides the highest reliability with a 95.6% PFA and a PCFA of 92.4% for the high ionospheric case, among the four sets of results.

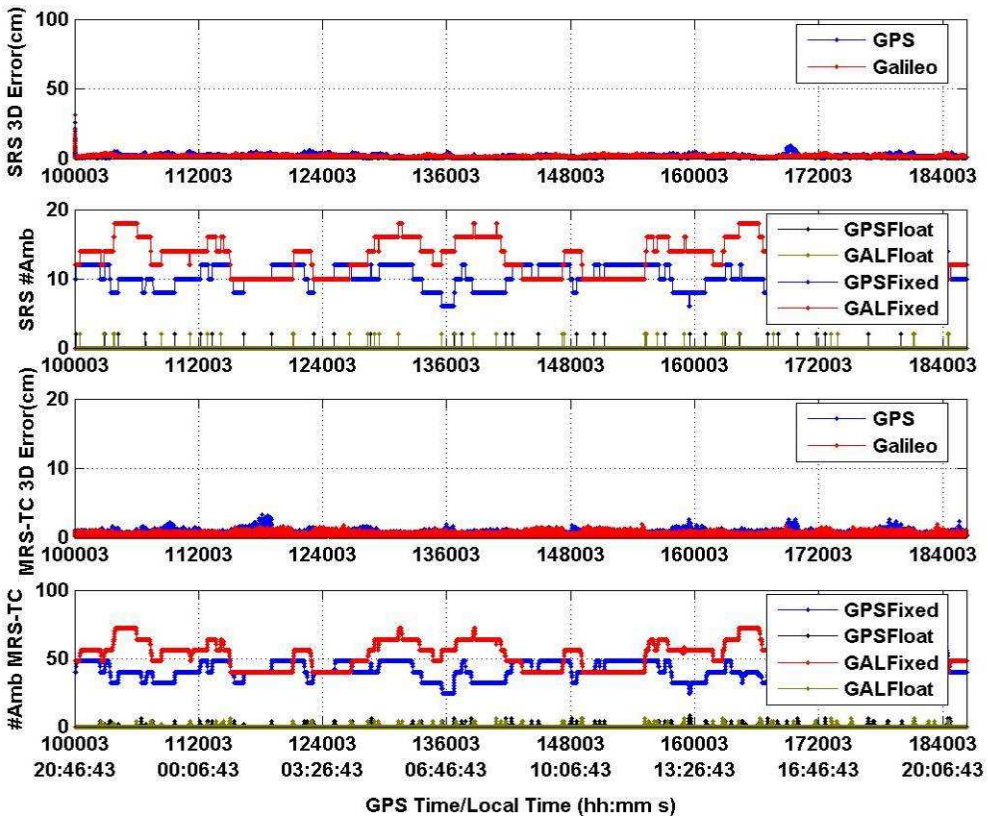

Figure 6.1 3-D RMS Error and Ambiguities Plot for the 30 km Baseline: Low Ionosphere

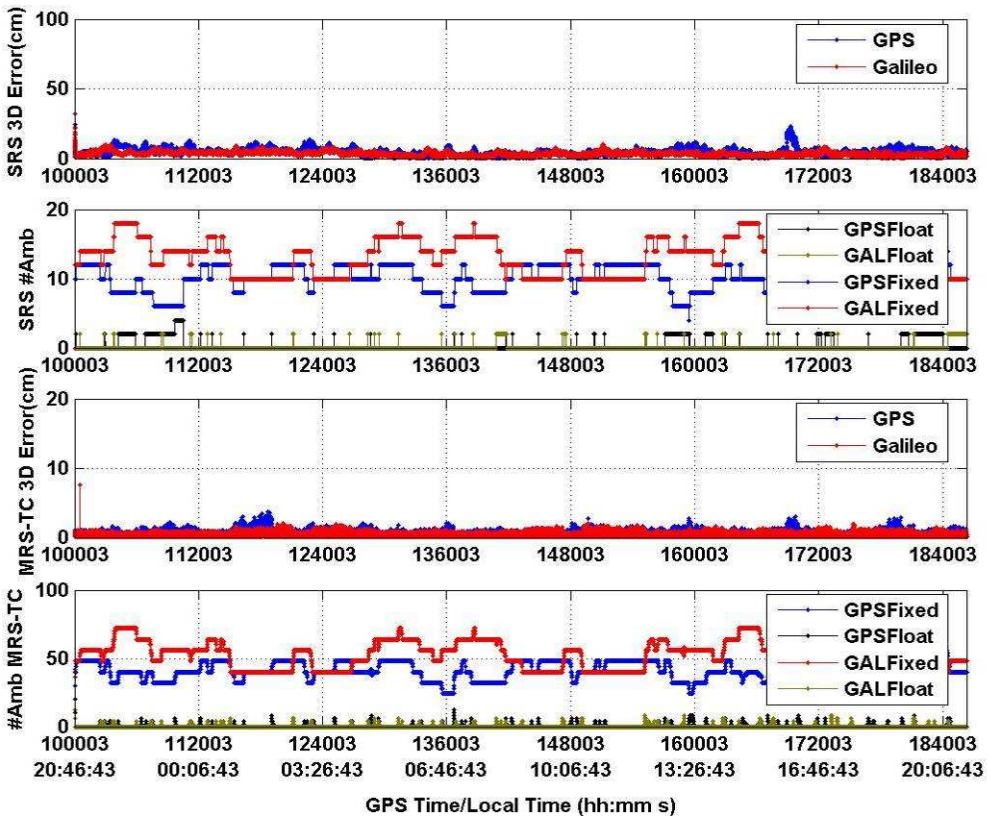

Figure 6.2 3-D RMS Error and Ambiguities Plot for the 30 km Baseline: Medium Ionosphere

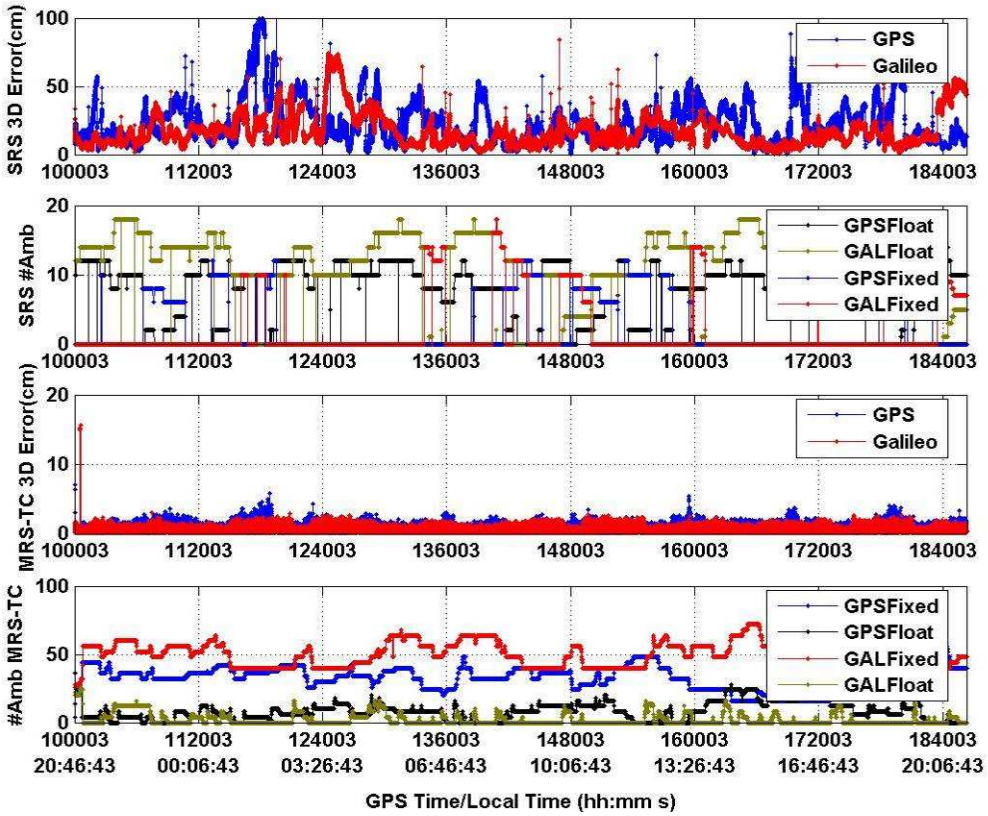

Figure 6.3 3-D RMS Error and Ambiguities Plot for the 30 km Baseline: High Ionosphere

Thus the results for small baselines using the SRS technique are reliable for low and medium atmospheric conditions, and deteriorate for high ionospheric conditions and become unreliable for both stand-alone GPS and stand-alone Galileo mode. Similar performance is shown for MRS-TC results except that the stand-alone Galileo high ionosphere case here shows better improvement providing around 95% reliable results.

6.2.2 Results for 60 km Baseline

Figure 6.4, Figure 6.5, and Figure 6.6 represent the 3-D RMS and ambiguities plots for the 60 km baseline. For the low ionospheric error case (Figure 6.6a), even though the SRS 3-D RMS errors are smooth and low, the Stand-alone GPS mode demonstrates less reliability with a PFA of 95.8%, compared to Stand-alone Galileo with a 99.8% PFA. The PCFA is 100% for both systems. As the ionospheric error level increases, the SRS number of fixed ambiguities has frequent jumps to zero in the ambiguity plot and discontinuities in the 3-D RMS error plots for both GPS and Galileo. Accordingly, the PFA figure for the SRS mode deteriorates to 61.6% and 71.5% for the medium ionospheric error case (Figure 6.5) for GPS and Galileo, respectively. It degrades further to 16.3% and 3.1% for the high ionospheric error case (Figure 6.6). The PCFA figure no longer stays at 100% and reduces to 96.2% and 97.5% for the medium ionospheric error and down to 6.6% and 10.3% for the high ionospheric error for GPS and Galileo respectively.

The 3-D RMS error does not remain smooth and within the decimetre level - it exceeds 25 cm for the high ionospheric error case. For low ionospheric error conditions, MRS-TC does not provide much improvement over SRS. However, MRS-TC nicely controls these error levels to the cm level, as compared to SRS for medium ionospheric error with a good PFA of 99% and 95% for Galileo and GPS, respectively. In the case of a high ionospheric error, the results show an improvement as compared to the SRS mode. The MRS-TC 3-D RMS error increases up to the decimetre level providing an unreliable solution which is indicated by a PFA of 39.2% and 45.8% and a PCFA of 24.8% and

55.5% for GPS and Galileo, respectively. The results are poor for high ionospheric conditions because the MRS-TC approach can compensate for only a small part of the ionospheric error due to an increase in the spatial decorrelation of the ionospheric error.

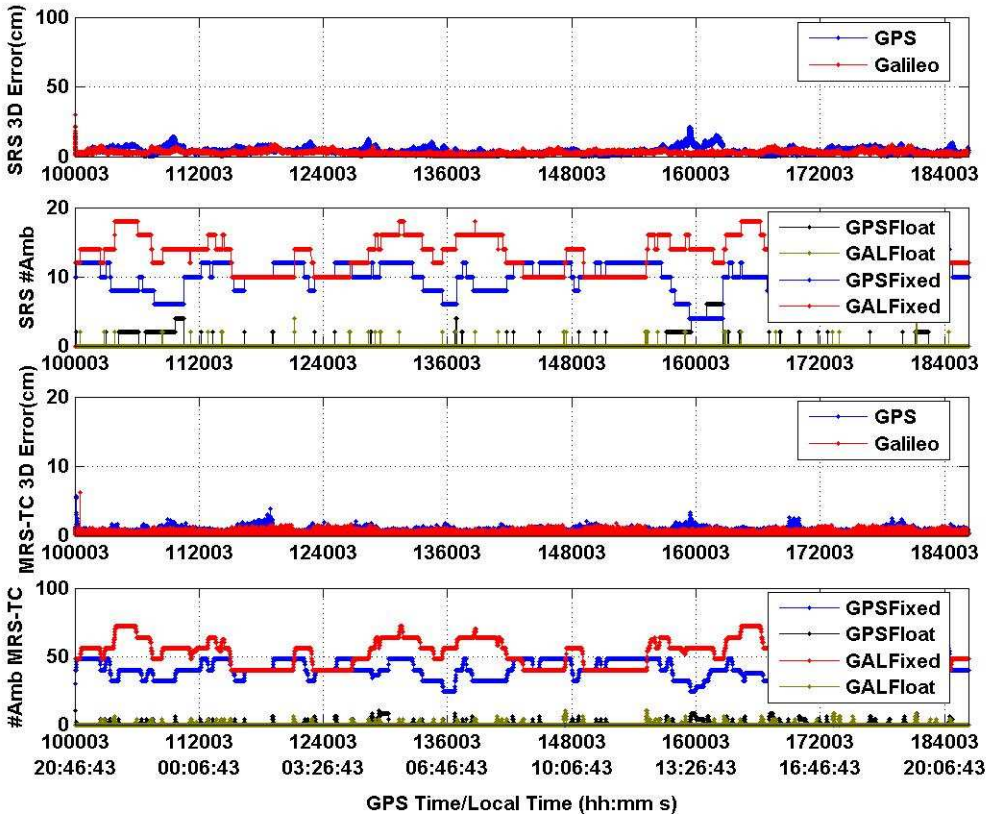

Figure 6.4 3-D RMS Error and Ambiguities Plot for the 60 km Baseline: Low Ionosphere

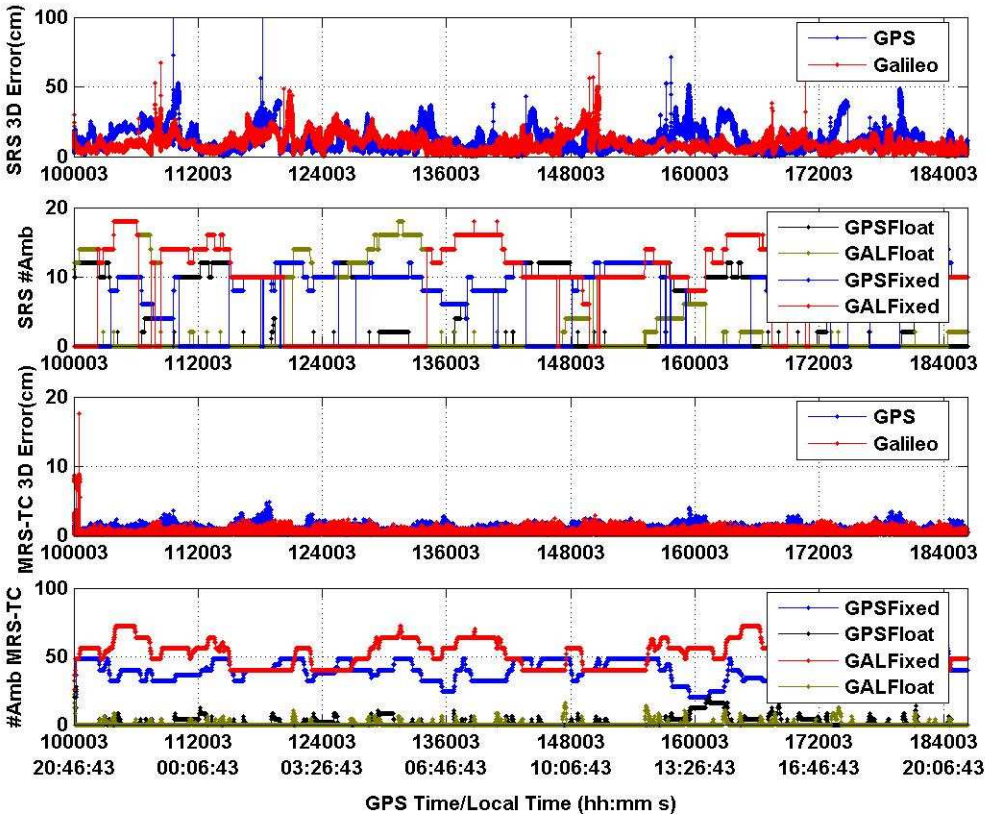

Figure 6.5 3-D RMS Error and Ambiguities Plot for the 60 km Baseline: Medium Ionosphere

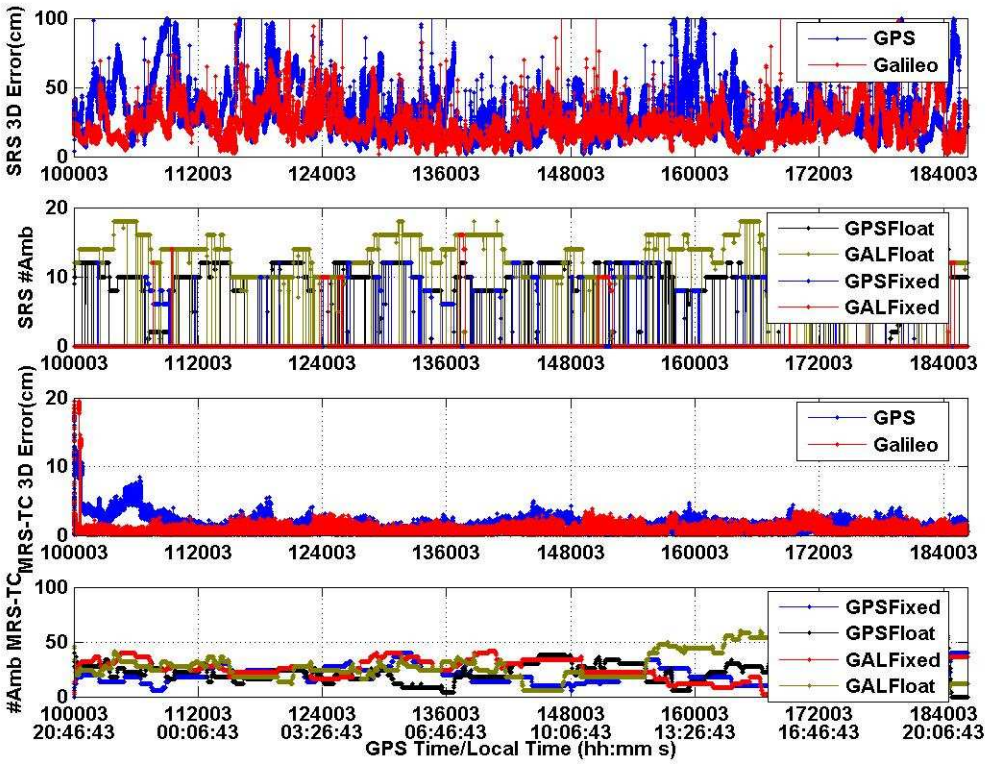

Figure 6.6 3-D RMS Error and Ambiguities Plot for the 60 km Baseline: High ionosphere

6.2.3 Results for 90 km Baseline

Figure 6.7, Figure 6.8, and Figure 6.9 presents the time series for the 3-D RMS errors and ambiguities for the 90 km baseline. For the low ionospheric error case (Figure 6.7), the SRS results produce decimetre-level 3-D RMS position errors, with a PFA of 89.6% and 98.7%, and a PCFA of 100% for GPS and Galileo. However, for both the medium and high ionosphere conditions, the SRS 3-D RMS errors shoot up to more than 19 cm

and 38 cm for the two systems. The solution is no longer reliable, showing PFAs of less than 28% and 20%, with PCFAs of 51.0% and 81.9% for medium ionospheric error GPS and Galileo solutions. For high ionospheric error conditions, the results decline further demonstrating very low PFA figures of 16.0% and 2.6% with PCFA values of 6.3% and 10.2% for GPS and Galileo. For low ionospheric error conditions as shown in Figure 6.7, the MRS-TC results do not show much improvement over the SRS results. However, MRS-TC stand-alone Galileo shows very good improvement under medium ionospheric errors, providing cm-level errors with a PFA of 95.7% and a PCFA of 90.6%. Under high ionospheric errors, the MRS-TC 3-D RMS error improves to the decimetre level compared to the SRS high ionospheric error level cases. However, the PFA only improves to 22.1% for Galileo, showing a higher number of float ambiguities in the ambiguity plot.

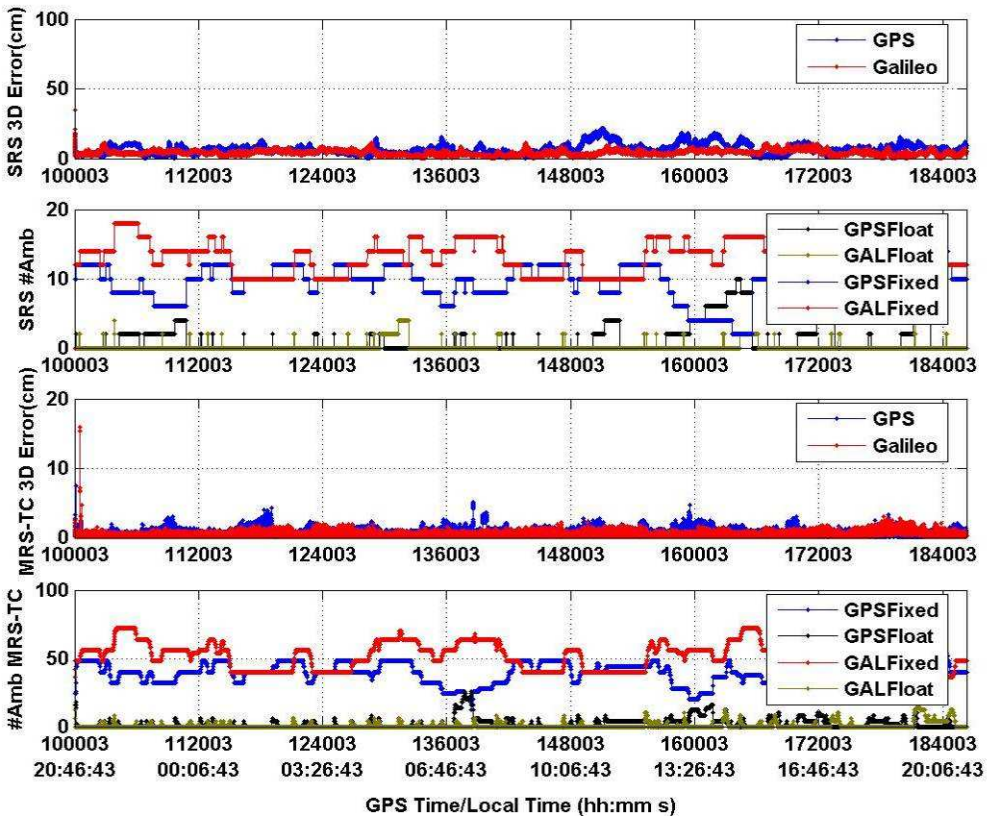

Figure 6.7 3-D RMS Error and Ambiguities Plot for the 90 km Baseline: Low Ionosphere

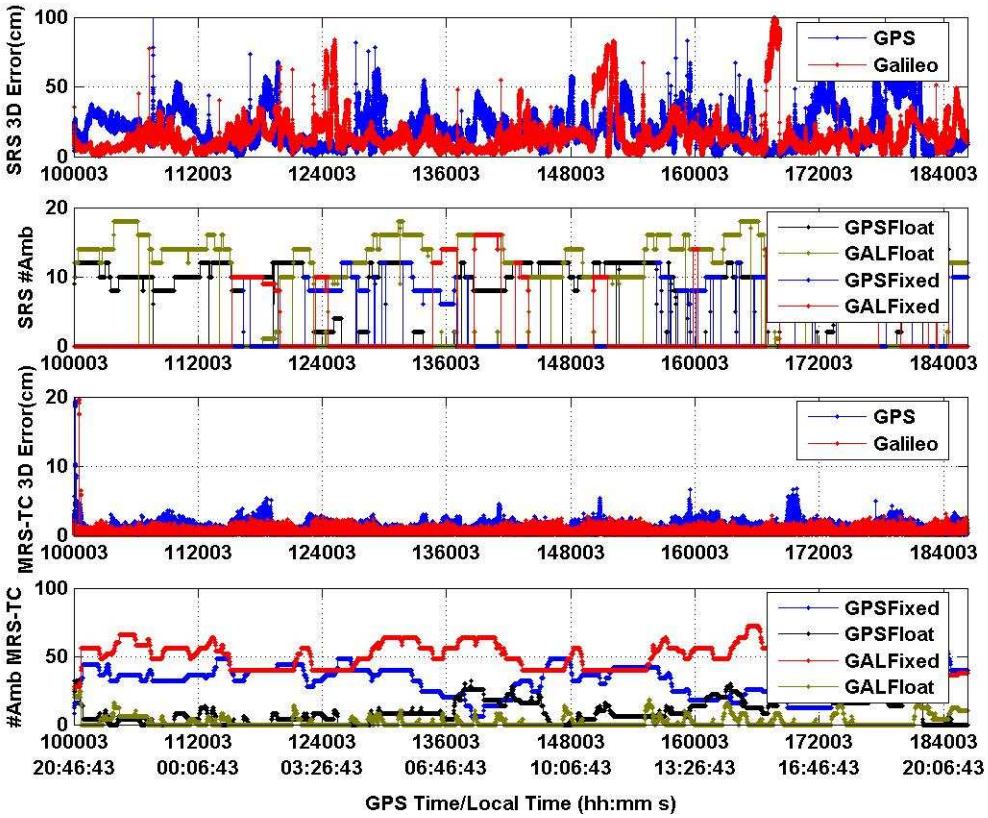

Figure 6.8 3-D RMS Error and Ambiguities Plot for the 90 km Baseline: Medium Ionosphere

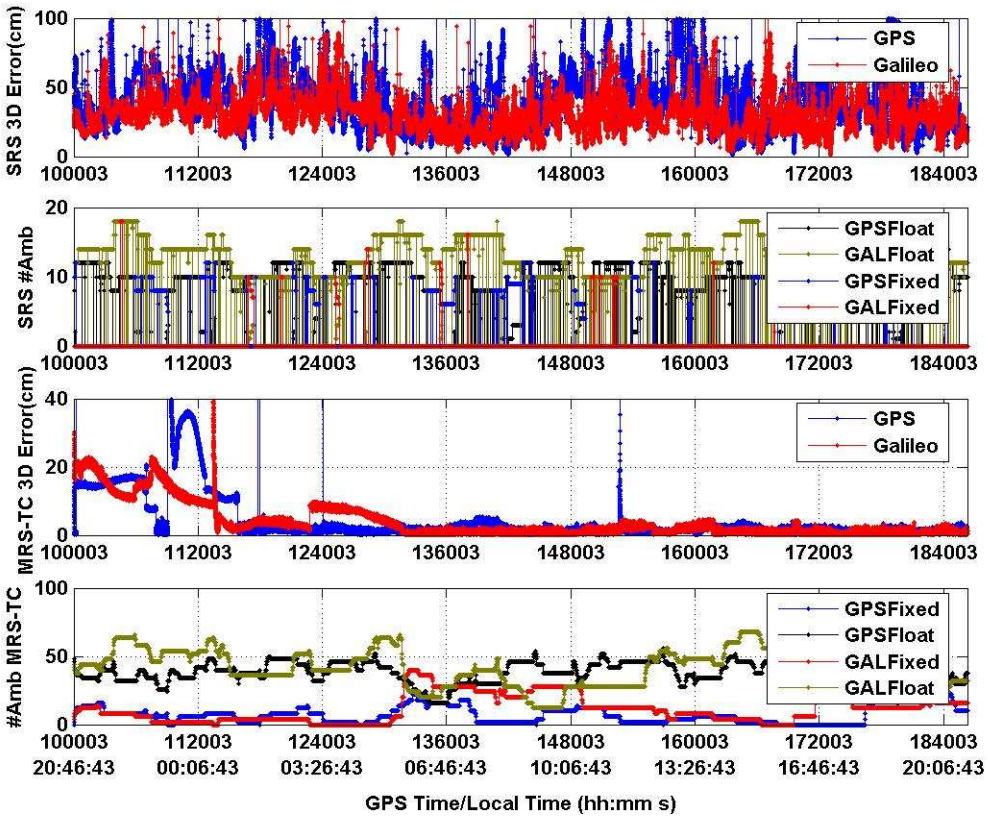

Figure 6.9 3-D RMS Error and Ambiguities Plot for the 90 km Baseline: High Ionosphere

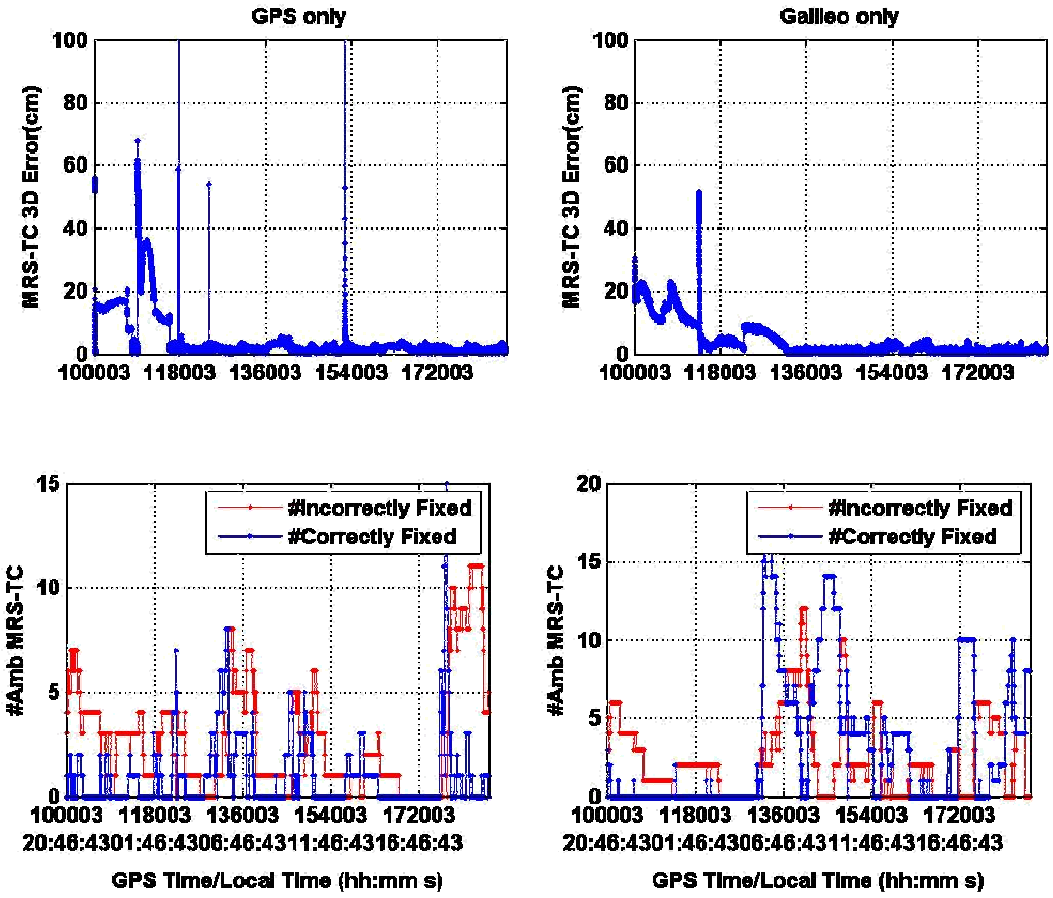

Figure 6.10 MRS-TC 3-D RMS Error, Number of Correctly and Incorrectly Fixed Ambiguities for 90 km Baseline: High Ionosphere Case

For the high ionospheric case, as shown in Figure 6.9, the 3-D RMS error in this case shows many discontinuities. In order to analyze their cause, a time series of MRS-TC 3-D RMS errors is plotted along with a time series of the number of correctly and incorrectly fixed ambiguities as given in Figure 6.10. It is evident from the figure that the discontinuity in the 3-D RMS error is due to incorrect fixing of ambiguities. Hence at

these affected epochs the number of incorrectly fixed ambiguities rises and the number of correctly fixed ambiguities drops.

6.2.4 Results for 120 km Baseline

Figure 6.11, Figure 6.12, and Figure 6.13 represents the 3-D RMS and ambiguity plots for the 120 km baseline. For the low ionospheric error case (Figure 6.11), the SRS results provide 3-D RMS errors of 7.6 and 7.1 cm with a PFA of 86.8% and 92.7% for the GPS and Galileo, respectively. The PCFA is 100% for both systems. These PFA figures reduce significantly to 18.1% and 21.1% with more than a 20 cm 3-D error for a medium ionospheric error. For a high ionospheric error, it further reduces to 9.2% and 2.0% with more than a 45 cm 3-D RMS error. The medium and high ionospheric error ambiguity plots (Figure 6.12 and Figure 6.13) show a higher number of float ambiguities with frequent jumps to zero representing a higher number of incorrectly fixed ambiguities. Hence the PCFA ambiguities are low in these cases. In case of MRS-TC, the low ionospheric error results are reliable at the cm level; however there is not much improvement over the SRS results. Under medium ionospheric errors, however, the MRS-TC shows very good improvement giving a cm-level error and a PFA of 77.7% and a PCFA of 73.4% for Galileo. In the case of a high ionospheric error, however, even if the 3-D RMS errors look statistically improved, they are not reliable as indicated by the PFA values of 6.8% and 8.4% and low PCFA figures for both GPS and Galileo.

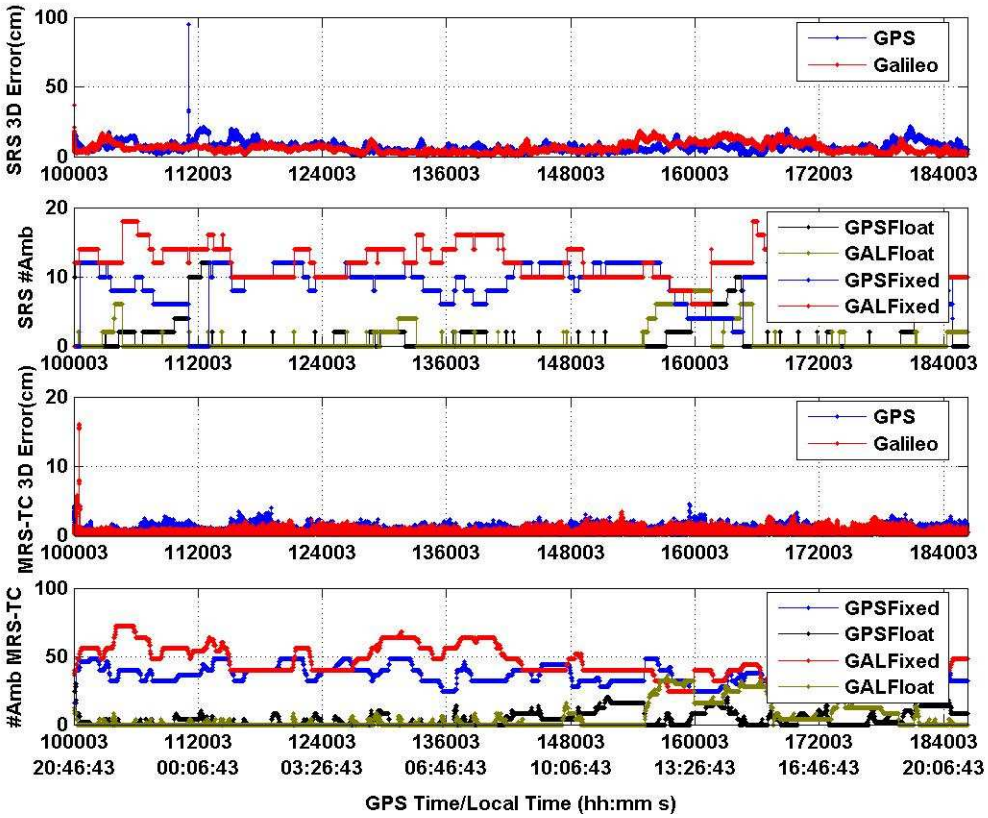

Figure 6.11 3-D RMS Error and Ambiguities Plot for the 120 km Baseline: Low Ionosphere

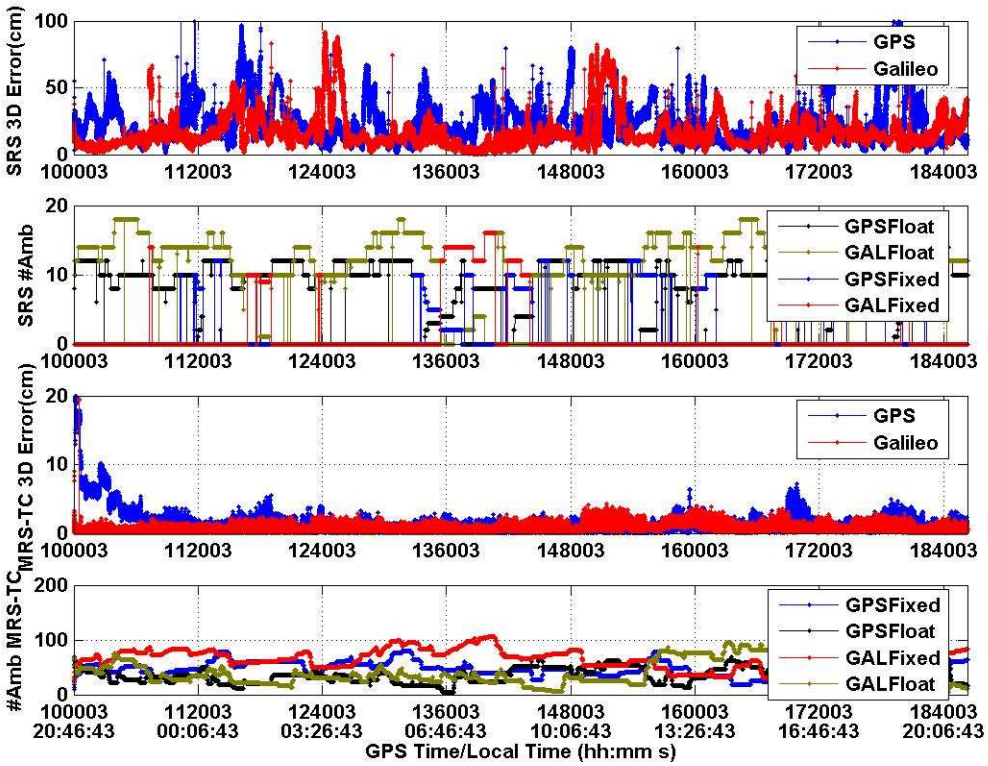

Figure 6.12 3-D RMS Error and Ambiguities Plot for the 120 km Baseline: Medium Ionosphere

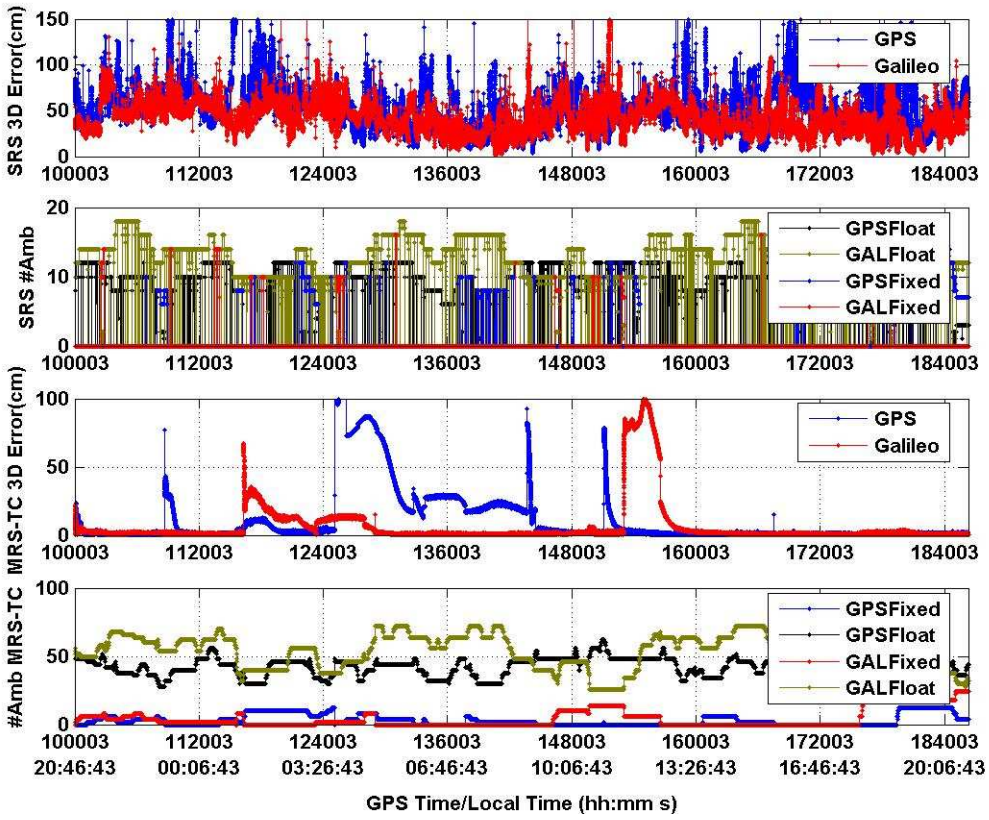

Figure 6.13 3-D RMS Error and Ambiguities Plot for the 120 km Baseline: High Ionosphere

Similar to the high ionospheric error MRS-TC 90 km case, high ionospheric errors in the 120 km baseline also causes large discontinuities in the 3-D RMS results (Figure 6.13). As explained in Figure 6.14, these occur at the instants when the numbers of correctly fixed ambiguities drop, or when there are no fixed ambiguities.

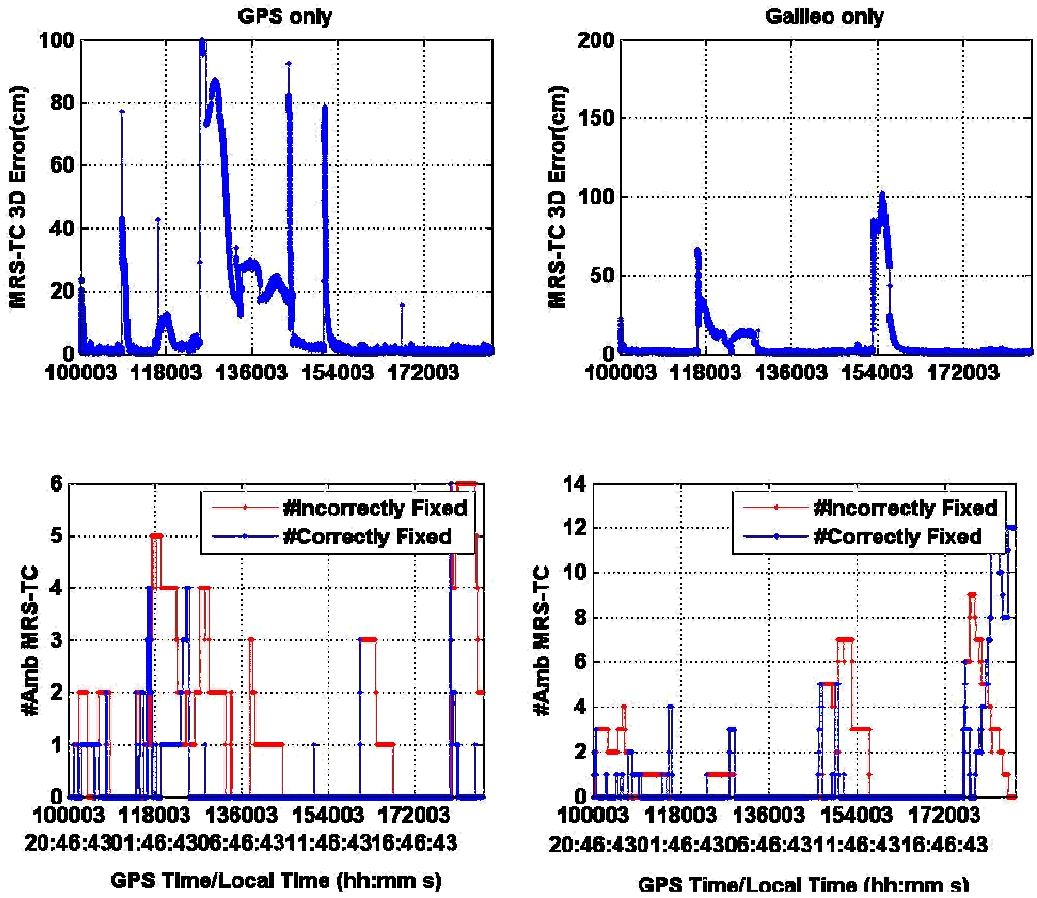

Figure 6.14 MRS-TC 3-D RMS Error, Number of Correctly and Incorrectly Fixed Ambiguities Plot for the 120 km Baseline: High Ionosphere Case

6.3 Ionosphere Estimation Error

The simulated ionosphere is the major source of error in all the scenarios hence the simulated DD ionosphere error is compared with the estimated DD ionosphere error using MRS-TC and SRS for all GPS and Galileo cases. Figure 6.15 and Figure 6.16 represent the time series of RMS values of simulated and estimated ionosphere using the MRS-TC approach and estimated ionosphere using the SRS approach for 120 km high ionosphere and medium ionosphere cases, respectively. From Figure 6.16 it is observed

that the ionospheric error is well estimated by the MRS-TC approach in the case of a moderate ionosphere. In case of increased ionosphere level demonstrates the elevated simulated ionosphere values specified by large green area in Figure 6.15. The SRS and MRS-TC ionosphere estimates do not approach the actual simulated values showing a large gap between the green area and the red and blue areas. This is due to correlation property of the ionospheric error which is utilised in the estimation models used in the SRS and MRS-TC approaches.

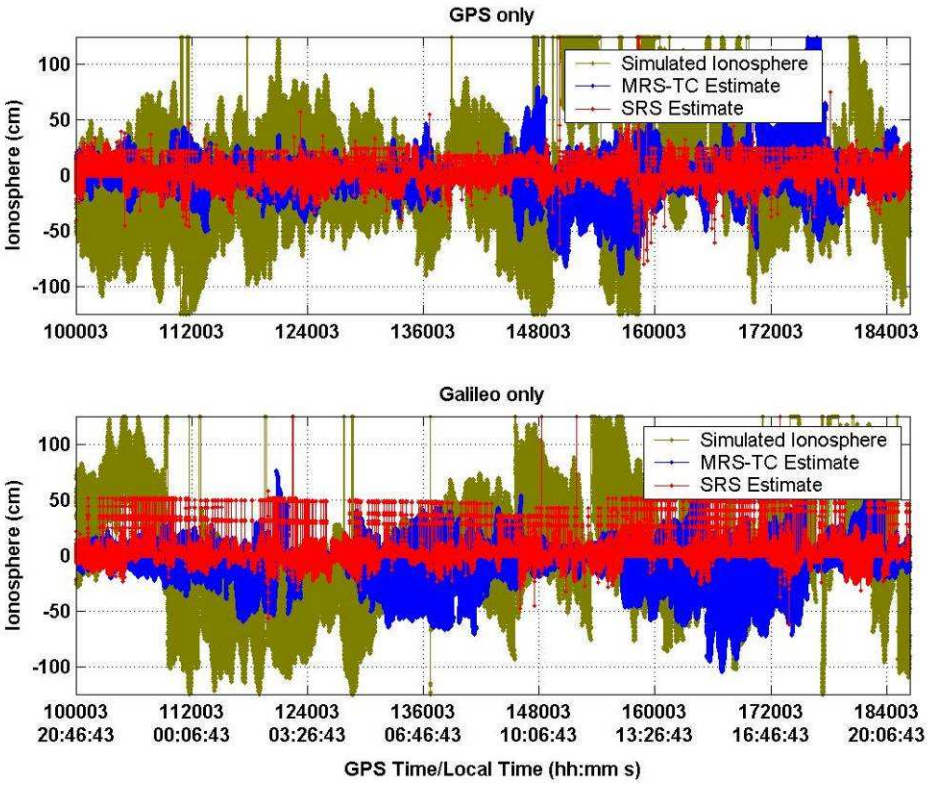

Figure 6.15 DD Ionosphere RMS Values for 120 km High Ionosphere Case

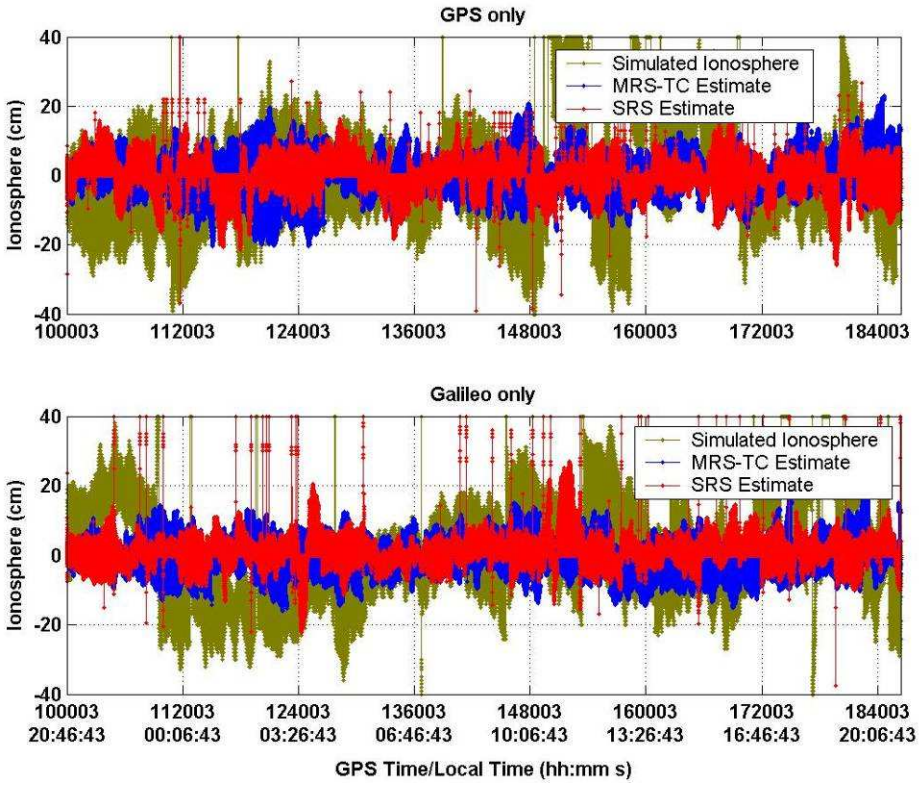

Figure 6.16 DD Ionosphere RMS Values for 120 km Medium Ionosphere Case

Table 6.7 and Table 6.8 represent the RMS error difference calculated by differencing the RMS times series of the simulated ionosphere and SRS estimates and the MRS-TC estimates respectively and taking the RMS of this differenced time series.

Table 6.7 Ionosphere Estimation Error in cm for the SRS

Baseline (km)	Medium Ionosphere		High Ionosphere	
	GPS	GAL	GPS	GAL
60	12.3	8.7	35.5	22.1
90	23.2	18.9	49.7	36.8
120	27.3	18.9	59.3	44.1

Table 6.8 Ionosphere Estimation Error in cm for the MRS-TC

Baseline (km)	Medium Ionosphere		High Ionosphere	
	GPS	GAL	GPS	GAL
60	0.3	0.3	1.6	0.9
90	1.0	0.5	7.1	5.2
120	1.9	0.7	22.3	16.2

These tables confirm that the MRS-TC approach performs better modelling of the ionospheric error compared to the SRS approach as discussed in Chapter 4. Also, it is observed that all Galileo only cases perform better than the corresponding GPS only cases since the better geometry of the simulated Galileo constellation results in better modelling of the ionosphere error.

6.4 Test Results with the 29/30 Constellation

The 29/30 GPS/Galileo constellation represents the presently operational 29 GPS satellites in space and 30 Galileo satellites uniformly distributed in three orbital planes as explained in Chapter 5. Since the new constellations have a higher number of satellites and better geometry compared to the originally designed 24/27 GPS/Galileo constellations as given by Table 5.8, this experiment aims to analyze how much improvement the new 29/30 constellation can provide compared to the 24/27 constellations in case of extended baselines and high ionosphere conditions, which are the most difficult. Hence simulated GPS and Galileo data with the new constellations was processed in SRS and MRS-TC modes for the medium and high ionospheric conditions for the 90 km and 120 km baselines. The results were analysed using the FOMs similar to all the cases analyzed for the 24/27 constellations. The results from two constellations are

compared in order to evaluate the performance improvement of the 29/30 constellations over the 24/27 constellations.

Table 6.9 and Table 6.10 list the comparisons for the overall 3-D RMS position error and Table 6.11 and Table 6.12 represent the comparisons for the PFA. Table 6.13 and Table 6.14, represent the comparisons for the PCFA of the two 24/27 and 29/30 GPS/Galileo constellations. The results for the 24/27 constellations are taken from the previous experiment, whereas the results for 29/30 constellations are discussed here in detail.

Table 6.9 Comparisons of 3-D RMS Errors for the 24/27 and 29/30 Constellations for SRS Processing (cm)

Baseline (km)	Medium Ionosphere				High Ionosphere			
	24 GPS/27 GAL		29 GPS/30 GAL		24 GPS/27 GAL		29 GPS/30 GAL	
	GPS	GAL	GPS	GAL	GPS	GAL	GPS	GAL
90	24.5	19.2	22.5	18.2	51.9	38.6	55.5	34.0
120	28.6	20.8	26.2	20.0	61.5	46.0	69.6	45.5

Table 6.10 Comparisons of 3-D RMS Errors for the 24/27 and 29/30 Constellations for MRS-TC Processing (cm)

Baseline (km)	Medium Ionosphere				High Ionosphere			
	24 GPS/27 GAL		29 GPS/30 GAL		24 GPS/27 GAL		29 GPS/30 GAL	
	GPS	GAL	GPS	GAL	GPS	GAL	GPS	GAL
90	1.1	0.6	0.8	0.5	8.8	6.7	4.0	3.9
120	2.5	0.9	1.1	0.9	26.4	18.0	30.5	15.1

Table 6.11 Comparisons of Percentage of Fixed Ambiguities for the 24/27 and 29/30 Constellations for SRS Processing (cm)

Baseline (km)	Medium Ionosphere				High Ionosphere			
	24 GPS/27 GAL		29 GPS/30 GAL		24 GPS/27 GAL		29 GPS/30 GAL	
	GPS	GAL	GPS	GAL	GPS	GAL	GPS	GAL
90	27.12	19.83	34.50	18.12	16.00	2.58	8.17	2.67
120	18.18	12.18	22.89	10.62	9.19	2.04	4.54	1.30

Table 6.12 Comparisons of Percentage of Fixed Ambiguities for the 24/27 and 29/30 Constellations for MRS-TC Processing (cm)

Baseline (km)	Medium Ionosphere				High Ionosphere			
	24 GPS/27 GAL		29 GPS/30 GAL		24 GPS/27 GAL		29 GPS/30 GAL	
	GPS	GAL	GPS	GAL	GPS	GAL	GPS	GAL
90	76.07	95.73	87.64	95.94	16.27	22.07	29.26	29.51
120	59.69	77.69	71.50	86.59	6.83	8.36	10.46	13.65

Table 6.13 Comparisons of Percentage of Correctly Fixed Ambiguities for the 24/27 and 29/30 Constellations for SRS Processing (cm)

Baseline (km)	Medium Ionosphere				High Ionosphere			
	24 GPS/27 GAL		29 GPS/30 GAL		24 GPS/27 GAL		29 GPS/30 GAL	
	GPS	GAL	GPS	GAL	GPS	GAL	GPS	GAL
90	51.04	81.92	72.48	80.25	6.33	10.15	6.49	18.31
120	50.41	80.94	22.46	55.20	2.29	3.36	3.39	12.03

Table 6.14 Comparisons of Percentage of Correctly Fixed Ambiguities for the 24/27 and 29/30 Constellations for MRS-TC Processing (cm)

Baseline (km)	Medium Ionosphere				High Ionosphere			
	24 GPS/27 GAL		29 GPS/30 GAL		24 GPS/27 GAL		29 GPS/30 GAL	
	GPS	GAL	GPS	GAL	GPS	GAL	GPS	GAL
90	79.04	90.57	91.67	96.92	15.02	41.94	45.38	55.19
120	68.01	73.37	82.83	84.31	11.34	26.66	18.59	39.12

6.4.1 Results for 90 km Baseline

Figure 6.18 presents the time series for 3-D RMS error and ambiguity plots for the 90 km baseline using the 29/30 GPS/Galileo constellations. The results show a similar behaviour as the results obtained with the 24/27 constellations discussed previously. For both medium and high ionosphere conditions (Figure 6.17 and Figure 6.18) the SRS 3-D RMS errors are more than 18 cm and 34 cm for the two systems. The solution is not reliable, showing a PFA of less than 34% and 19%, with a PCFA of 72.5% and 80.2% for medium ionospheric error GPS and Galileo solutions. For high ionospheric error conditions, the results deteriorate further demonstrating very low PFA figures of 8.1% and 2.7% with PCFA values of 6.5% and 18.3% for GPS and Galileo.

MRS-TC Galileo results only show very good improvement under medium ionospheric errors, providing cm level errors with a PFA of 95.9% and a PCFA of 96.9%. Under high ionospheric errors, the MRS-TC 3-D RMS error improves to the decimetre level compared to the SRS high ionospheric error levels. However, the PFA only improves to 29.5% for Galileo, showing a higher number of float ambiguities in the ambiguity plot. The time series of the 3-D RMS error for MRS-TC mode (Figure 6.18) shows discontinuities caused by incorrectly fixed ambiguities, similar to the results obtained with 24/27 constellations as seen previously.

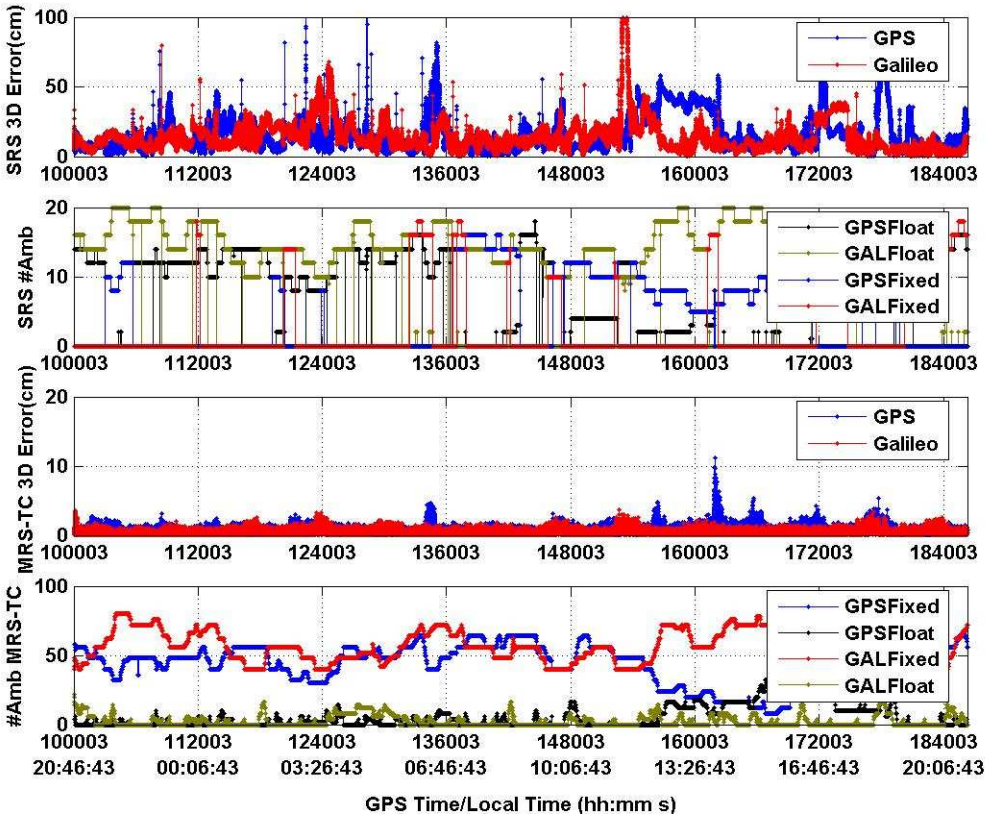

Figure 6.17 3-D RMS Error and Ambiguities Plots for the 90 km Baseline: Medium Ionosphere using 29/30 GPS/Galileo Constellations

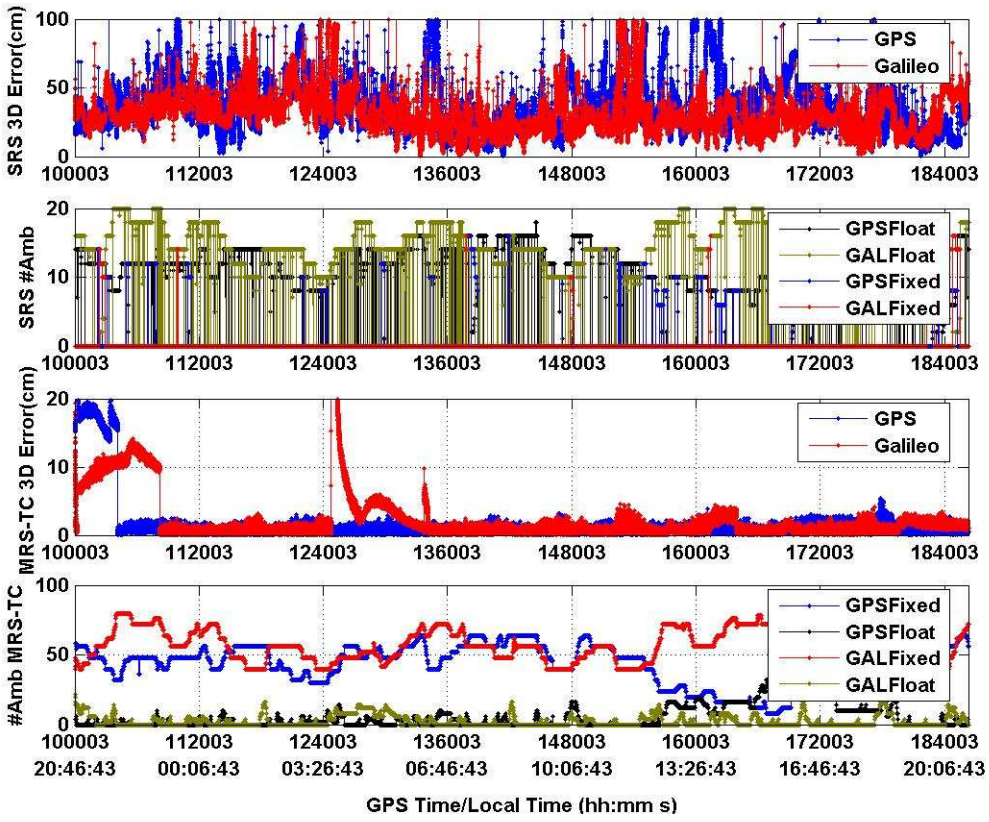

Figure 6.18 3-D RMS Error and Ambiguities Plots for the 90 km Baseline: High ionosphere using 29/30 GPS/Galileo Constellations

6.4.2 Results for 120 km Baseline

Figure 6.19 and Figure 6.20 represent the time series for 3-D RMS error and ambiguity plots for the 120 km baseline using the 29/30 GPS/Galileo constellations. The SRS results show a 3-D RMS error of more than 20 cm for medium ionospheric conditions with low PFAs figures of 22.9% and 10.6% for the GPS and Galileo. For high ionospheric errors, it further reduces to 4.5% and 1.3% with more than a 45 cm 3-D RMS error. Similar to the results obtained with the 24/27 constellations, the medium and high

ionospheric error ambiguity plots (Figure 6.19and Figure 6.20) show a higher number of float ambiguities with frequent jumps to zero representing a higher number of incorrectly fixed ambiguities, implying low PCFA figures. In the case of the MRS-TC approach, the medium ionospheric results show very good improvement giving a cm level error and an 86.6% PFA and an 84.3% PCFA compared to the SRS results for the stand-alone Galileo case. For high ionospheric conditions, the results are not reliable as indicated by low PFA values of 13.7% and 10.5%, and PCFA figures of 39.1% 18.6% for Galileo and GPS, respectively. As shown in Figure 6.20, the time series of the 3-D RMS error for MRS-TC shows discontinuities caused because of incorrectly fixed ambiguities similar to as seen previously in the 90 km and 120 km high ionosphere cases for the 24/27 constellations.

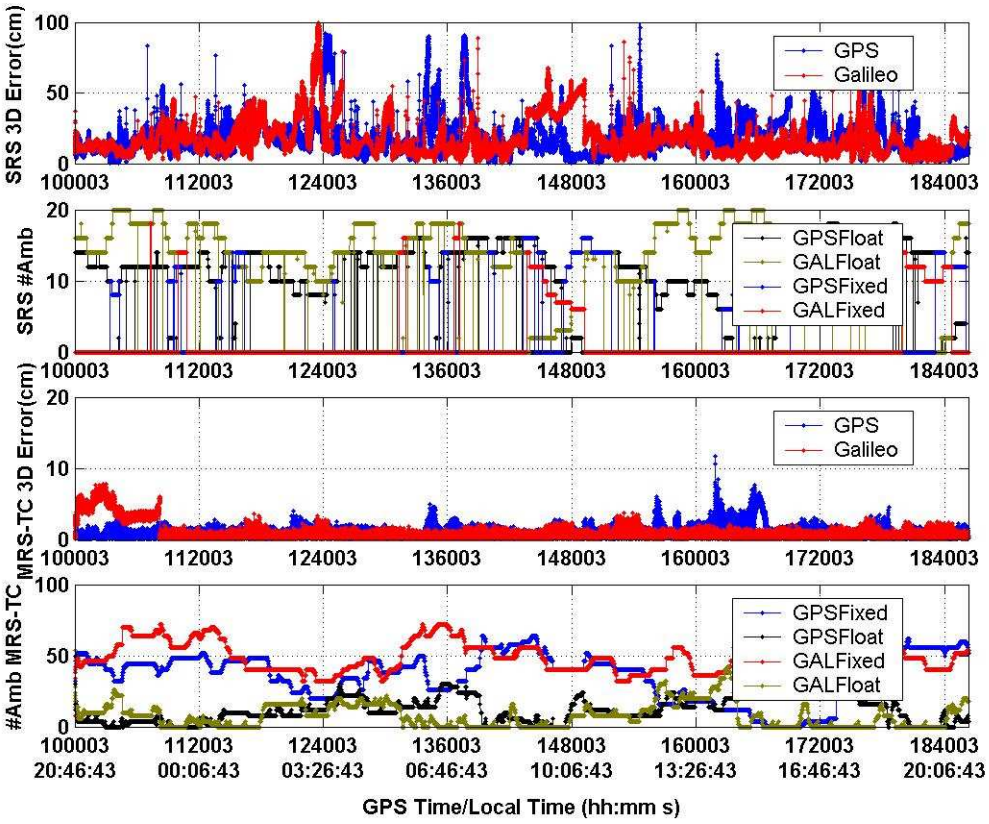

Figure 6.19 3-D RMS Error and Ambiguities Plots for the 120 km Baseline: Medium Ionosphere using 29/30 GPS/Galileo Constellations

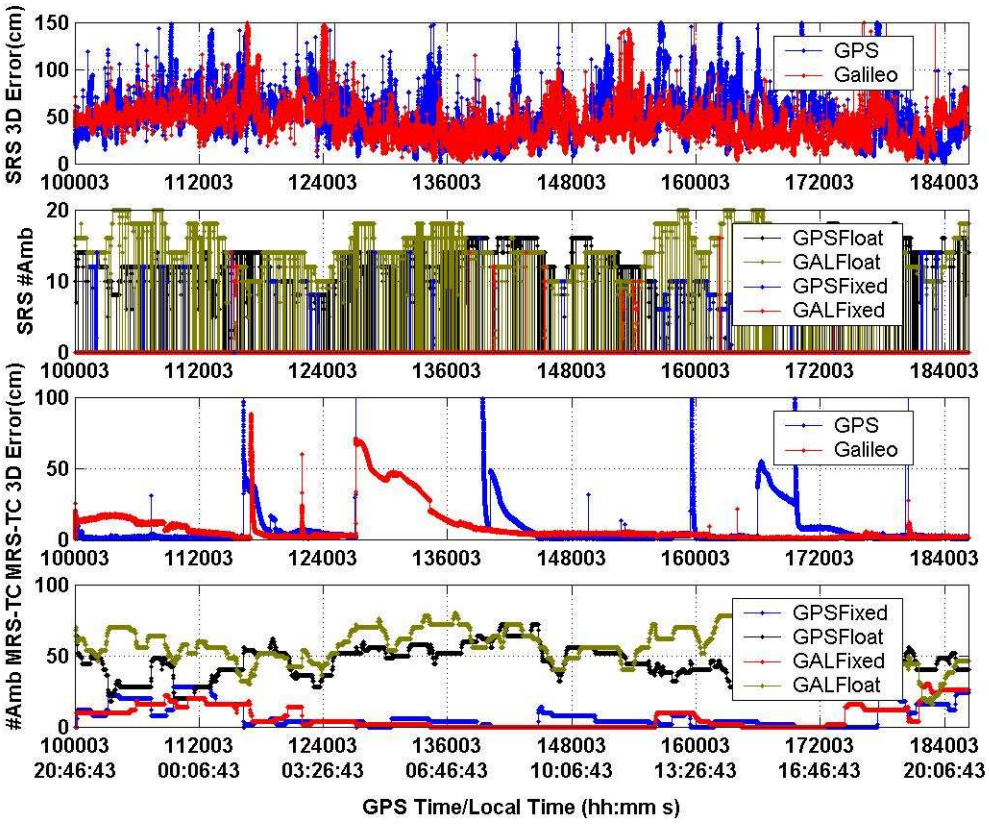

Figure 6.20 3-D RMS Error and Ambiguities Plots for the 120 km Baseline: High Ionosphere using 29/30 GPS/Galileo Constellations

6.5 FOM Results Summary

6.5.1 Summary of Results for 24/27 GPS/Galileo Constellations

Figure 6.21s, Figure 6.22 and Figure 6.23 present a summary of the overall simulation results for the 24/27 GPS/Galileo constellation, and hence can be used to compare the 3-D RMS error, as well as PFA and PCFA values for all 48 simulation scenarios. From Figure 6.21, it can be seen that Galileo always provides better position estimates compared to GPS for both the SRS and MRS-TC approaches. The MRS-TC solution

always shows an improvement compared to the SRS results and the MRS-TC Galileo scenarios provide the best solutions for all simulated scenarios.

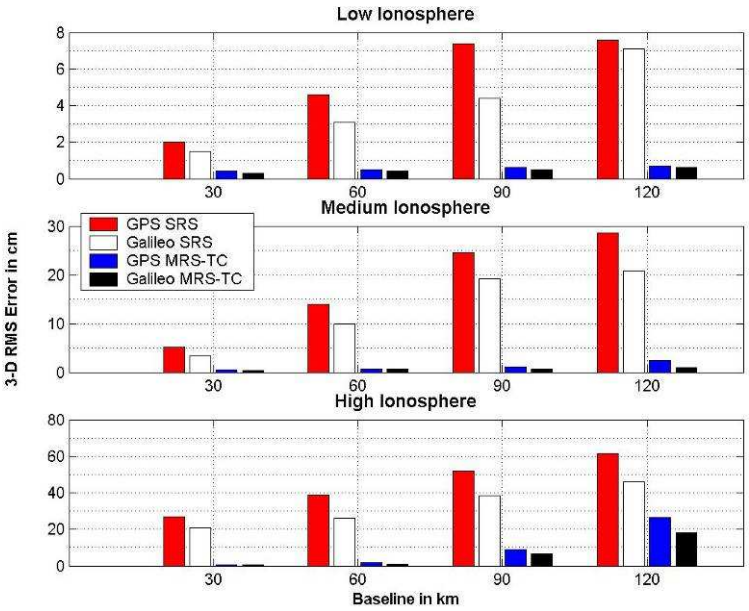

Figure 6.21 3-D RMS Errors for All Simulated Cases of the 24/27 Constellations

Figure 6.22 and Figure 6.23 show the reliability of the position estimates represented by Figure 6.21. For low ionospheric errors, the PFA and PCFA figures are comparable at about 90% for all four baselines and all four processing modes. For the medium ionosphere case, however, they are comparable only in the case of the 30 km baseline, beyond which the SRS PFA figures drop drastically and the MRS-TC PFA figures show very good improvement over the SRS results.

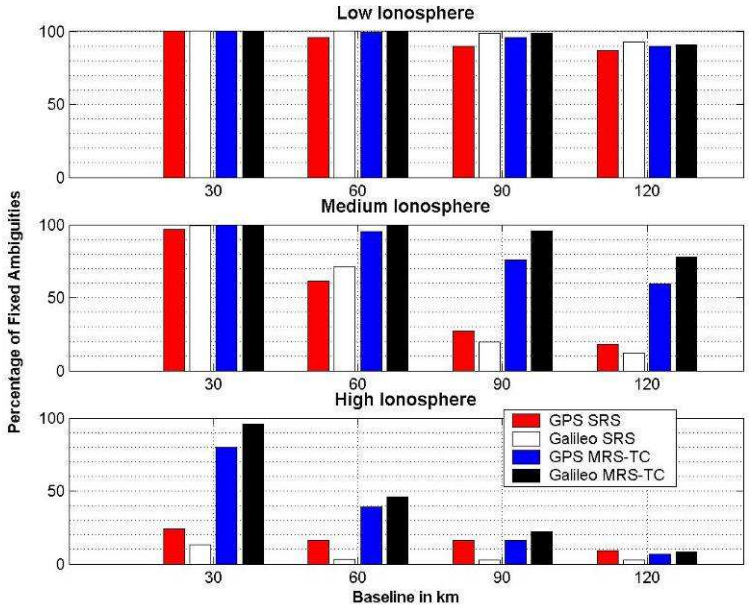

Figure 6.22 Percentages of Fixed Ambiguities for All Simulated Cases of the 24/27 Constellations

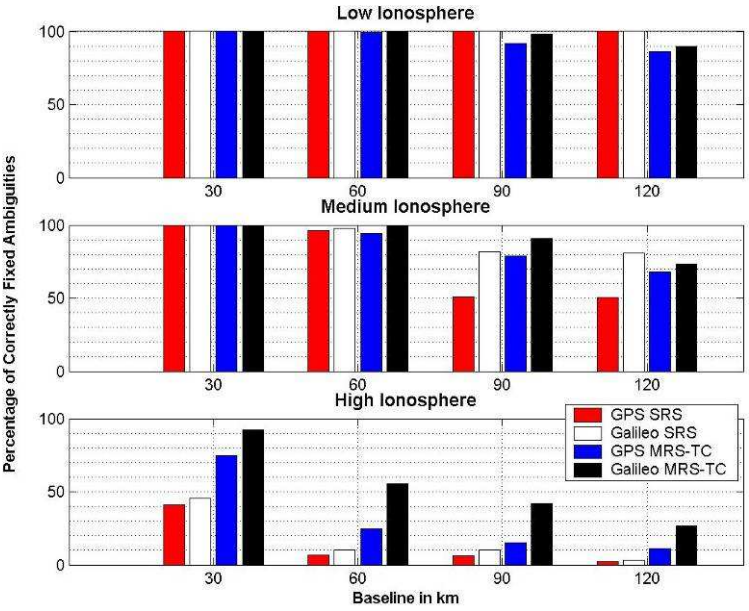

Figure 6.23 Percentages of Correctly Fixed Ambiguities for All Simulated Cases of the 24/27 Constellations

For high ionospheric errors, MRS-TC shows improved PFA values over the SRS approach only for the 30 km baseline, beyond which due to increase in the spatial decorrelation of the ionospheric ionosphere error, both the SRS and MRS-TC approaches deteriorate and are no longer reliable. For medium and high ionospheric error conditions, MRS-TC Galileo provides the best PFA for all baselines. In the SRS case for medium and high ionospheric errors, GPS provides a slightly higher PFA as compared to Galileo. This is because, for the SRS approach, ionospheric modelling estimates additional ionosphere states. For Galileo, since a higher number of satellites is available compared to GPS, it takes much longer to converge, and hence provides a lower number of fixed ambiguities. However, in terms of PCFA, the stand-alone Galileo solution is always better than stand-alone GPS for both the SRS and MRS-TC approaches.

6.5.2 Comparison of Results for 24/27 and 29/30 GPS/Galileo Constellations

Figure 6.24, Figure 6.25, and Figure 6.26 represent the plots derived using comparison results for three FOMs using the 24/27 and 29/30 constellations listed in Table 6.9, Table 6.10, Table 6.11, Table 6.12, Table 6.13 and Table 6.14.

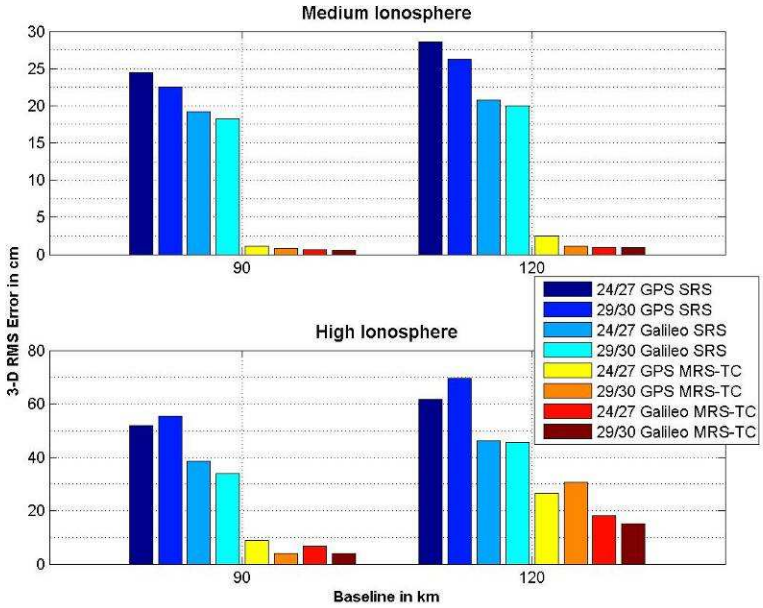

Figure 6.24 Comparisons of 3-D RMS Error for the 24/27 and 29/30 GPS/Galileo Constellations

From Figure 6.24, a comparison of the 3-D RMS errors show that the results obtained using both the 24/27 and 29/30 GPS/Galileo constellations are comparable. If we compare the SRS and MRS-TC results for each of the four simulated error cases, the stand-alone Galileo results are always better than the stand-alone GPS case. Also, the MRS-TC stand-alone Galileo 30 satellite constellation provides the best results providing the lowest 3-D RMS error among all processing modes, as expected.

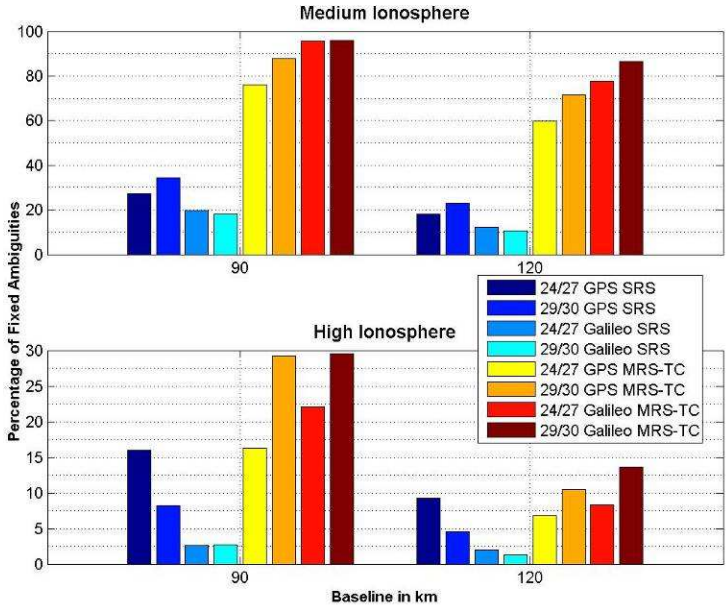

Figure 6.25 Comparisons of PFA for 24/27 and 29/30 GPS/Galileo Constellations

From Figure 6.25, a comparison of the PFA for the 24/27 and 29/30 GPS/Galileo constellations shows that, for medium ionospheric conditions, the PFA figures are comparable for both constellations. For high ionospheric conditions, the MRS-TC 29/30 constellation results show a significant improvement over the 24/27 constellations. However, these improved figures are still well below the reliability requirements for the PFA FOM. The MRS-TC stand-alone Galileo 30 satellite constellation again provides the best results by showing the highest PFA for all simulated error cases.

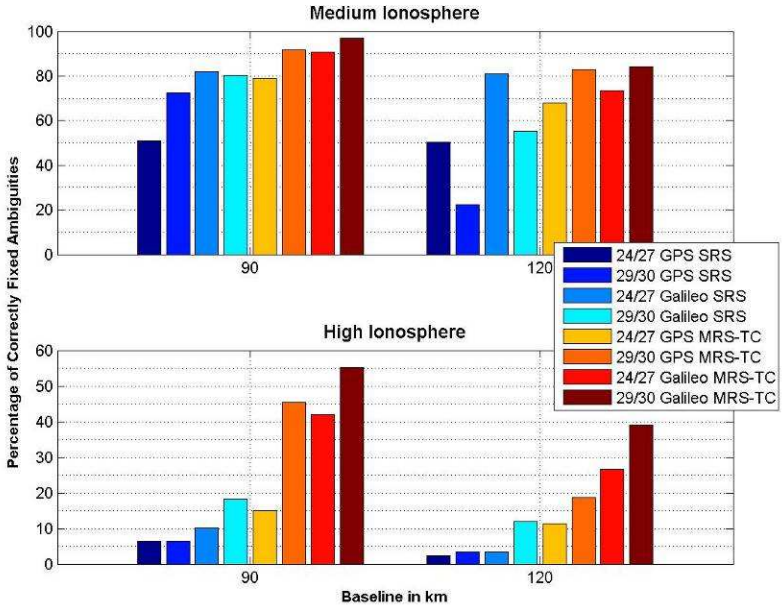

Figure 6.26 Comparisons of PCFA Values for the 24/27 and 29/30 GPS/Galileo Constellations

From Figure 6.26, a comparison of the PCFA for the 24/27 and 29/30 GPS/Galileo constellations shows a similar behaviour as in the results for the PFA given in Figure 6.25. Again for this FOM, the MRS-TC stand-alone Galileo approach with the 30 satellite constellation provides the best results by showing the highest PCFA for all simulated error cases.

Chapter 7 Conclusions and Recommendations

This research focused on a comparison of the SRS and MRS approaches for GPS and Galileo, for different baseline lengths and ionospheric conditions. The MRS-TC approach was chosen for evaluation referring to Alves (2004) and Dao et al. (2004) which showed that it provides improved accuracy and ambiguity resolution performance compared to a traditional collocation-based MRS approach. The study simulated two sets of stand-alone GPS and Galileo observations based on two constellations: the first constellation of 24 GPS and 27 operational Galileo satellites according to their original constellation designs, and another one based on the current GPS constellation with 29 GPS satellites and the future Galileo constellation with all 30 satellites. The simulated stand-alone GPS and Galileo observations for the baselines ranging from 30 to 120 km in low to high (i.e. 1 ppm to 6 ppm) ionospheric conditions were tested using the MRS-TC and SRS approaches and the results were evaluated in terms of positioning accuracy and ambiguity resolution performance. Given the test setup and the specific errors that were simulated, the following conclusions can be drawn:

- Galileo always provided better results in terms of the 3-D RMS error for both the MRS-TC and SRS approaches compared to GPS in the case of low and medium ionospheric conditions due to the improved availability and hence geometry of satellites. The simulation studies show that Galileo provides higher satellite availability, i.e. 6 to 10 satellites, compared to 4 to 8 GPS satellites. Also the Galileo geometry shows PDOP values of 1.5 to 3.3 compared to PDOP values of

1.6 to 5.8 for stand-alone GPS for the 24/27 GPS/Galileo constellation. Therefore, as anticipated, Galileo always provided better results in terms of the 3-D RMS error for both the MRS-TC and SRS approaches compared to GPS in the case of low and medium ionospheric conditions due to the improved availability and geometry of satellites.

- For all simulated scenarios, the improved geometry and availability from the Galileo constellation results in better ionospheric error estimation compared to the GPS only case. Also, it is confirmed that the MRS approach improves ionospheric estimation compared to the SRS approach.
- For all the simulated baselines and error levels, the MRS-TC approach applied to Galileo always offers the best results compared to SRS GPS and Galileo and the MRS-TC GPS cases. This due to combined benefits of Galileo and MRS-TC, i.e.: improved availability geometry of Galileo and addition of more information (rover observations) to the MRS-TC network filter.
- For low ionospheric error conditions, the MRS-TC approach for Galileo delivers cm-level positioning errors with 0.6 cm 3-D RMS error with 91% PFA and 90% PCFA for extended baselines up to 120 km. However these PFA and PCFA figures still need to be improved further in order to attain a 99% reliable results reliability level for practical applications.
- For low ionospheric error cases for all baselines, the MRS-TC provides approach provided an improved accuracy (~0.6 cm) compared to the SRS approach (~7.0 cm) in terms of 3-D RMS results, however both algorithms provided comparable results in terms of reliability, i.e. PFA and PCFA figures for both GPS as well as

Galileo. This is due to the larger reduction of correlated ionospheric errors when using MRS-TC compared to SRS.

- For medium and high ionospheric conditions, MRS-TC stand-alone Galileo provides reliable cm-level positioning errors results for baselines up to 30 and 90 and 30 km, with a 96% PFA in both cases and PCFA values of 90% and 92% PCFA %, respectively.
- For high ionospheric conditions and extended baselines beyond 30 km, none of the systems provide reliable results using the simulated data, since in both cases the uncorrelated residuals errors play a major role in making the systems unreliable.
- For all the simulated baselines and error levels, the MRS-TC approach applied to Galileo always offered the best results compared to the SRS GPS and Galileo and MRS-TC GPS cases. This was due to the combined benefits of Galileo and MRS-TC, i.e.: improved availability geometry of Galileo when compared to GPS and addition of more information (reference and rover observations) when SRS is compared to the MRS-TC due to better modelling of GNSS errors at the network filter.

This research deals with dual frequency results and treats GPS and Galileo independently, providing some interesting results for positioning improvements when using MRS-TC Galileo. However this thesis recommends further evaluation of the MRS-TC approach considering:

- Triple Frequency Techniques: GPS and Galileo will provide three frequencies to civil users out of which two are common to both systems. Based on these available triple frequencies new techniques for ambiguity resolution applied to the SRS approach were discussed in Chapter 3. Inspiring from these new findings in SRS triple frequency GPS/Galileo positioning, this thesis therefore recommends further evaluation of an MRS-TC approach for a GPS/Galileo combined system employing the same techniques i.e.: using triple frequency tight coupling and ionospheric weighted model or cascading ambiguity resolution with integrated triple frequency techniques as a future work. These triple frequency techniques applied to MRS-TC approach expects to improve the performance further for high ionospheric conditions over extended baselines.
- Real Galileo Data: In order to confirm these simulations based results further evaluation of Galileo MRS-TC approach using real MRS data is recommended when Galileo attains the full operational capability at the end of deployment phase and Galileo observations are available. Using the real data, MRS-TC can be evaluated for the GPS and Galileo systems independently as implemented in this thesis and for the combined GPS/Galileo system as recommended in the future work. However, while dealing with the combined GPS/Galileo system, interoperability issues such as different time reference frames and geodetic datums, as discussed in Chapter 2, need to be considered.

References

Alexander, K. (2006) ***U.S. Space Based PNT Policy and GPS Modernization,*** National Space-Based PNT Coordination Office, United Nations/Zambia/ESA Regional Workshop on the Applications of GNSS Technologies in Sub-Saharan Africa June 26-30, 2006.

Alves P., Y. W., Ahn and G., Lachapelle (2003) ***The Effects of Network Geometry on Network RTK Using Simulated GPS Data***, CD-ROM, Proceedings of ION GPS/GNSS 03, Institute of Navigation, Portland, Oregon, USA, 11 pages.

Alves, P. (2001) ***Effect of Galileo on Carrier Phase Ambiguity Resolution***, Proceedings of ION GPS 2001, Salt Lake City, Utah, Sept. 2001, CDROM, 10 pages.

Alves, P. (2004) ***Development of Two Novel Carrier Phase-Based Methods for Multiple Reference Station Positioning***, PhD Thesis, UCGE Report No 20203, Department of Geomatics Engineering, University of Calgary, Calgary, Canada.

Alves, P., Y.W., Ahn, J., Liu, G., Lachapelle, D., Wolfe, and A., Cleveland (2004) ***Improvements of USCG RTK Positioning Performance Using External NOAA Tropospheric Corrections Integrated with a Multiple Reference Station Approach,*** Proceedings of ION National Technical Meeting-04, San Diego, USA, pp. 689-698.

Ashjaee, J. and R., Lorenz (1992) ***Precise GPS Surveying After Y-Code,*** Proceedings of the 5th International Technical Meeting of the Satellite Division of the Institute of Navigation (ION GPS-92), Albuquerque, New Mexico, pp. 657-659.

Behrend, D., L., Cucurull, E., Cardellach, A., Rius, M.J., Sedo, and A., Nothnagel (2001) ***The Use of NWP Products in Near Real-Time GPS Data Processing***, In Proceedings of ION GPS-01, Salt Lake City, USA, pp. 2499-2506.

Black, H.D. and A. Eisner (1984) ***Correcting Satellite Doppler Data for Tropospheric Effects,*** Journal of Geophysical Research, Vol. 89, No. D2, pp. 2616-2626.

Brown, R.G. and P.Y.C., Hwang (1992) ***Introduction to Random Signals and Applied Kalman Filtering***, 2nd Ed. John Wiley & Sons, Inc., New York.

Brown, R.G., and P.Y.C., Hwang (1992) ***Introduction to Random Signals and Applied Kalman Filtering***, 2nd Ed. John Wiley & Sons, Inc., New York.

Can it Get?, Proceedings of ION GPS-02, 24-27 September, Portland, OR, pp. 493-502.

Cannon, M.E. (1991) ***Airborne GPS/INS with an Applications to Aerotriangulations***, UCSE Reports No. 20040, Department of Surveying Engineering, University of Calgary.

Cannon, M.E. (2001) ***GPS Modernization and the Emergence of New GNSS Systems and Applications***, Keynote Address, Proceedings of the Japanese GPS Conference, Tokyo, November 15-16, pp. 9-18.

Cannon, M.E., G., Lachapelle, and G., Lu (1993) ***Kinematic Ambiguity Resolution With a High Precision C/A Code Receiver***, Journal of Surveying Engineering, Amer. Soc. Civil Eng, Vol. 119, No. 4, pp. 147-155.

Chao, C. C. (1974) ***The Tropospheric Calibration Model for Mariner Mars***, 1971, JPL TR32-1587, Jet Propulsion Laboratory, Pasadena, CA.

Chen, D., and G., Lachapelle (1994) ***A Comparison of the FASF and Least-Squares Search Algorithms for On-the-Fly Ambiguity Resolution,*** Journal of the Institute of Navigation, Vol. 42, No.2, pp.371-390.

Chen, D., and G., Lachapelle (1995) ***A Comparison of the FASF and Least Squares Algorithms for Ambiguity Resolution On the FLY***, Navigation, Journal of The Institute of Navigation, Alexandria, VA, Vol. 42, No. 2, pp. 371-390.

Colombo, O.L., M., Hernandez-Pajares, J., Miguel Juan, J., Sanz (2000) ***Ionospheric Tomography Helps Resolve GPS Ambiguities On The Fly At Distances Of Hundreds Of Kilometers During Increased Geomagnetic Activity***, Proceedings IEEE PLANS 2000 Meeting, San Diego, March 2000.

Dai, L., S., Han, J., Wang, and C., Rizos (2004) ***Comparison of Interpolation Algorithms in Network Based GPS Techniques***, Navigation, Journal of The Institute of Navigation, Vol. 50, No. 4, pp. 277-293.

Dao, T. H. D., P., Alves, and G., Lachapelle (2004) ***Performance Evaluation of Multiple Reference Station GPS RTK for a Medium Scale Network***, International Symposium on GNSS/GPS 2004, Sydney, Australia, Dec. 2004, CDROM, 15 pages.

Dao, T.H.D. (2005) ***Performance Evaluation of Multiple Reference Station GPS RTK for a Medium Scale Network***, M. Sc. Thesis, UCGE Report No 20214, Department of Geomatics Engineering, University of Calgary, Calgary, Canada.

Dellago, R., E., Detoma and F., Luongo (2003a) ***Galileo-GPS Interoperability and Compatibility: A Synergetic Viewpoint***, Proceedings of ION GPS/GNSS-03, 9-12 September, Portland, OR, pp. 542-548.

Dellago, R., G., Galati, M., Leonardi, P., Magarò, and M., Sanna, (2003b) ***Galileo System Performance for Precision Approach with the Local Element,*** Proceeding of GNSS 2003, Graz, Austria, April 2003.

Dong, L. (2004) ***SimGNSSII^{TM} Algorithm Design Document,*** Released by PLAN Group, Department of Geomatics Engineering University of Calgary, March 31, 2004, Calgary, Canada.

Enge, P. (2003) ***GPS Modernization: Capabilities of the New Civil Signals,*** Australian International Aerospace Congress, Brisbane, Australia, *2*9 July – 1 August 2003.

European Commission (2006a) ***The Galilei project: GALILEO Design Consolidation***, online available at http://ec.europa.eu/dgs/energy_transport/galileo/documents.

European Commission (2006b) ***High Level Mission Definition version 3.0***, online available at http://ec.europa.eu/dgs/energy_transport/galileo/documents.

European Space Agency (ESA), Galileo Joint Undertaking (GJU) (2006) ***Galileo Open Service Signal In Space Interface Control Document***, (OS SIS ICD), Draft 0, Retrieved in June 2006 from http://www.galileoju.com.

Forssell, B., M., Martin-Neira, and R. A., Harris (1997) ***Carrier Phase Ambiguity Resolution,*** Proceedings of ION GPS-97, 16-19 September, Kansas City, MO, pp. 1727 - 1736.

Fortes, L. P. S. (2002) ***Optimising the Use of GPS Multi-Reference Stations for Kinematic Positioning***, Ph.D. thesis, UCGE Report No. 20158, Department of Geomatics Engineering, The University of Calgary, Calgary, Canada.

Fotopoulos, G. (2000) ***Parameterization of DGPS Carrier Phase Errors Over a Regional Network of Reference Stations***, M.Sc. thesis, UCGE Report No. 20142, Department of Geomatics Engineering, The University of Calgary, Calgary, Canada.

Frei, E. (1991) ***GPS-Fast Ambiguity Resolution Approach "FARA": theory and Application,*** Paper presented at XX General Assembly of the IUGG, IAG-Symposium, Vienna, August 11-24.

Fyfe, P., K., Davis, I., Jeng, C., Kelley, and C., Mosley (2002) ***GPS and Galileo-Interoperability for Civil Aviation Applications***, Proceedings of ION GPS-02, 24-27 September, Portland, OR, pp. 289 - 302.

Ganguly, S., A., Jovancevic, and J., Noronha (2004) ***Interoperability Study Between GPS and Galileo***, Proceedings of ION GNSS-04, 21-24 September, Long Beach, CA, pp. 670-680.

Gao, Y., and A., Wojciechowski (2004) ***High Precision Kinematic Positioning Using Single Dual-frequency GPS Receiver,*** XXth ISPRS Congress, 12-23 July 2004 Istanbul, Turkey. pp. 845-849.

Gao, Y., Z., Li, and J., McLellan (1997) ***Carrier Phase Based Regional Area Differential GPS for Decimetre-Level Positioning and Navigation***, Proceedings of ION GPS-97, Institute of Navigation, Kansas City, Missouri, USA, pp. 1305-1313.

Garin, L., F. V., Diggelen, Rousseau, and Jean-Michel (1996) ***Strobe And Edge Correlator Multipath Mitigation For Code,*** The 1996 9th International Technical Meeting of the Satellite Division of the Institute of Navigation, ION GPS-96. Part 1 (of 2); Kansas City, MO; USA; 17-20 Sept. 1996. pp. 657-664. 1996.

GPS World (2004) ***Global View: GALILEO Moves Ahead***, Retrieved in December 2005, from http://www.gpsworld.com/gpsworld/article/articleDetail.jsp?id=105343

GPS World (2006a) ***Galileo Gets Up- Sat Launched, Signal Received, Contract Signed***, Retrieved in February 2006, from http://www.gpsworld.com/gpsworld/article/articleDetail.jsp?id=300336

GPS World (2006b) ***Galileo ICD Released***, Retrieved in May 2006, from http://www.gpsworld.com/gpsworld/article/articleDetail.jsp?id=329192.

Han, S., and C., Rizos (1996) ***GPS Network Design and Error Mitigation for Real-Time Continuous Array Monitoring Systems***, Proceedings of ION GPS-96, Institute of Navigation, Kansas City, Missouri, USA, pp. 1827-1836.

Han, S., and C., Rizos (1997): ***Instantaneous Ambiguity Resolution for Medium-Range GPS Kinematic Positioning Using Multiple Reference Stations,*** In Proceedings of the International Association of Geodesy Symposia, vol. 118, Advances in Positioning and Reference Frames, Rio de Janeiro, Brazil, pp. 283-288.

Hatch, R. (1990) ***Instantaneous Ambiguity Resolution,*** In Kinematic Systems in Geodesy, Surveying, and Remote Sensing, Eds Schwarz, KP, Springer, pp. 299-308.

Hatch, R. (1991) ***Ambiguity Resolution while Moving-Experimental Results,*** In Proceedings of ION GPS 91, Albuquerque, New Mexico, September, pp. 707-713.

Hein, G.W., J., Godet, J., L., Issler, J., C., Martin, P., Erhard, R., Lucas-Rodriguez and T., Pratt (2002) ***Status of Galileo Frequency and Signal Design***, Proceedings of ION PS-02, 24-27 September, Portland, OR, pp. 266 - 277.

Hein, G.W., J., Godet, J.-L., Issler, J.-C., Martin, P., Erhard, R., Lucas-Rodriguez and T.,

Hein, G.W., J., Godet, J.-L., Issler, J.-C., Martin, P., Erhard, R., Lucas-Rodriguez and T., Pratt (2001) ***The Galileo Frequency Structure and Signal Design***, Proceedings of ION GPS-01, 11-14 September, Salt Lake City, UT, pp. 1273 - 1282.

Hopfield, H.S. (1969) ***Two-Quartic Tropospheric Refractivity Profile for Correcting Satellite Data,*** Journal of Geophysical Research, Vol. 74, No. 18, pp. 4487- 4499.

Hothem, L. (2006) ***GPS Modernization Program Current Status and Plans***, Presentation at IGS Workshop 2006, Darmstadt, Germany, May 2006.

Internaltional GPS Service (IGS) (2005) IGS Product Table, Retrieved in February 2005, from http://igscb.jpl.nasa.gov/components/prods.html.

Jan, Shau-Shiun (2003) ***Aircraft Landing Using A Modernized Global Positioning System And The Wide Area Augmentation System***, Phd Thesis, The Department Of Aeronautics And Astronautics, Stanford University, USA.

Jensen, A.B.O. (2002) ***Numerical Weather Prediction for Network RTK,*** PhD Thesis, University of Copenhagen, Publication Series 4, Vol. 10, National Survey and Cadastre, Denmark.

Julien, O., P., Alves, M.E., Cannon and G., Lachapelle (2004) ***Improved Triple-Frequency GPS/GALILEO Carrier Phase Ambiguity Resolution Using a Stochastic Ionosphere ModelingModelling***, Proceedings of ION NTM 2004, Institute of Navigation, January 2004, CDROM, 12 pages.

Julien, O., P., Alves, M.E., Cannon, and W., Zhang (2003) ***A Tightly Coupled GPS/GALILEO Combination for Improved Ambiguity Resolution***, Proceedings of ENC-GNSS 2003, Graz, Austria, April 2003, CDROM, 14 pages.

Jung, J, P., Enge, and B., Pervan (2000) ***Optimization of Cascade Integer Resolution with Three Civil GPS Frequencies***, Proceedings of the ION GPS-00, September 2000, Salt Lake City, UT, pp. 2191-2201.

Klobuchar, J. A. (1996) ***Ionospheric Effects on GPS***, Parkinson B., W., and Jr., J., J., Spilker, eds., Global Positioning System: Theory and Applications, volume I, chapter 12, American Institute of Aeronautics and Astronautics, Inc., Washington D.C., USA, pp. 486-516.

Lachapelle, G. (1983) ***Use of Kalman Filtering for GPS Aided Marine Navigation,*** Published in Geodesy in Transition, Publ. 60002, Division of Surveying Engineering, University of Calgary, pp. 301-312.

Lachapelle, G. (1990) ***GPS Observables and Error Sources for Kinematic Positioning, P r eceeding of Kinematic Systems***, Geodesy, Surveying, and Remote Sensing (IAG Symposium 107), Banff, Alberta, Sept. 10-13, pp.17-26.

Lachapelle, G. (2004) Advanced GPS – Theory and Applications, ENGO625 Lecture Notes, Department of Geomatics Engineering, University of Calgary.

Lachapelle, G., M.E., Cannon, and G., Lu (1992) ***Ambiguity Resolution On The Fly - A Comparison of P Code and High Performance C/A Code Receiver Technologies***, Proceedings of ION GPS-92, Institute of Navigation, Alexandria, VA, pp. 1025-1032.

Leonard, A., and I., Izquierdo (2002) ***GPS and GALILEO Interoperability and Synergies***, Proceedings of ION GPS-02, 24-27 September, Portland, OR, pp. 330 - 341.

Litton, J.D., G., Russell, K.T., Woo (1996) ***Method and Apparatus for Digital Processing in a Global Positioning Receiver***, U.S. Patent No.5,576,715, Nov.1996.

Liu, J. (2004) ***Implementation and Analysis of GPS Ambiguity Resolution Strategies in Single and Multiple Reference Station Scenarios***, M. Sc. Thesis, UCGE Report No 2016, Department of Geomatics Engineering, University of Calgary, Calgary, Canada.

Liu, J., Cannon, M.E., and G. Lachapelle (2003) ***FLYKIN+^{TM} Operator's Manual***, version 1.0, Department of Geomatics Engineering, University of Calgary.

Marini, J. W. (1972) ***Correction of Satellite Tracking data for an Arbitrary Tropospheric Profile,*** Radio Science, Vol. 7, No. 2, pp. 223-231.

McDonald, K. (2002) ***The Modernization of GPS: Plans, New Capabilities and the Future Relationship to Galileo***, Journal of Global Positioning System, Vol.1, No. 1: 1-17.

Miller, J. (2004) ***GPS &GALILEO: Evolution Towards GNSS***, Presentation at ION NTM-04, 26-28 January, San Diego, CA, pp. 73-91.

Misra, P., and P., Enge (2006) ***Global Positioning System: Signals, Measurements and Performance***, Ganga-Jumuna Press, 2nd edition, 2006.

Niell, A.E. (1993). ***A New Approach for the Hydrostatic Mapping Function,*** Proceedings of the International Workshop for Reference Frame Establishment and Technical Development in Space Geodesy, Communications Research Laboratory, Koganei, Tokyo, Japan, pp. 61-68.

O'Keefe, K., S. Ryan, and G. Lachapelle (2002) ***Global Availability and Reliability Assessment of the GPS and Galileo Global Navigation Satellite Systems,*** Canadian Aeronautics and Space Journal, Canadian Aeronautics and Space Institute, Vol. 48, 2, pp. 123-132.

Odijk, D. (2000) ***Weighting Ionospheric Correction to Improve Fast GPS Positioning Over Medium Distances***, Proceedings of ION NTM 2000, Institute of Navigation, September 2000, Salt Lake, USA, pp. 1113 - 1124.

Odijk, D. (2002) ***Fast Precise GPS Positioning In The Presence Of Ionosphereic Delays***, Optima Grafische Communicatie, the Netherlands.

Pany, T., P., Pesec, and G., Stangl (2001) ***Elimination of Tropospheric Path Delays in GPS Observations with the ECMWF Numerical Weather Model***, Physics and Chemistry of the Earth(A), Vol.26, No.6-8, pp. 487-492.

Parkinson, B. W. (1996) ***GPS Error Analysis***. Parkinson B., W., and Jr., J., J., Spilker, eds., Global Positioning System: Theory and Applications, volume I, chapter 11, American Institute of Aeronautics and Astronautics, Inc., Washington D.C., USA, pp. 469-485.

Perz, C.M. (2004) ***GPS Modernization Update***, Presentation at IEEE Plans, Session D4, 28 April, Monterey, CA.

Pratt (2002), ***Status of Galileo Frequency and Signal Design***, Proceedings of ION GPS-02, 24-27 September, Portland, OR, pp. 266 - 277.

Raquet, J. (1998) ***Development of a Method for Kinematic GPS Carrier-Phase Ambiguity Resolution Using Multiple Reference Receivers***, PhD thesis, UCGE Report No 20116, Department of Geomatics Engineering, University of Calgary, Calgary, Canada.

Ray, J. K. (2000) ***Mitigation of GPS Code and Carrier Phase Multipath Effects Using a Multi-Antenna System,*** Ph.D. Thesis, UCGE report 20136, Department of Geomatics Engineering, The University of Calgary, Calgary, Canada.

Ray, J. K. (2000) ***Mitigation of GPS Code and Carrier Phase Multipath Effects Using a Multi-Antenna System***, Ph.D. Thesis, UCGE report 20136, Department of Geomatics Engineering, The University of Calgary, Canada.

Rodriguez, J., M., Irsigler, G. W., Hein and T., Pany (2004) ***Combined Galileo/GPS Frequency and Signal Performance Analysis***, Proceedings of ION GNSS-04, 21-24 September, Long Beach, CA, pp. 632-649.

Rodriguez, J., M., Irsigler, G., W., Hein and T., Pany (2004) ***Combined Galileo/GPS Frequency and Signal Performance Analysis***, Proceedings of ION GNSS-04, 21-24 September, Long Beach, CA, pp. 632-649.

Ryan, S. (2000) ***Multiple Blunders in Marine Application,*** Proceedings of ION GPS-2000, the Institute of Navigation, Alexandria, VA.

Saastamoinen, J. (1972) ***Atmospheric Correction for the Troposphere and Stratosphere in Radio Ranging of Satellites***, Geophysics Monograph. Series, American Geophysical Union, Washington, DC, Vol. 15.

Saastamoinen, J. (1973) ***Contribution to the Theory of Atmospheric Refraction***, Bulletin Géodésiqué, Vol. 107, pp. 13-34.

Salgado, G., S., Abbondanza, R., Blondel, and S., Lannelongue (2001) ***Constellation Availability Concepts for Galileo***, Proceedings of ION NTM 2001, Institute of Navigation, Long Beach, CA, January 2001,, pp. 778-786.

Sandhoo, K., D., Turner and M., Shaw (2000) ***Modernization of the Global Positioning System***, Proceedings of ION GPS-00, 19-22 September, Salt Lake City, UT, pp. 2175-2183.

Skone S. (2003) Atmospheric Effects on Satellite Navigation Systems. ENGO 633 Lecture Notes, Department of Geomatics Engineering, University of Calgary.

Skone, S. (1998) ***Wide Area Ionosphere Grid Modelling in the Auroral Region***, PhD Thesis, UCGE Report Number 20123, Department of Geomatics Engineering, University of Calgary, Calgary, Canada.

Spilker, Jr., J., J., and B., W., Parkinson (1994) ***Overview of GPS Operation and Design***, Parkinson B., W., and Jr., J., J., Spilker, eds., Global Positioning System: Theory and Applications, volume I, chapter 2, American Institute of Aeronautics and Astronautics, Inc., Washington D.C., USA, pp. 29-55.

Swider, R. (2001) ***GPS Policy Update***, Presentation at Civil GPS Service Interface Committee, Department of Defense, 9-11 September, Salt Lake City, UT.

Teunissen, P.J.G. (1994) ***A New Method for Fast Carrier Phase Ambiguity Estimation***, Proceedings of the IEEE PLANS'94, Las Vegas, pp. 562-573.

Teunissen, P.J.G. (1998) ***Success Probability of Integer GPS Ambiguity Rounding and Bootstrapping***, Journal of Geodesy, Springer-Verlag 1998, Vol. 72, pp. 606-612.

Tsujii, T., J., Wang, L., Dai, C., Rizos, M., Harigae, T.T., Inagaki, T., Fujiwara, and T. Kato (2001) ***A Technique for Precise Positioning of High Altitude Platforms System (HAPS) using a GPS Ground Reference Network***, Proceedings of ION GPS-01, pp. 1017-1026.

U. S. Coast Guard (2006) ***GPS Status & Outage Information,*** online at http://www.navcen.uscg.gov/gps.

Varner, C. (2000) ***DGPS Carrier Phase Networks and Partial Derivative Algorithms***, Ph.D. Thesis, UCGE Report No. 20129, University of Calgary, Department of Geomatics Engineering Calgary, Canada.

Varner, C., and M. E., Cannon (1997) ***The Application of Multiple Reference Stations and the Determination of Multipath and Spatially Decorrelating Errors,*** In Proceedings of ION NTM-97, Santa Monica, California, pp. 323-333.

Vollath U., A., Buerchl, H., Landau, C., Pagels and B., Wagner (2000) ***Long-Range RTK Positioning Using Virtual Reference Stations***, Proceedings of ION GPS 2000, 13th International Technical Meeting of the Satellite Division of the Institute of Navigation, September 2000, Salt Lake City, Utah.

Vollath, U., S., Birnbach, and H., Landau (1998) ***Analysis of Three-Carrier Ambiguity Resolution (TCAR) Technique for Precise Relative Positioning***, Proceedings of ION GPS-98, Nashville, USA, 1998, pp. 417-426.

Wanninger, L. (1995) ***Improved Ambiguity Resolution by Regional Differential ModelingModelling of the Ionosphere***, Proceedings of ION GPS-95, Institute of Navigation, Palm Springs, CA, USA, pp. 55-62.

Weill, L. R. (2002) ***Multipath Mitigation Using Modernized GPS Signals: How Good***

Wells, D., N., Beck, D., Delikaraoglou, A., Kleusgerg, E. J., Kraviswisky, Lachapelle, G., R., Langley, M., Nakiboglu, K. P., Schwarz, J. M., Tranquilla, and P., Vanicek (1986) ***Guide to GPS Positioning***, Canadian GPS Associates, Fredericton.

Wells, D.E., N., Beck, D., Delikaraoglou, A., Kleusberg, E.J., Krakiwsky, G., Lachapelle, R.B., Langley, M., Nakiboglou, K.P., Schwarz, J.M., Tranquilla and P., Vanicek (1986) ***Guide to GPS Positioning***, University of New Brunswick Graphic Services, Fredericton.

Wübbena, C., A., Bagge, G., Seeber, B., Volker, and P., Hankemmeier (1996) ***Reducing Distance Dependent Errors for Real -time Precise DGPS Applications by Establishing Reference Station Networks***, Proceedings of ION GPS-96, Institute of Navigation, Kansas City, Missouri, USA, pp. 1845-1852.

Zandbergen, R., S., Dinwiddy, J., Hahn, E., Breeuwer and D., Blonski (2004) ***Galileo Orbit Selection***, Proceedings of ION GNSS-04, 21-24 September, Long Beach, CA, pp. 616- 623.

Zhang, W. (2005) ***Triple Frequency Cascading Ambiguity Resolution for Modernized GPS and GALILEO,*** MSc Thesis, UCGE Report No. 20228, Department of Geomatics Engineering, The University of Calgary, Calgary, Canada.

Zhang, W., M.E., Cannon, O., Julien, and P., Alves (2003) ***Investigation of Combined GPS/GALILEO Cascading Ambiguity Resolution Schemes***, Proceedings of U.S. ION GPS/GNSS, Institute of Navigation, Portland, OR, September 2003, pp. 2599-2610.